FUNDAMENTAL PHOTOELECTROCHEMICAL PROPERTIES OF TiO_2/WATER INTERFACES: RELEVANCE FOR HAZARDOUS WASTE REMEDIATION

Thesis by

Janet M. Kesselman

In Partial Fulfillment of the Requirements

for the Degree of

Doctor of Philosophy

California Institute of Technology

Pasadena, California

1997

(Submitted October 2, 1996)

Acknowledgments

During my graduate career, I have had the benefit of not one, but two excellent advisors, and I would like to start off by thanking them for their support—financial, scientific, and otherwise. I've learned so much from both of them, it would take too long to enumerate it here.

There are also many people in both research groups I would like to thank for their scientific contributions to my thesis and for their moral support in surviving graduate school. Ming Tan showed me the ropes when I first joined Nate's group, and I'm grateful for her continued friendship. Gary Shreve made significant contributions to the work described in Chapter 2 during numerous and lengthy discussions of the analysis of the results. I'd like to thank Kathy Pomykal, my compatriot from UCSD and inimitable captain of our illustrious softball team, for being my best friend and sounding board for all my dilemas— scientific and otherwise. From Michael's group I would especially like to thank Ron Siefert for his help with computers and ion chromatography, and Wonyong Choi, Nicole Peill, and Scot Martin, members of the TiO_2 foursome, for many stimulating discussions about TiO_2 photocatalysis. I'd like to thank Scot Martin for getting me involved in the research described in Chapter 4— I learned a lot by working with him. I'd also like to thank Nicole for helping to keep me sane, especially during this last year while looking for a job and trying to finish up.

Most of all, I would like to thank my family, especially my parents, for always being there whenever I needed them, for teaching me the value of hard work, and for making me believe I could accomplish anything.

Abstract

TiO_2 photocatalysis is a promising technology for the treatment of aqueous or gaseous systems contaminated by low levels of organic pollutants. The research described in this thesis explores fundamental mechanistic and kinetic questions for both TiO_2 photocatalytic and electrocatalytic degradation of aqueous organic contaminants. A recurring theme in this thesis is the use of TiO_2 electrodes to investigate kinetic and mechanistic aspects of the TiO_2 photocatalytic process. The use of electrodes provides additional experimental control of system parameters that is not possible in conventional TiO_2 slurry reactors.

The first study reports the kinetics of oxygen reduction at single-crystal, rutile TiO_2 electrodes as a function of applied potential. Platinum deposits are found to catalyze the reduction of oxygen at this surface. Application of a flux-matching condition to the independently measured reduction and photooxidation currents predicts significant recombination losses for TiO_2 particles operating under steady-state photocatalytic conditions.

In a second project, the contributions of direct and hydroxyl radical mediated oxidation pathways are determined at Nb-doped, polycrystalline TiO_2 electrodes.[1-3] In addition to quantifying the branching ratio of these two mechanisms for a variety of organic substrates, the results suggest that surface interactions are important in determining the predominant reaction pathway in these systems.

Finally, the adsorption of 4-chlorocatechol at the TiO_2/H_2O interface is investigated as a function of pH and solution concentration. Quantitative measurements of the extent of adsorption are reported as well as spectroscopic evidence for the structure of the adsorbed complex. Further work correlates observed photocatalytic degradation rates with the extent of adsorption under various solution conditions.

References

(1) Weres, O.; Hoffmann, M. R., *Electrochemical Method and Device for Generating Hydroxyl Free Radicals and Oxidizing Chemical Substances Dissolved in Water*, U.S. Patent #5,364,508, Nov. 15, 1994.

(2) Weres, O.; Hoffmann, M. R., *Electrode, Electrode Manufacturing Process and Electrochemical Cell*, U.S. Patent #5,419,824, May 30, 1995.

(3) Weres, O.; Hoffmann, M. R., *Electrochemical Device for Generating Hydroxyl Free Radicals and Oxidizing Chemical Substances Dissolved in Water*, U.S. Patent #5,439,577, Aug. 8, 1995.

Table of Contents

List of Illustrations

Chapter 1.

Introduction

Contamination of ground water supplies is a pervasive problem in the United States. Organic pollutants typically found in contaminated ground water include BTEX compounds (benzene, toluene, ethyl benzene, and xylene) from fuels and lubricants; chlorinated hydrocarbons such as trichloroethylene and perchloroethylene which have been used as degreasers, solvents, and dry-cleaning agents; and halogenated aromatic compounds such as DDD [1,1-dichloro-2,2-bis(p-chlorophenyl)ethane] and various PCB (polychlorinated biphenyl) compounds used as pesticides.[1] Ground water contamination can be traced to many sources, including leaky underground storage tanks, landfill leaching, surface impoundments, waste disposal injection wells, municipal and industrial septic systems, and direct application to soil (e.g., pesticide use).[1]

According to the Office of Technology Assessment, there are 2.5 million underground storage tanks in the U. S.[1] An EPA survey found that of the 800,000 underground tanks used for fuel storage, 35% were leaky.[1] A 1982 EPA report found that 95% of the 27,000 industrial surface impoundment sites were within 1 mile of a drinking water well and 70% were unlined.[1] Over 25 states report ground water contamination from pesticides.[1] The cost for remediation of U.S. military sites alone has been estimated at $30 billion over the next ten years.[2]

Technologies that have been developed to treat contaminated water include: bioremediation, UV/peroxide and UV/ozone, carbon adsorption, and high temperature incineration.[1-3] Bioremediation is a promising treatment technology; however, some pollutants of interest are resistant to microbial degradation. UV/peroxide and UV/ozone systems effectively oxidize organic contaminants. However, the consumption of ozone and peroxide in the process adds to the treatment costs. Carbon adsorption removes organic contaminants from the water, but does not chemically destroy them. High temperature incineration is often politically unfeasible. Thus, research into new waste treatment technologies continues.

TiO_2 photocatalysis is a promising alternative technology for the treatment of water contaminated by low concentrations of organic molecules.[2, 3] TiO_2 is a semiconductor with a band gap energy of 3.0 eV for the rutile crystal phase, and 3.2 eV for the anatase phase.[4] When TiO_2 is illuminated with photons of energy equal to or greater than the band gap energy, an electron, e^-, is excited from the valence band to the conduction band (Figure 1). The resulting electron vacancy in the valence band is called a hole, h^+. Due to the valence band edge position of TiO_2 (+3.2 V vs. the normal hydrogen electrode, NHE, at pH 0 for anatase[4, 5]), the hole is a strong oxidant and can oxidize organic molecules, RH, eventually mineralizing them to CO_2. Similarly, the hole can oxidize water to form hydroxyl radicals, •OH, which are also effective oxidants of organic compounds. For chlorinated hydrocarbons of the general formula, $C_xH_yCl_z$, the mineralization reaction can be written with the following stoichiometry [2]:

$$C_xH_yCl_z + \left(x + \frac{y-z}{4}\right)O_2 \xrightarrow{h\nu, TiO_2} xCO_2 + zH^+ + zCl^- + \left(\frac{y-z}{2}\right)H_2O \qquad (1)$$

In order for the process to continue effectively, the photogenerated electrons must also be removed from the TiO_2. Typically, oxygen is used as the electron acceptor. Oxygen can be reduced to the superoxide anion radical, which may participate in the degradation reactions of the organic molecules, or be further reduced to hydrogen peroxide or water.

Electrons and holes which are not removed from the TiO_2 by reaction with solution species recombine in the particle to produce heat. This reaction is an unproductive pathway and limits the efficiency of the system. Unproductive reactions of electrons and holes with solution species, such as the complete oxidation of water to molecular oxygen, represent additional loss mechanisms. As a result of these unproductive pathways, typical quantum yields for the degradation of organic molecules by TiO_2 photocatalysis are less than 0.1.[6, 7] Recent research has thus focused on

improving our understanding of the fundamental chemical and physical processes occurring in TiO_2 photocatalysis, and on determining how various system parameters affect the observed quantum efficiencies. Factors that have been shown to be important include: (1) the preparation method and resulting crystal phase of the TiO_2 catalyst;[6, 8-12] (2) the incident light intensity,[7, 13] and more recently, the use of pulsed illumination;[14] (3) the concentration of dissolved oxygen[7, 15] or alternate electron scavengers;[13, 16] (4) solution pH;[7, 17] (5) adsorption of the substrate to the TiO_2 surface;[2, 18-20] and (6) the use of metal deposits to catalyze electron transfer to oxygen.[21, 22]

There is a great deal of interest in using TiO_2 for waste treatment due to the low cost of the TiO_2 catalyst as well as the potential for using sunlight as the energy source. TiO_2 photocatalysis has not yet been widely commercialized, however, due primarily to the low efficiency of the process and the use of more expensive artificial light sources to enable continuous operation.

The goal of the research described in this thesis is to build upon the work of previous researchers in order to understand better the factors affecting reaction mechanisms and rate-limiting processes for TiO_2 photocatalysis. By understanding the parameters that control the efficiency of TiO_2 photocatalysis, rational design of improved systems for the degradation of organic pollutants in water can in principle be achieved.

In Chapter 2, the possible rate-limiting behavior of oxygen reduction in TiO_2 photocatalysis is evaluated. Single-crystal, rutile TiO_2 electrodes are used to examine oxidation and reduction half reactions independently. Rate constants for electron transfer to oxygen are determined as a function of applied potential. These results are then compared to expected values based on literature calculations using Marcus/Gerischer theory, and to estimates of the electron/hole pair generation rates for particles exposed to solar irradiation.[23, 24] These experiments determine the potential conditions under which electron transfer to oxygen is slower than the electron generation rate, and thus "rate-

limiting." Further experiments compare the potential dependence of the dark reduction current and the photooxidation current to predict the operating potential of TiO_2 particles. The flux of electrons and holes across the TiO_2/H_2O interface at this potential is shown to be much less than the photogeneration rate of electron/hole pairs implying significant recombination losses for particles operating under steady-state conditions. The influence of platinum deposits on the potential dependence of the oxidation and reduction currents indicates that platinum catalyzes the reduction of oxygen and would thus improve degradation efficiencies.

The goal of the work described in Chapter 3 is to determine the predominant oxidation mechanism for commercially prepared, Nb-doped, polycrystalline TiO_2 electrodes operated under strong anodic bias and without UV illumination. To distinguish between •OH mediated and direct electron transfer mechanisms, the relative degradation rates of a series of chlorinated acetates are compared to the known and expected trends for •OH and direct mechanisms, respectively, for these compounds. Further work quantifies the contribution of each pathway for a number of organic substrates by comparing the increase in current density upon addition of substrate (a measure of the direct oxidation pathway) with the observed degradation rate (the sum of both pathways). The results of these experiments also suggest the importance of surface interactions in determining degradation mechanisms for various substrates.

Abundant evidence exists for the importance of substrate adsorption as a determining factor in TiO_2 photodegradation rates. Chapter 4 describes a collaborative effort to determine the surface structures of a strongly adsorbing organic molecule, 4-chlorocatechol, on TiO_2. The amount of 4-chlorocatechol adsorbed on TiO_2 as a function of initial solution concentration and pH is quantified by measurement of the loss of 4-chlorocatechol from solution upon equilibration with a slurry of TiO_2 particles. The surface structure of the adsorbed molecule is determined by attenuated total reflectance

Fourier transform infrared spectroscopy (ATR-FTIR) combined with modeling studies incorporating surface reaction stoichiometries.

Chapter 5 is a continuation of the work begun in Chapter 4. The photodegradation rates of 4-chlorocatechol as a function of initial solution concentration and pH can be compared to the extent of adsorption measured under similar conditions in Chapter 4. The observations indicate that the degradation rate is linearly correlated with the concentration of adsorbed 4-chlorocatechol.

A recurring theme in this thesis is the use of TiO_2 electrodes to investigate kinetic and mechanistic aspects of TiO_2 photocatalysis. Electrochemical experiments offer additional control of system parameters that is not possible in conventional TiO_2 slurry reactors. Several different types of TiO_2 electrodes have been used in this work. As discussed above, Chapter 2 describes experiments using single-crystal, rutile TiO_2 electrodes to monitor independently the oxidation and reduction reactions occurring at the TiO_2/H_2O interface. At the surface of illuminated TiO_2 particles, both oxidation and reduction reactions occur simultaneously. At TiO_2 electrodes, however, by controlling the applied potential and performing experiments either (a) in the dark in the presence of dissolved oxygen, or (b) under illumination in the absence of oxygen, the oxidation and reduction half reactions can be monitored separately (Figure 2). The experiments in Chapter 3 employ commercially developed, Nb-doped, polycrystalline TiO_2 electrodes operated under strong anodic bias and without UV illumination to distinguish between •OH and direct electron transfer oxidation mechanisms. The ability to measure the current due to direct oxidation of organic substrates allows the determination of the relative contributions of direct and hydroxyl radical mediated oxidation. Finally, Chapter 5 makes use of undoped, polycrystalline TiO_2 electrodes to compare degradation rates of 4-chlorocatechol over a range of solution concentration and pH conditions. In this case, because the photogenerated electrons can be removed through the external electrical

circuit, the use of TiO_2 electrodes permits the measurement of 4-chlorocatechol degradation in nitrogen purged solutions. This avoids complications in the analysis of the data that are present when competing homogeneous oxidative coupling reactions occur in the presence of oxygen at high pH.

References

(1) Bedient, P. B.; Rifai, H. S.; Newell, C. J. *Ground Water Contamination Transport and Remediation*; Prentice Hall PTR: Englewood Cliffs, New Jersey, 1994.

(2) Hoffmann, M. R.; Martin, S. T.; Choi, W.; Bahnemann, D. W. *Chem. Rev.* **1995**, *95*, 69-96.

(3) Venkatadri, R.; Peters, R. W. *Haz. Waste. & Haz. Mat.* **1993**, *10*, 107-149.

(4) Finklea, H. O. In Semiconductor Electrodes; H. O. Finklea, Eds.; Elsevier: New York 1988; p 43-146.

(5) Nozik, A. J. *Ann. Rev. Phys. Chem.* **1978**, *29*, 189-222.

(6) Choi, W.; Termin, A.; Hoffmann, M. R. *J. Phys. Chem.* **1994**, *98*, 13669-13679.

(7) Kormann, C.; Bahnemann, D. W.; Hoffmann, M. R. *Environ. Sci. Technol.* **1991**, *25*, 494-500.

(8) Martin, S. T.; Herrmann, H.; Choi, W.; Hoffmann, M. R. *J. Chem. Soc. Faraday Trans.* **1994**, *90*, 3315-3322.

(9) Martin, S. T.; Herrmann, H.; Hoffmann, M. R. *J. Chem. Soc. Faraday Trans.* **1994**, *90*, 3323-3330.

(10) Rivera, A. P.; Tanaka, K.; Hisanaga, T. *Appl. Catal. B: Env.* **1993**, *3*, 37-44.

(11) Riegel, G.; Bolton, J. R. *J. Phys. Chem.* **1995**, *99*, 4215-4224.

(12) Sclafani, A.; Palmisano, L.; Schiavello, M. *J. Phys. Chem.* **1990**, *94*, 829-832.

(13) Cunningham, J.; Sedlák, P. *J. Photochem. Photobiol. A: Chem.* **1994**, *77*, 255-263.

(14) Sczechowski, J. G.; Koval, C. A.; Noble, R. D. *J. Photochem. Photobiol. A: Chem.* **1993**, *74*, 273-278.

(15) Bideau, M.; Claudel, B.; Faure, L.; Kazouan, H. *J. Photochem. Photobiol. A.: Chem* **1991**, *61*, 269-280.

(16) Schwitzgebel, J.; Ekerdt, J. G.; Gerischer, H.; Heller, A. *J. Phys. Chem.* **1995**, *99*, 5633-5638.

(17) Mills, A.; Morris, S. *J. Photochem. Photobiol. A: Chem.* **1993**, *71*, 75-83.

(18) Ollis, D. F.; Pelizzetti, E.; Serpone, N. In Photocatalysis: Fundamentals and Applications; N. Serpone and E. Pelizzetti, Eds.; John Wiley & Sons: New York 1989; p 603-637.

(19) Al-Ekabi, H.; Serpone, N.; Pelizzetti, E.; Minero, C.; Fox, M. A.; Draper, R. B. *Langmuir* **1989**, *5*, 250-255.

(20) Al-Sayyed, G.; D'Oliveira, J.-C.; Pichat, P. *J. Photochem. Photobiol. A: Chem.* **1991**, *58*, 99-114.

(21) Izumi, I.; Dunn, W. W.; Wilbourn, K. O.; Fan, F.-R. F.; Bard, A. J. *J. Phys. Chem.* **1980**, *84*, 3207-3210.

(22) Wang, C.-M.; Heller, A.; Gerischer, H. *J. Am. Chem. Soc.* **1992**, *114*, 5230-5234.

(23) Gerischer, H.; Heller, A. *J. Phys. Chem.* **1991**, *95*, 5261-5267.

(24) Gerischer, H.; Heller, A. *J. Electrochem. Soc.* **1992**, *139*, 113-118.

Figures

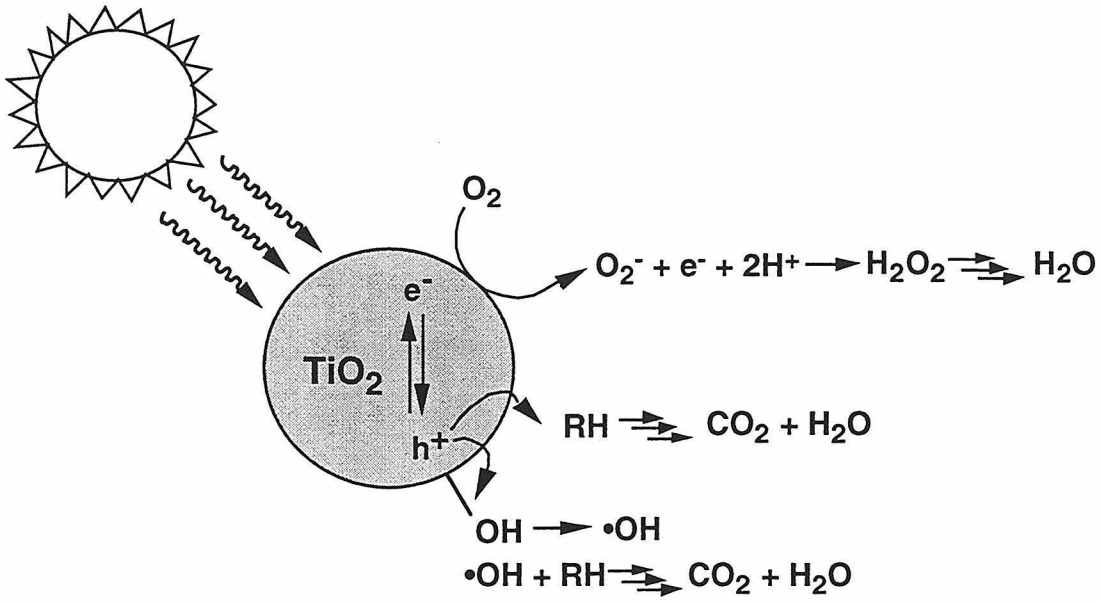

Figure 1. Schematic representation of processes occurring in TiO_2 photocatalysis.

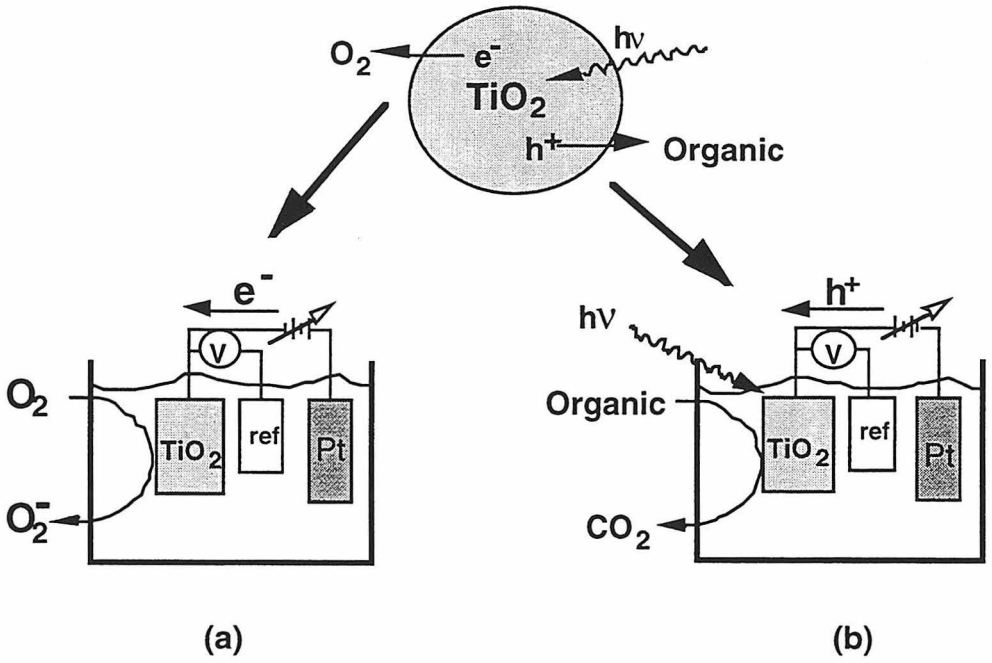

Figure 2. Three-electrode experiments at single-crystal TiO_2— separating oxidation and reduction. (a) Measurement of the current due to the reduction of O_2 at a TiO_2 electrode in an air-saturated solution in the dark. (b) Measurement of the photooxidation current at an illuminated electrode in a N_2-purged solution.

Chapter 2.

Flux-Matching Conditions at TiO_2 Photoelectrodes: Is Interfacial Electron Transfer to O_2 Rate-Limiting in the TiO_2-Catalyzed Photochemical Degradation of Organics?

(The text of this chapter appeared in Kesselman, J. M.; Shreve, G. A.; Hoffmann, M. R.; and Nathan S. Lewis, *J. Phys. Chem.*, **1994**, *98(50),* 13385-13395.)

Abstract

A flux-matching condition has been applied to determine whether O_2 reduction is rate-limiting under photocatalytic conditions for the degradation of $CHCl_3$ at rutile TiO_2 single-crystal electrodes. In this approach, the potential dependence of the photooxidation current density is compared to the potential dependence of the current density for O_2 reduction. The potential at which the oxidation and reduction fluxes are equal determines the operating potential, and the steady-state flux, that will flow through the crystal under no applied bias. If this flux-matching condition occurs when the cathodic flux equals the flux of photogenerated carriers, then the predicted quantum yield should approach unity; otherwise, recombination should be significant in the TiO_2. Our measurements indicate that significant recombination will occur for the oxidation of typical organic molecules in H_2O over a range of pH values. The data also indicate that Pt catalysis of O_2 reduction should be beneficial for the oxidation of organic molecules, as would the use of alternate electron acceptors such as $Fe(CN)_6^{3-}$. The O_2 reduction data and rotating disk electrode data collected in this work allow a quantitative comparison to theoretical estimates of the electron transfer rate constant for O_2 reduction at TiO_2. We also present an elucidation of the previously published theoretical treatments of TiO_2 charge transfer rate constants in view of the new data collected herein.

Introduction

TiO_2 particles have been utilized to promote the photocatalytic degradation of organic compounds often found in contaminated waste streams. Halocarbons,[1-4] pesticides,[5,6] and surfactants[7,8] are among the variety of compounds that have been photocatalytically degraded using TiO_2. For many of these compounds, the only consumables are sunlight, atmospheric $O_2(g)$ and $H_2O(l)$, with the organic material being completely oxidized to CO_2. For these reasons, TiO_2-based photooxidation has been recognized as a promising technology for remediation of toxic organic wastes.

Despite the extensive interest in this process from both the applied and fundamental viewpoints, there is still controversy regarding the rate-determining step in the photooxidation process. When TiO_2 is exposed to light of energy greater than the band gap energy (3.0 eV for rutile TiO_2, 3.2 eV for anatase TiO_2),[9] an electron is excited from the TiO_2 valence band into the TiO_2 conduction band. The photogenerated electron vacancy (hole) generally initiates the oxidation of the organic (either through direct oxidation of the organic molecule or through formation of OH radicals followed by Fenton[10]chemistry), while the photogenerated electron must be removed from the particle by transfer to a suitable electron acceptor. In most cases of interest, atmospheric $O_2(g)$ is employed as the electron scavenger.[1-4,6-8] Because the steady-state quantum yields for organic oxidation in the presence of air are typically much less than unity,[1,2] a key question is whether electron transfer or hole transfer from the particle is limiting the quantum yield and efficacy of the photocatalytic process.

Theoretical studies by Gerischer and Heller have suggested that the rate of electron transfer from TiO_2 to dioxygen may be slow compared to the electron-hole pair generation rate.[11,12] Some experimental support for interfacial electron transfer as the rate limiting step in photocatalysis has been obtained from the accumulation of excess

negative charge on TiO_2 particles during the photocatalyzed oxidation of 1.6 *M* $CH_3OH(aq)$.[13] Other experimental studies, however, have suggested that electron transfer to dioxygen is not rate-limiting in photocatalytic degradation processess.[2,14] For example, Kormann *et al.*[2] have reported that the rate of oxidation of $CHCl_3$ in an aqueous suspension of TiO_2 displays Langmuir-type saturation behavior with respect to the concentration of dioxygen. Under air-saturation conditions, they observed that the rate of $CHCl_3$ degradation was essentially independent of the $O_2(g)$ concentration.[2] Similarly, Bideau and co-workers reported that the rate of oxidation of acetic acid by TiO_2 became independent of the concentration of dioxygen for $[O_2(g)] > 3$ ppm.[14] This observation either implies that above $[O_2(g)] \approx 3$-5 ppm, photogenerated electrons were effectively scavenged by dioxygen, or that electron transfer to surface sites was rate-limiting and that in air-saturated solutions, adsorbed dioxygen filled all of the available surface sites.

An alternative approach to evaluating the rate-limiting step in heterogeneous photodegradation is to perform electrochemical measurements at single-crystal TiO_2 photoelectrodes.[9,15,16] Two classes of such experiments will be described in this report. In one set of experiments, rotating disk electrodes have been used to determine the rate of O_2 reduction at single-crystal TiO_2 electrodes.[17,18] O_2 reduction rates have been determined at several electrode potentials and oxygen concentrations, and these values have been compared to the theoretical predictions made by Gerischer and Heller.[12] In the second set of experiments, the magnitudes of photooxidation current densities for a variety of aqueous solutions in the absence of oxygen have been compared to oxygen reduction current densities in air-saturated solutions. A current-matching condition can then be used to predict the net flux of electrons and holes that would occur at TiO_2 particles for this photogeneration rate. These results provide valuable information about the important kinetic factors in these systems, and allow the formulation of predictions

that can be tested for particulate systems. These results also suggest methods by which operating TiO_2 photocatalysts might be made more efficient.

Background

We first present a brief description of theoretical expectations for the flux-matching experiments, and then discuss a theoretical formalism for treating heterogeneous rate constants at semiconductor electrodes. This formalism will provide a basis for analysis of the current density vs. potential (J-*E*) data presented in Section IV.

Qualitative Analysis of Flux-Matching Data

Figure 1 presents the four basic fluxes of interest in the TiO_2 mediated photocatalytic oxidation of aqueous phase organic molecules in the presence of oxygen. A flux of absorbed photons, Γ_o, will create electron-hole pairs in the TiO_2. Unless these photogenerated charge carriers transfer across the solid/liquid interface, the carriers will recombine in the solid, producing a recombination flux, U_{rec}. The interfacial charge transfer flux of holes, U_p, includes oxidation of water and direct oxidation of the organic donor. The interfacial charge transfer flux of electrons, U_n, primarily involves reduction of the electron acceptor, generally considered to be O_2 during oxidative degradation processes.

At steady-state, U_p must equal U_n. Using single-crystal electrodes, it is possible to evaluate separately the potential dependence of U_p and U_n. For example, in an air-saturated solution under no illumination, slow scan J-*E* curves can directly yield the steady-state potential dependence of the flux for dioxygen reduction (Figure 2a) at TiO_2. In this measurement, the hole transfer flux is not important, because electrons are rapidly resupplied by the potentiostat to the back contact of the crystal. The potential

dependence of U_p can be determined independently by obtaining J-E data for TiO_2/H_2O-organic junctions under illumination and in the absence of $O_2(g)$ (Figure 2b). Thus, in each J-E measurement, only one interfacial reaction is rate-determining, so at single-crystal electrodes each important interfacial charge transfer process can be studied separately.[15,16]

For a given light intensity, there will be only one potential at which the oxidation current density equals the reduction current density, *i.e*, where $U_n(E) = U_p(E)$. This flux matching approach to photoelectrochemical degradation processes is closely analogous to the classical treatments of electrochemical corrosion processes, in which a corroding metallic electrode adopts the potential at which the anodic and cathodic current densities are equal. This flux-matching condition can be used to predict the "operating potential," E_{op}, of the TiO_2 photocatalyst under no external bias. It also yields the net flux of electrons and holes that will cross the TiO_2 surface at the specific electron-hole pair generation rate of interest. It is not important whether the interfacial reactions occur through one-electron intermediates or through more complicated chemical processes, because only the potential dependences of the total fluxes, U_n and U_p, are required to perform the desired analysis. Recombination processes are implicitly included in the net J-E data under illumination, so the flux-matching procedure is valid even if significant carrier recombination occurs on the TiO_2 surface.

Figures 2c and 2d illustrate this experiment for two possible limiting cases. When the flux-matching condition occurs at a potential for which $U_n(E_{op}) = U_p(E_{op}) = \Gamma_o$, the rate of photocatalysis is limited by the generation rate of electron/hole pairs (Figure 2c). This will occur when the onset of cathodic current density is sufficiently positive that the desired flux, Γ_o, is achieved at potentials where the photocurrent is independent of potential. The other limiting case, $U_n(E_{op}) = U_p(E_{op}) << \Gamma_o$, occurs when the onset of cathodic current density does not occur at positive potentials relative to the photocurrent

plateau region (Figure 2d). In this situation, the interfacial flux of electrons and of holes at $E = E_{op}$ will be much less than the incident photon flux; thus, the rate of photocatalysis will be limited by the rate of charge transfer. In addition, when $U_n(E_{op}) = U_p(E_{op}) << \Gamma_o$, significant charge recombination must occur and will result in a lower overall efficiency for the photocatalytic process.

Theoretical Rate Constant Calculations

It is also possible to assess whether the reduction current density and/or oxidation current density at a given electrode potential is in accord with theoretical expectations. The charge transfer rate constant for a donor (D) and acceptor (A) separated by a fixed distance in a homogeneous solution can be broken down into a frequency factor, ν_n, an electronic term, κ_{el}, and a nuclear term, κ_n:[19]

$$_{D,A} = \nu_n \kappa_{el} \kappa_n \qquad (1)$$

In eq 1, κ_{el} is a function of the distance, r, between species A and species D. For nonadiabatic electron transfers, κ_{el} generally displays an exponential dependence on distance: $\kappa_{el} = \kappa_{el,o}\exp\{-\beta(r-r_o)\}$, where β is typically 10^8 cm^{-1}, r_o is the center-to-center distance between D and A at contact, and $\kappa_{el,o}$ is the value of κ_{el} at $r = r_o$. κ_n is a function of the activation energy for the electron transfer event, and is classically related to the reorganization energy, λ, and to the driving force for reaction, ΔG^o.[19] For a heterogeneous reaction in which the donors are confined to one phase and the acceptors are confined to the other phase, Marcus has shown that integration of eq 1 over the relevant distances and angles for all donor-acceptor pairs yields:[20,21]

$$k_{het,D,A} = \nu_n\{2\pi(r_D + r_A)\beta^{-3}\}\left\{\exp\left(\frac{-(\lambda_A + \lambda_D + \Delta G^\circ)^2}{4kT(\lambda_A + \lambda_D)}\right)\right\} \qquad (2)$$

where r_D and r_A are the effective radii of the donor and acceptor ions, respectively, and λ_D and λ_A are the reorganization energies for the donor and acceptor species. The first term in brackets represents κ_{el} and the second term corresponds to κ_n.

Suitable modification of this expression for a bimolecular charge transfer process at a semiconductor/liquid interface, where the delocalized electron in the solid is the donor and the acceptor is dissolved in the solution, yields:

$$k_{sc} = \nu_n\{2\pi(r_A + r_e)\beta^{-3}\}\left\{\exp\left(\frac{-(\lambda + \Delta G^{\circ'})^2}{4kT\lambda}\right)\right\} \qquad (3)$$

where r_e is the effective radius of the electron in the semiconductor and λ is the reorganization energy of A near the surface of the semiconductor.[22,23] The driving force for the interfacial charge transfer reaction at an n-type semiconductor electrode is $\Delta G^{o'}$, with $\Delta G^{o'} = \mathbf{E}_{cb}-\mathbf{E}^{o'}$ for electron transfer from the conduction band to an acceptor species (with $\mathbf{E}^{o'}$ the formal electrochemical potential of the acceptor/donor pair and $\mathbf{E}_{cb}$ the energy of the conduction band edge at the solid/liquid contact).[24-28] Taking the effective radius of the electron, r_e, as 10^{-7} cm, $r_A \approx 3\times10^{-8}$ cm, $\beta = 10^8$ cm^{-1} and $\nu_n = 10^{13}$ s^{-1}, yields a maximum value for $k_{sc} = 10^{-17}$ cm^4-s^{-1} at $\kappa_n = \exp[-(\lambda + \Delta G^{o'})^2/(4kT\lambda)] = 1.0$ (optimal driving force).[22]

Gerischer has derived an analogous expression for reactions of dissolved redox species at a planar semiconductor electrode by assuming an effective distance for electron transfer and a constant rate of transfer over this distance.[29] Summing over all possible donor-acceptor pair distances at the interface yields:

$$k_{sc} = \nu_n (r_e)^3 \delta \exp\left\{\frac{-(\lambda + \Delta G^{o'})^2}{4kT\lambda}\right\} \qquad (4)$$

where r_e = the effective radius of the electron in the semiconductor, δ = the effective electron transfer distance, and λ = the reorganization energy of the acceptor species in solution. Taking values of $r_e = 10^{-7}$ cm, $\delta = 3 \times 10^{-8}$ cm, and $\kappa_n = 1$ yields a value of $k_{sc} = 3 \times 10^{-16}$ cm^4-s^{-1},[11,12,22,29] which is within an order of magnitude of that obtained from eq 3.[11,12] Gerischer and Heller have used this type of expression, with an estimated value of $\kappa_n = 10^{-3}$, to assess whether electron transfer to O_2 is rate-limiting in the photocatalytic oxidation of organic molecules using TiO_2 particles. This would predict that k_{sc} is lower than the maximum value of 10^{-17} cm^4 sec^{-1} and is on the order of $k_{sc} \approx 10^{-20}$ cm^4 sec^{-1}.

The rate constant k_{sc} can be directly related to the experimentally observed current density at a planar semiconductor electrode. The explicit assumption of a bimolecular rate law in the derivation of eqs 2 through 4 yields:

$$J(E) = -q\, k_{sc} n_s [A]_s \qquad (5)$$

where n_s equals the concentration of electrons at the surface of the semiconductor (and is a function of the applied potential in depletion), and $[A]_s$ is the concentration of the acceptor species at the surface of the electrode. In the flux-matching experiments described below, k_{sc} will be determined from the observed current density divided by the estimated value of n_s at the potential of measurement. This will allow an experimental validation of the values of κ_n used in the theoretical treatment of Gerischer and Heller.[11,12]

A slightly different formalism is required to relate the RDE data to the fundamental rate constant, k_{sc}, and to the value of κ_n for the electron transfer process. At an RDE, the observed current density is related to the kinetic current density and the mass transport current density as follows:[30]

$$\frac{1}{J} = \frac{1}{J_k} + \frac{1}{J_{lim}} \tag{6}$$

Here, $J_k = -q\, k_n'\, [O_2]$ and $J_{lim} = -0.62 n_e F [O_2] D^{2/3} \nu^{-1/6} \omega^{1/2}$, where n_e is the number of electrons transferred per molecule of O_2 reduced, F is the number of coulombs per mole of electrons, ω is the rotation rate of the electrode, ν is the kinematic viscosity of the solution, and D is the diffusion coefficient of the electroactive species. Thus, the kinetic parameter that describes the rate constant for O_2 consumption at a given electrode potential must be the product of k_{sc} and n_s:

$$k_n' = k_{sc} n_s \tag{7}$$

Our RDE experiments have been performed in accumulation, so n_s is on the order of the atom density in the solid and is relatively independent of potential. Use of eq 7, however, requires an accurate estimation of the value of n_s under accumulation conditions. An alternative approach is to treat the rate constant in the standard fashion for metal electrodes,[20,22,31,32] which yields the following expression for k_n':

$$k_n' = \nu_n \beta^{-1} \kappa_n \tag{8}$$

Solving eq 8 for κ_n by use of $\nu_n = 10^{13}$ s^{-1}, $\beta = 10^8$ cm^{-1} and then using the value of κ_n in either eqs 3 or 4 relates k_n' and k_{sc}. This calculation therefore provides the required link between the data of the flux-matching experiments and those of the RDE experiments.

Experimental

TiO_2 Rotating Disk Electrodes (RDEs)

Single crystals of TiO_2 were obtained from Commercial Crystal Laboratories Inc. (Naples, FL). The crystals had been polished on one side and were oriented to expose the (001) face. The crystals were doped n-type by heating for approximately 90 min at 800 °C in a quartz tube furnace (Lindberg; Watertown, WI) under a flowing atmosphere of forming gas (95% N_2, 5% H_2). The crystals were then allowed to cool for 2-3 hours under the flowing forming gas. During doping, the crystals changed from a transparent yellowish color to dark blue-black, and exhibited some visible surface damage. Following doping, the crystals were etched in hot (≈250 °C) concentrated sulfuric acid for ≈ 2.5 hours.[33] This etching procedure caused visible changes in the surface but did not remove all of the surface damage caused by the doping process.

Ohmic contact to the crystal was made by rubbing a Ga:In eutectic mixture onto the back of the sample. Electrically conductive silver epoxy (Epoxy Technology Inc.; Billerica, MA) was used to attach the crystal to a stainless steel rod. The crystals, which were approximately 3 mm on a side, were then ground into a circular shape using a wet grinder. The edges of the crystal were then sealed with white epoxy 1C (Dexter Corp.; Seabrook, NH) and the stainless steel rod/crystal assembly was encased in a Teflon shield. The area of the electrode was determined photographically and/or by comparison of the slopes of Koutecky-Levich plots for the TiO_2 electrode in $K_3[Fe(CN)_6](aq)$

solutions with those of Pt rotating disk electrodes (RDEs) of known areas in the same solutions.

Prior to each scan in the RDE measurements, the TiO_2 was etched for 15-30 s in HF/HNO_3 (1:1). After each etch, the electrode was rinsed in flowing water and was dried in a stream of $N_2(g)$.

TiO_2 Electrodes for Flux-Matching Experiments

The same crystals and doping/etching/ohmic contact procedures were employed for electrodes used in the flux-matching experiments. After making ohmic contacts with Ga:In eutectic, the back of the crystal was attached to a Cu wire with electrically conductive silver epoxy. The wire was encased in a glass tube and the edges of the crystal were sealed with white epoxy to expose surface areas between 0.03 and 0.08 cm^2. The electrodes were cleaned in aqua regia and were stored in deionized water between J-*E* scans.

Platinum was electrodeposited onto TiO_2 electrodes from a 1.0 *M* NaCl (aq)- 20-40 *mM* $Na_2PtCl_4 \cdot H_2O$ solution. The pH of this solution was adjusted to between 3 and 5 using HCl(aq). The platinization was performed at a potential for which the Pt reduction current was at least an order of magnitude greater than the background current in 1.0 *M* NaCl(aq) of the same pH. Kogo *et al.*, using a similar deposition technique, observed that Pt was deposited in the form of small islands that did not completely cover the TiO_2 surface.[34] The maximum amount of Pt deposited on the surface was estimated by the number of coulombs passed during platinization. The Pt coverages determined by X-ray photoelectron spectroscopy (XPS) were substantially less than the upper limit calculated using coulometry, indicating that not all of the platinum adhered to the electrode surface.

Electrochemical Cells and Measurement Techniques

The electrochemical cell used in the RDE experiments was fabricated from Pyrex. The cell used in the flux-matching experiments was also made from Pyrex, but had a flat quartz bottom to maximize optical transmission in the UV spectral region. Potassium hydroxide, sodium hydroxide, sodium carbonate/sodium bicarbonate buffer, and tris(hydroxymethyl)aminomethane (TRIZMA) buffer solutions were used as electrolytes to provide solutions with a range of pH values between 14 and 7.2. The KOH, NaOH, and $NaHCO_3$ were reagent grade and used as obtained from the supplier (EM; Gibbstown, NJ). TRIZMA Base and Na_2CO_3 (J. T. Baker; Phillipsburg, NJ) and TRIZMA HCl (Sigma; St. Louis, MO) were also of reagent grade and used as received. For area determination experiments and for experiments in which an alternate electron acceptor was desired, $K_3Fe(CN)_6$ (Mallinkrodt; Paris, KY) was added to the electrolyte solutions. $CHCl_3$ and $K_4Fe(CN)_6$ (J. T. Baker; Phillipsburg, NJ) were used as alternate electron donors in some photooxidation experiments. These compounds were also at least reagent grade and were used as received.

Various O_2(aq) concentrations were obtained by passing H_2O-saturated gas mixtures continuously through the electrolyte. The gases were appropriate combinations of pre-purified N_2, air, and/or O_2. The partial pressure of O_2 over the cell was adjusted with a flow controller/meter. The concentration of O_2 in solution was measured with an Orion Ag/AgCl oxygen sensitive electrode (Orion; Boston, MA).

A Barnsted NANOpure water purifier (Boston, MA) provided 17.8 MΩ-cm resistivity deionized water for the RDE experiments. For the flux-matching experiments, more reproducible results were obtained by using Millipore Milli-Q^{UV} Plus 18 MΩ resistivity water (Van Nuys, CA). Prior to each experiment, this water was pre-electrolyzed under a N_2(g) purge. The working electrode for preelectrolysis was a fibrous carbon cloth which was maintained at reducing potentials for several hours. All

flux-matching data discussed in this work, except for Figures 8 and 10, were obtained in pre-electrolyzed solutions.

In all J-*E* experiments, a two-compartment cell was used. The counterelectrode compartment was separated from the working electrode compartment by a ceramic frit (Corning; Corning, NY). The counterelectrode was made from carbon fibers, and the reference electrode was a saturated calomel electrode (SCE). In the RDE experiments, the experimental configuration consisted of a TiO_2 RDE working electrode, a Pt counterelectrode (with a much larger area than the working electrode), and a SCE reference. The Pt counterelectrode was separated from the main compartment of the cell by a Nafion frit.

In photoelectrochemical experiments, illumination was provided by a 300 W ELH-type W-halogen bulb (Wiko; Orland Park, IL) with a dichroic rear reflector.[35] The incident light intensity was controlled by adjusting the distance between the lamp and the cell and/or by the use of neutral density filters. Although the ELH lamp has its maximum spectral irradiance in the visible region,[36] the lamp provided sufficient intensity in the near ultraviolet to achieve the desired electron-hole pair generation rates in our TiO_2 samples.

J-*E* scans obtained in the dark were generally initiated at positive potentials, and the potential was scanned to the negative limit to trigger a reversal in scan direction. Conversely, J-*E* scans of photooxidation current were initiated at negative potentials and were scanned to a limiting positive potential. At the slow scan rates employed in these studies (generally ≤ 5 mV-s^{-1}), the forward and reverse scans exhibited only a small amount of hysteresis (*cf* Figures 3a and 4). Steady-state values of the current were estimated from the mean of the currents measured at a given potential in the forward and reverse directions. Several attempts were made to collect reliable data for dioxygen reduction at acidic pH values. A variety of electrolyte solutions was explored at acidic

pH, but J-*E* curves in all cases exhibited substantial hysteresis between forward and reverse potential scans. In addition, the J-*E* curves obtained in acidic media ($2 < pH < 5$) did not display the 60 mV/pH unit shift in current density that was observed for $7.2 < pH < 14$. Our inability to obtain reliable, reproducible J-*E* data at low pH values for n-TiO_2 is curious considering the published results of other researchers.[18,37,38]

Electrochemical and Surface Science Instrumentation

A Pine Instrument Co. Model RDE 3 Potentiostat with an ASR Rotator (Grove City, PA) was used for all RDE experiments. J-*E* data for flux-matching experiments were obtained using a Princeton Applied Research (Princeton, NJ) Model 175 Universal Programmer coupled to Model 173 Potentiostat/Galvanostat equipped with a Model 179 Current-to-Voltage Converter or similar potentiostatic instrumentation. The J-*E* data for all experiments were recorded on a Houston Instruments Model 2000 Omnigraphics X-Y recorder (Houston, TX).

XPS measurements were carried out on a Surface Science Instruments/Fisons (San Carlos, CA) M-Probe instrument. The background pressure in the instrument was typically $(4 \pm 1) \times 10^{-9}$ torr, and monochromatic X-rays from the Al K_α line, collamated to spot sizes of either 300 μm or 400 μm x 1000 μm, were used as the source. An electron energy analyzer pass energy of 150 V was used for the desired low resolution (1.5 eV) scans. The XPS spectra were analyzed using the M-Probe ESCA 1.34 software package (Surface Science Instruments/Fisons, CA) on a HP Vectra RS/20C-20 MHz-DOS 5.0 computer. XPS peaks were referenced to the signal arising from adventitious carbon, which was assigned an absolute energy of 284.6 eV.

Results

Flux-Matching Conditions for n-TiO_2/1.0 *M* NaOH(aq) Interfaces

Figure 3a depicts the J-*E* behavior for reduction of air-saturated (0.26 *mM* O_2(aq)) water in the dark at TiO_2. For $-0.95 < E < -0.85$ V vs. SCE, the O_2 reduction current increased exponentially as *E* became more negative. Ten determinations using several different electrodes yielded average values for the diode quality factor, $A = (q/kT)/\{\partial(\ln J)/\partial V\}$, of 1.4 ± 0.1, and for the exchange current density, J_o, of $(2 \pm 3) \times 10^{-18}$ A cm^{-2} (Figure 3b). Of particular note in regard to our flux-matching analysis is that the current density for 0.26 *mM* O_2 reduction did not exceed the electron-hole pair generation flux for 30 nm radius TiO_2 particles under 1 Sun illumination[12] (i.e., 2.1 μA cm^{-2} or 1.3×10^{13} carriers cm^{-2} s^{-1}) until $E_{TiO_2} < -0.875$ V vs. SCE.

Figure 4 displays the J-*E* curves for TiO_2/1.0 *M* NaOH(aq) interfaces under several different light intensities. These experiments were performed in N_2 purged solutions. Of particular note with regard to the flux-balance condition is that the photocurrent density in Figure 4 did not equal the electron-hole pair generation current density until $E_{TiO_2} > -0.75$ V vs. SCE. Essentially identical J-*E* behavior was observed for the anodic photocurrent of n-TiO_2/1.0 *M* NaOH in the presence of organic donors, such as saturated aqueous solutions of $CHCl_3$.

Combining the data of Figures 3a and 4 allowed determination of the flux that would flow through the TiO_2 sample under photocatalytic conditions. The electron transfer rate for the n-TiO_2/1.0 *M* NaOH-0.26 *mM* O_2(aq) interface only matched the hole transfer rate for the n-TiO_2/1.0 *M* NaOH(aq) or n-TiO_2/1.0 *M* NaOH(aq)-$CHCl_3$(sat'd) interfaces at a flux that was far smaller than the electron-hole pair generation rate (Figure 5). For comparison to TiO_2 photocatalysts, the electron-hole pair generation rates used in these experiments were comparable to those expected for TiO_2 particles with radii, r_{TiO_2}, = 30 nm-100 nm, under 1 Sun illumination conditions.[12] For example, assuming negligible recombination, electron-hole pair generation would yield a current density of

2.1 μA cm^{-2} over the surface of a 30 nm radius TiO_2 particle.[12] Our experiments indicate that this flux could not be sustained at steady-state through an unbiased TiO_2 crystal that must reduce 0.26 *mM* O_2(aq) and oxidize H_2O and/or the organic donor (Figure 5). Thus, the actual current density through the TiO_2 will be less than the electron-hole pair generation current density, and substantial recombination will occur in the semiconductor.

pH Dependence of the Flux-Matching Conditions for n-TiO_2/H_2O Interfaces

The potential of the n-TiO_2 conduction band edge (E_{cb}) shifts ≈-59 mV/pH unit in aqueous solutions due to a protonation-deprotonation equilibrium on the TiO_2 surface.[9,39] The anodic J-*E* curves for n-TiO_2/H_2O contacts should therefore onset at more negative potentials as the pH is raised, because the onset of photocurrent at n-type semiconductors is a strong function of the position of the conduction band edge. A negative potential shift in the anodic J-*E* behavior would improve the flux-matching condition, provided that $U_n(E)$ did not also exhibit a corresponding pH dependence.

Two factors need to be considered, however, in predicting the pH dependence of $U_n(E)$. At 300 K, a -59 mV conduction band edge shift will lead to a ten-fold reduction in n_s at a given potential vs. a reference electrode. The resulting reduction in cathodic current density (eq 5) would lead to an exact compensation of the shift in anodic J-*E* properties as the pH is changed, so no change in the net flux at $E = E_{op}$ should be observed. However, if the rate-determining step in O_2 reduction were the formation of free O_2^-(aq) with no proton transfer (i.e., $E^{o'}(O_2/O_2^-)$ is independent of pH), as postulated previously,[12] then changes in κ_n (and therefore in k_{sc}) would be expected due to the pH dependence of $\Delta G^{o'} = E_{cb}-E^{o'}(O_2/O_2^-)$. This additional dependence of k_{sc} on pH should

result in a change in $U_n(E_{op})$ as the pH is varied. To investigate this possibility, flux-matching experiments were performed for n-TiO_2 electrodes as a function of pH.

As displayed in Figure 6, the photooxidation J-E data for n-TiO_2 in contact with aqueous, N_2-purged solutions shifted by ≈ -60 mV/pH unit. As the pH was varied, the dioxygen reduction J-E data for n-TiO_2 electrodes also shifted ≈ -60 mV/pH unit (Figure 6). The lack of any additional pH dependence in the J-E data, above that expected from the TiO_2 band edge shift, indicated that k_{sc}, and thus κ_n, was not a strong function of pH for $7 \leq pH \leq 14$. Thus, although E_{op} was a function of pH, increasing the pH from 7 to 14 did not yield significant improvements in the net interfacial flux at $E = E_{op}$.

Improvement of the n-TiO_2/H_2O Flux-Matching Condition Through the Use of Alternate Donors and Acceptors

Although variations in pH were not successful in changing the flux-matching conditions, the kinetic model depicted in Figure 1 implies that it should be possible to improve the quantum yield of photocatalysis if either U_n or U_p could be increased. It was thus useful to determine whether increases in U_n or U_p could be achieved readily for TiO_2/H_2O interfaces. To address this point, a series of experiments was performed in which alternate electron acceptors and donors were added to aqueous solutions in contact with rutile n-TiO_2 electrodes.

Figure 7 compares the cathodic J-E data for n-TiO_2/1.0 M NaOH(aq) contacts in the presence of 0.10 M $K_3Fe(CN)_6$ (N_2-purged) to those in the presence of 0.26 mM O_2(aq). At a given potential, substitution of 0.10 M $K_3Fe(CN)_6$(aq) produced a significant increase in $U_n(E)$ relative to that observed in 1.0 M NaOH-0.26 mM O_2(aq). This increase in $U_n(E)$ is consistent with eq 5, because $[A]_s$ is larger in 0.10 M $K_3Fe(CN)_6$(aq) than in 0.26 mM O_2(aq). The rate constant, k_{sc}, might also have increased

when the electron acceptor was changed from O_2 to $Fe(CN)_6^{3-}$. Comparing the flux-matching condition for the cases of O_2 and $K_3Fe(CN)_6$ as electron acceptors implies that a higher steady-state current density would flow through the TiO_2 sample if 0.10 *M* $Fe(CN)_6^{3-}$(aq) were the electron acceptor than if 0.26 *mM* O_2 were the electron acceptor (Figure 7). In fact, the cathodic current density in the presence of 0.10 *M* $K_3Fe(CN)_6$ was so large that $U_n(E_{op}) = U_p(E_{op}) \approx \Gamma_o$ under illumination (Figure 7). Thus, electron-hole pair generation would be predicted to be the rate-limiting step in a photocatalytic system operated under these conditions.

The use of alternate electron donors, however, did not alter the photooxidation curves observed at TiO_2/1.0 *M* NaOH(aq) contacts. Figure 8 displays the J-*E* curves under illumination in 1.0 *M* NaOH and after addition of $CHCl_3$ or 0.10 *M* $K_4Fe(CN)_6$(aq). For a constant electron-hole generation rate (*i.e.*, $q\Gamma_o \approx 8$ $\mu A\text{-}cm^{-2}$), the potential for the onset of photocurrent was the same in all three solutions. Thus, no change in E_{op} would occur through the use of these additional electron donor species. This result is readily explained given the strong oxidizing power of holes in the valence band[9,39-41] and the high concentration of water at the surface of the electrode (> 55 *M*) compared to the concentration of alternate donor ($\leq$ 0.1 *M*).

Evaluation of the Flux-Matching Condition for Platinized TiO_2 Surfaces

Another approach to improving the flux-matching condition would be to catalyze the H_2O oxidation process and/or the O_2(aq) reduction process at TiO_2 surfaces. It has been suggested that deposition of islands of Pt, Pd or other noble metals on TiO_2 should catalyze O_2 reduction and should improve the rate of photocatalytic degradation of organic molecules. [12] Prior work at TiO_2 single-crystal electrodes has investigated the changes in $U_n(E)$ for O_2 reduction after platinization,[18,34,37] but has not thoroughly

investigated the effects of platinization on the photooxidation portion of the TiO_2/NaOH(aq) J-*E* data. Furthermore, experimental results with Pt- or Pd-loaded TiO_2 particles have been varied, with some authors reporting increased rates of photodegradation[13,34,42] and others reporting decreases in catalytic activity.[43] Because the oxidation and reduction reactions occur simultaneously at the surface of particles, it is difficult to determine experimentally whether the noble metal deposits are predominantly catalyzing the reduction of O_2, the photooxidation of organic molecules, or are reducing the inherent rate of electron/hole pair recombination at the TiO_2 surface. These effects can be distinguished at TiO_2 electrodes in a three electrode configuration, as described below.[15,18,34,37]

Figures 9 and 10 show the J-*E* data (in the dark) observed for n-TiO_2/1.0 *M* NaOH(aq)-0.26 *mM* O_2(aq) contacts before (*cf.* Figure 9(b), 10(b)) and after (*cf.* Figure 9(d), 10(d)) deposition of Pt onto the surface of the TiO_2. Two different thicknesses of Pt were deposited, one approximately 6 Å thick and one approximately 70 Å thick, as determined by XPS measurements. As depicted in Figures 9 and 10, platinization led to an increase in U_n at a given electrode potential. As expected, the electrode with the larger Pt coverage exhibited the larger cathodic current density. For the electrode with 70 Å thick coating of Pt, the cathodic current density at a given potential vs. SCE was nearly as large as that measured for unplatinized n-TiO_2/H_2O-0.10 *M* $K_3Fe(CN)_6$ interfaces (*cf.* Figures 7 and 10).

Figures 9 and 10 also compare the J-*E* behavior of TiO_2 electrodes in contact with N_2(g)-purged 1.0 *M* NaOH(aq) solutions before (*cf.* Figure 9a, 10a) and after (*cf.* Figure 9c, 10c) platinization. These data indicate that the Pt overlayer also increased the current density for H_2O reduction. For the thin Pt overlayer, addition of O_2(g) produced a measurable increase in $U_n(E)$ relative to that in N_2(g) purged solution. However, for the thick Pt overlayer, $U_n(E)$ in N_2(g)-purged solutions was virtually the same as that

observed in air-saturated solutions, for -700 < E < -200 mV vs. SCE (Figure 10). Thus, for thick Pt deposits, the cathodic flux under 1 atm air likely consisted of a mixed reaction of O_2 and H_2O reduction, whereas O_2 reduction predominated when very thin Pt deposits were employed.

Both platinized TiO_2 specimens were tested for Schottky diode behavior by comparing their open circuit voltages in 0.0050 *M* $K_4Fe(CN)_6$-0.0050 *M* $K_3Fe(CN)_6$(aq) and 0.10 *M* $K_4Fe(CN)_6$-0.0050 *M* $K_3Fe(CN)_6$ or in 0.050 *M* $K_4Fe(CN)_6$-0.0025 *M* $K_3Fe(CN)_6$(aq) and 0.0050 *M* $K_4Fe(CN)_6$-0.0025 *M* $K_3Fe(CN)_6$ solutions in 1.0 *M* NaOH(aq) at the same light intensity. For a bare TiO_2 electrode and for the platinized electrode shown in Figure 9, the open circuit voltages were different by an amount equal to the difference in cell potentials of the two solutions. This is the behavior expected for a "hybrid" semiconductor/metal-liquid junction in which the semiconductor recombination properties are affected by the properties of the electrolyte solution.[44-46] However, for the platinized electrode in Figure 10, the open circuit voltages were the same in the two different electrolyte solutions. This indicated that the recombination in this device was insensitive to the constituents of the liquid phase, and was dominated by the semiconductor/metal contact.[44] Thus, the TiO_2 surfaces coated with ≈ 6 Å of Pt were useful for our kinetic studies, but electrodes with nominal coverages of 70 Å of Pt only provided information on the nature of the Schottky barrier between the TiO_2 and the Pt, as opposed to the desired information on k_{sc} for O_2 reduction at TiO_2 in the presence of catalytic amounts of Pt.

For the TiO_2 sample coated with 6 Å of Pt, the J-E curves under illumination (Figure 11) did not provide a direct measure of $U_p(E)$. Because the Pt overlayer catalyzed H_2O reduction as well as O_2 reduction, the interfacial fluxes for electrons and holes could not be determined independently under illumination. Thus, the J-E data under illumination represented a superposition of $qU_n(E)$ and $qU_p(E)$ at each potential. It

was nevertheless possible to calculate $qU_n(E_{op})$ from the J-E data. For the photooxidation curve shown in Figure 11(a), the potential at which $J_{tot} = 0$ (i.e., the open circuit potential, E_{oc}) corresponded experimentally to the potential at which the dark reduction current density equaled the limiting photogeneration current density. Because the photooxidation curve is the superposition of $qU_n(E)$ and $qU_p(E)$, the operating potential of the system under illumination can be predicted from the open circuit potential. Since $qU_n(E) = q\Gamma_o$ at this potential, electron-hole pair generation was the rate-limiting process for this system at $E = E_{op}$. Since $U_n(E)$ was greater for this surface under O_2(g) than under N_2(g), electron-hole pair generation must also be rate-limiting when O_2 is present.

Rotating Disk Voltammetric Measurements of O_2 Reduction at Rutile TiO_2 Crystals in 1.0 *M* KOH(aq)

As described in eqs 6-8, it is also possible to determine the rate constant for O_2 reduction under accumulation conditions in the semiconductor using a RDE.[17,18] At the rather large current densities that are present in accumulation, both kinetic polarization at the interface and mass transport polarization in the electrolyte can be important in limiting the interfacial flux. Rotating disk electrode experiments have been performed to assess this situation quantitatively.

Figure 12 displays the J-E behavior for TiO_2/1.0 *M* KOH(aq) contacts as a function of the electrode rotation rate, ω. For $E < \approx$-1000 mV vs. SCE, the observed current was a function of ω. Figure 13 shows the resulting Koutecky-Levich plots (J^{-1} vs. $\omega^{-1/2}$) for various electrode potentials.[30] Such plots yield the number of electrons transferred, n, from their slopes, and yield the heterogeneous charge transfer rate

constant, k_n', from their intercepts. Table I summarizes the values of n and k_n' obtained from such data.

Over the potential range of our measurements, n values ranged between 2 and 4. This is commonly observed for reduction of $O_2(g)$ at various electrodes, and results from the possibility of 1, 2, or 4-electron reduction processes to yield O_2^- (or HO_2), H_2O_2, or H_2O, respectively.[17,30,47] The heterogeneous rate constant k_n' was more significant for the kinetic measurements of interest in our work, and typically was in the range of 10^{-2}-10^{-3} cm s^{-1}. Because the RDE experiments were done at potentials in which the semiconductor was in accumulation, n_s, and therefore k_n', varied only weakly as a function of potential. Assuming that reduction of dioxygen can be described as a one-electron transfer reaction with the electrochemical step being the rate-limiting process, the use of eq 8 allows us to calculate a value of 10^{-7} for κ_n , using k_n' determined from the RDE experiments and taking $\nu_n = 10^{13}$ s^{-1} and $\beta = 10^8$ cm^{-1}. A value of $k_{sc} = 3 \times 10^{-23}$ cm^4 sec^{-1} is then obtained from eq 4 with $r_e = 10^{-7}$ cm and $\delta = 3 \times 10^{-8}$ cm. Similarly, using eq 7, with $n_s \approx 10^{20}$ cm^{-3} in accumulation yields $k_{sc} = 10^{-22}$ cm^4 sec^{-1}.

Discussion

Flux-Matching Behavior and "Rate Determining" Steps Under Photocatalytic Conditions

The flux-matching constraint, applied to the J-*E* data depicted in this work, indicates that significant recombination should be present at TiO_2/H_2O interfaces under photocatalytic conditions. In fact, the observations can be used to predict that, under a steady-state carrier generation flux of 1.3×10^{13} cm^{-2} s^{-1}, over 75% of the photogenerated charge carriers would recombine for the particular surfaces and reaction

pairs (reduction of 0.26 *mM* O_2 coupled with oxidation of H_2O or oxidation of $CHCl_3$(aq)) investigated (Figure 5). This is consistent with the experimental data on particulate TiO_2 systems, which display relatively low quantum yields for organic oxidation under analogous steady-state illumination conditions.[11,12] These flux-matching comparisons thus allow assessment of the rate-determining processes without any theoretical analysis of the charge transfer rate constants.

Because the three fundamental carrier decay pathways depicted in Figure 1 are all intimately related under conditions of significant recombination, no individual process, U_n, U_p, or U_{rec} can be stated to be "rate-determining." In terms of the J-*E* data, either a negative shift in the photoanodic J-*E* scan, or a positive shift in the cathodic J-*E* characteristic, would produce an increased quantum yield for the process (Figures 2c,d). A decrease in the inherent recombination rate of the TiO_2 would produce a negative shift in the photoanodic J-*E* data and would therefore also result in higher values of U_n and U_p at the flux-matching potential.

This conclusion is supported by the analytical expression for the quantum yield in terms of the reaction rates depicted in Figure 1. Expressions for n_s and p_s under steady-state conditions can be obtained by writing U_n as the product of the electron concentration at the surface of the TiO_2, n_s, and the rate constant for interfacial electron transfer, k_n; writing U_p as the hole concentration at the surface of the TiO_2, p_s, multiplied by the rate constant for interfacial hole transfer, k_p; and by writing U_{rec} as a bimolecular process with a rate constant k_{rec}. Thus, at steady-state,

$$\frac{dn}{dt} = 0 = \Gamma_o - k_n n_s - k_{rec} n_s p_s \qquad (9)$$

$$\frac{dp}{dt} = 0 = \Gamma_o - k_p p_s - k_{rec} n_s p_s \qquad (10)$$

and,

$$n_s = \frac{\Gamma_o}{k_n + p_s k_{rec}} \tag{11}$$

$$p_s = \frac{\Gamma_o}{k_p + n_s k_{rec}} \tag{12}$$

The steady-state quantum yield, Φ, is then readily calculated as:

$$\Phi = \frac{U_n}{\Gamma_o} = \frac{U_p}{\Gamma_o} = \frac{k_n k_p}{2\Gamma_o k_{rec}}\left[\sqrt{1 + \frac{4\Gamma_o k_{rec}}{k_n k_p}} - 1\right] \tag{13}$$

From eq 13 with $\Phi < 1.0$, no single rate constant, nor single rate process, can be arbitrarily stated to be "rate-determining" or "efficiency-limiting." When $4\Gamma_o k_{rec}/k_n k_p >> 1$ eq 13 simplifies to the following expression:

$$\Phi = \left(\frac{k_n k_p}{\Gamma_o k_{rec}}\right)^{1/2} \tag{14}$$

In this limit, increasing k_n or k_p, or decreasing k_{rec} or Γ_o, would all serve to increase Φ. This analytical solution is in accord with the qualitative conclusions discussed above regarding the J-*E* behavior, but is different than prior conclusions that have emphasized primarily the importance of electron transfer processes to O_2 as rate-determining in the photodegradation of organic molecules using TiO_2.[11-13] Interdependences of Φ on k_n, k_p, k_{rec}, and sometimes on Γ_o, are also generally obtained from other kinetic models of the photocatalytic processes at TiO_2.[48]

Methods for Improving the Quantum Yield Under Photocatalytic Conditions

The discussion and experimental data presented above suggest several strategies for improving photocatalytic toxic waste remediation. It is conceptually useful to distinguish between several approaches for accelerating the rate of photocatalysis: catalysis of electron transfer and catalysis of hole transfer. Each of these methods is analyzed briefly below in the context of our experimental results.

Catalysis of Electron Transfer Rates. One obvious strategy to increase the photocatalytic rate is to accelerate the electron transfer process. This is the approach suggested by Gerischer and Heller.[11,12] The pronounced increase in J upon addition of 0.10 *M* $K_3Fe(CN)_6$ to 1.0 *M* NaOH solutions (Figure 7) validates this strategy conceptually. In addition, an increase in the electron transfer flux was also observed as a result of electrodeposition of Pt onto the TiO_2 surface (Figures 9, 10).

The limit for improvement in electron transfer rates can be evaluated for the case of TiO_2 electrodes. In principle, catalysis of the electron transfer process can yield an increase in cathodic current density at an electrode until the rate is limited by the electron supply to the TiO_2/H_2O interface or by other mass-transport-limiting processes in the electrolytic cell. For a barrier height, E_{cb}-$E(O_2/H_2O)$ = 1.18 V, the charge-supply limited rate can be calculated from thermionic emission/diffusion theory to produce an exchange current density of 6 x 10^{-15} A cm^{-2}.[49] For a direct comparison to data obtained in this work, thermionic emission/diffusion theory predicts a cathodic current density of 300 A cm^{-2} at E = -0.875 V vs. SCE, which significantly exceeds the J measured experimentally for the TiO_2/NaOH-O_2(aq) system (*cf.* Figure 3a). Thus, catalysis of the electron transfer process is a promising approach for designing improved photocatalysts.

Catalysis of Hole Transfer Rates. It is also possible to enhance the net photocatalytic rate by acceleration of the hole transfer process. In this case, the J-E data

for TiO_2 photoanodes would be "shifted" negatively along the voltage axis. The flux-matching condition would then yield a higher charge carrier flux through the TiO_2 even if the electron transfer rate remained unchanged.

Like electron transfer, catalysis of hole transfer also has a finite limit for effecting improvements in the photocatalytic rate. For a semiconductor electrode, 0.2-0.3 V of built-in electric potential is generally required to effectively separate the photogenerated charges. [50] Since $E_{cb} \approx$ -1.066 V vs. SCE for TiO_2 at pH = 14.0, this implies that the electron-hole pair generation flux could, in principle, be collected effectively for $E_{TiO2} \approx$ -0.75 to -0.85 V vs. SCE. Thus, catalysis of the hole-transfer process might be sufficient to yield electron-hole pair generation as the rate-limiting step in certain systems. However, due to the fundamental limit on the anodic J-*E* shift, hole-transfer catalysis appears not to offer as large a potential for rate improvement as electron-transfer catalysis.

Comparison of Experimental Results to Theoretical Predictions

It is interesting to compare theory with experimental data for the reduction of O_2(g) at rutile TiO_2. It has been argued that when $U_n > \Gamma_o$ at potentials positive of the TiO_2 conduction band potential, the cathodic charge-transfer process will not be rate-limiting in photocatalysis, and Φ will approach 1.0.[11,12] Specifically, Gerischer and Heller assumed that if $n_s \leq 10^{17}$ cm^{-3} when $U_n(E) = \Gamma_o$, recombination would not be excessive and electron transfer to O_2 would not be rate-limiting in the photocatalytic process.[11,12] For our experiments, taking the conduction band potential, E_{cb}, as approximately equal to -1.066 V vs. SCE (i.e., approximately $E(H_2O/H_2)$ for 1 atm H_2 at pH = 14.0) implies that $n_s = 5.9 \times 10^{15}$ cm^{-3} at -0.875 V vs. SCE (i.e., where $U_n(E) = \Gamma_o = 2.1$ μA cm^{-2}).[51,52] Thus, Figure 5 indicates that the required constraint, $n_s \leq 10^{17}$ cm^{-3} when $U_n(E) = \Gamma_o$, was indeed satisfied for the n-TiO_2/H_2O junctions studied in this work.

Within the assumptions adopted by Gerischer and Heller, this would indicate that electron flow to the acceptor is adequate to support the photogenerated charge flux, and would produce $\Phi \approx 1.0$.

However, the flux-matching condition described herein imposes a more stringent requirement on $U_n(E)$. It is necessary not only that $U_n(E) = \Gamma_o$ when $E > E_{cb}$, but also that $U_p(E) = \Gamma_o$ where $U_n(E) = \Gamma_o$. Figure 5 clearly indicates that this more stringent constraint was not met under our conditions. As shown in this work, $U_p(E) << \Gamma_o$ even when $n_s < 10^{17}$ cm^{-3}, so recombination was significant under these conditions and $\Phi <<$ 1.0 at E_{op}.

It is also interesting to compare the experimental values of $U_n(E)$ to the theoretical predictions based on a one-electron, outer-sphere reduction step of O_2(aq) to O_2^-(aq).[11,12] We will first consider the situation at pH = 7, and will compare our experimentally observed current density at -0.470 ± .025 V vs. SCE (which is the potential at which $U_n(E) = \Gamma_o = 2.1$ μA cm^{-2} as calculated at 1 Sun for $r_{TiO_2} = 30$ nm[12]) to the current density expected at this potential according to the literature model.[11,12] Prior theoretical treatments have assumed that the reorganization energy for the one electron transfer from O_2 to O_2^- was 1.0 eV, that $E^{o'}(O_2/O_2^-)$ was -0.571 V vs. SCE, that the effective radius of the electron was 10^{-7} cm, and that the effective transfer distance was 3 x 10^{-8} cm.[11,12] Using these same quantities in eq 4 implies that $k_{sc} = 8.4 \times 10^{-21}$ cm^4-s^{-1} at pH = 7.0 for O_2 reduction at TiO_2. Taking the value of $[O_2(aq)] = 1.6 \times 10^{17}$ cm^{-3} (as measured experimentally in this work), along with the calculated value of $k_{sc} = 8.4 \times 10^{-21}$ cm^4 s^{-1} implies that a current density of 1.3×10^{-6} A cm^{-2} should be observed for $n_s = 5.9 \times 10^{15}$ cm^{-3} (E = -0.470V)(Eq 5). The observed value of J at pH = 7 and $n_s = 5.9 \times 10^{15}$ cm^{-3} was 2.1×10^{-6} A cm^{-2}, so theory and experiment for $U_n(E)$ are in reasonable agreement when measurements of $U_n(E)$ performed at pH = 7.0 are considered.

A discrepancy arises when the pH dependence expected theoretically for a rate-determining step involving a one-electron transfer to O_2 is considered in view of the lack of change in k_{sc} that was observed experimentally for $7 < pH \leq 14$ (Figure 6). The prior theoretical treatment predicts[11,12] a 300-fold increase in k_{sc} if the pH were to be increased from 7 to 14, but the experimental data obtained herein yielded almost identical values for k_{sc} (3×10^{-20} cm^4-s^{-1}) over this range of pH values. Thus, the theoretical estimate of $U_n(E)$ significantly overestimates the observed cathodic flux at pH = 14.0. In fact, the theoretical estimate of k_{sc} based on a one-electron transfer from O_2 to yield O_2^- would predict that for $q\Gamma_o = 2.1 \times 10^{-6}$ A cm^{-2}, $U_n(E) = q\Gamma_o$ at $n_s = 3 \times 10^{13}$ cm^{-3} instead of the experimentally observed value of $n_s = 5.9 \times 10^{15}$ cm^{-3}. This theoretically predicted current density implies that at E_{op} the electron-hole generation would be rate-limiting at pH = 14, and that recombination would be minimal. Such behavior was not observed experimentally, with $U_n(E) << q\Gamma_o$ at $E = E_{op}$ (Figure 5). Thus, a simple outer sphere one-electron reduction of O_2(aq) to O_2^-(aq) cannot satisfactorily describe the cathodic reduction of O_2(aq) at rutile TiO_2 crystals, and further theoretical development is warranted to more fully describe this process.

The RDE experiments depicted in Figures 12 and 13 at pH = 14 yield estimated values of k_{sc} and $U_n(E)$ that are in reasonable agreement with the observed J-E data. Using the value of $k_{sc} = 3 \times 10^{-23}$ cm^4-s^{-1}, calculated from eqs 4 and 8, yields $J \approx 5 \times 10^{-9}$ A cm^{-2} at $n_s = 5.9 \times 10^{15}$ cm^{-3} (eq 5). These values for k_{sc} and J are thus somewhat smaller than, but in qualitative agreement with, the values determined from the observed J-E data between pH 14 and 7.

Given the semi-quantitative agreement between theory and experiment for O_2 reduction at TiO_2 at near-neutral pH, it is interesting to reevaluate the predictions of the Gerischer/Heller model for rate-limitations in photocatalysis.[11,12] Although the rate of electron transfer to O_2 was estimated to be sufficiently rapid to remove photogenerated

electrons from TiO_2 particles under 1 Sun illumination (for $n_s \leq 10^{17}$ cm^{-3} and assuming rapid hole transfer), Gerischer and Heller proposed that electron transfer to O_2(aq) would most likely occur through surface traps that covered only a fraction of the TiO_2 surface. In this approach, the total surface trap density was assumed to be only 1% of the TiO_2 atom surface density.[11,12] A reduced driving force for electron transfer from trap levels, combined with the relatively low trap density, then led to an alternative estimate of the electron transfer rate. This revised, smaller rate of interfacial electron transfer led to the prediction that electron transfer would be rate-limiting for the largest TiO_2 particles at pH 8.2 (the pH of their calculations).[11,12] However, when two parallel pathways for electron transfer are available, the overall rate of electron scavenging by O_2 is given by the sum of the rates for the two parallel paths. In most scenarios, addition of a pathway involving surface traps will only increase the predicted steady state flux above the value estimated for the direct electron transfer pathway alone. While our data do not distinguish between the two pathways for O_2 reduction at rutile TiO_2, our data do show that $U_n(E) = \Gamma_o$ for $n_s \approx 10^{15}$ cm^{-3}. Although this would seem to imply that recombination would be negligible according to prior theoretical treatments, the key constraint, emphasized above, is whether $U_n(E) = U_p(E) = \Gamma_o$ at $E = E_{op}$. As described above, this more restrictive constraint was not met for any of the systems investigated to date.

Extension of J-*E* Data on TiO_2 Single Crystals to Particulate TiO_2 Photocatalysts

It is important to emphasize that all of the data and conclusions described above only apply rigorously to the behavior of rutile TiO_2 single crystals. The data are extremely useful in evaluating the theoretical treatments of charge transfer processes at TiO_2 surfaces and also serve as a guide to obtaining improved photocatalysis in slurry reactors using particulate TiO_2. However, the electrochemical conditions employed in this study certainly do not correspond exactly to the photocatalytic situation obtained

using TiO_2 slurries. Any extension of our data to particulate systems explicitly assumes that the behavior of single-crystal rutile TiO_2 electrodes will be similar to that of TiO_2 particles, which have a variety of exposed surfaces and are typically composed of ≈75% anatase.[53] However, the J-*E* data allow several predictions regarding the photocatalytic behavior of particulate systems to be made. When recombination is significant, increases in either the electron or hole transfer rate constants should increase the overall oxidation rate of the organic donor. This prediction is difficult to test experimentally because many variables are generally changed at once, and it is difficult to show that only one rate has been changed when the experimental conditions are varied. For instance, if the species obtained from the reduction of $O_2(g)$ is also involved as an intermediate in the oxidation of the organic donor, then replacement of $O_2(g)$ with another acceptor will not provide a suitable test of this prediction. In addition, added redox reagents can act as recombination sites, so the overall photocatalytic rate could increase, decrease, or remain unchanged in the presence of such reagents. Clearly, caution must be taken in designing an experiment to test the predictions described above on an actual photocatalytic process. However, our experiments on single crystals of TiO_2 can serve as a useful guide to the behavior of particulate photocatalytic systems, if such experiments can be performed under suitably well-defined and controlled conditions.

Conclusions

For TiO_2 electrodes at pH = 7, the cathodic electron flux equaled the photogenerated carrier flux at 1 Sun for surface electron concentrations less than 10^{16} cm^{-3}. Within a prior model for photocatalysis, this would imply that electron-hole recombination should be minimal under photocatalytic conditions. However, the key constraint identified herein, and evaluated experimentally, is whether the cathodic and anodic fluxes sustained at the operating potential of the system each equal the flux of

photogenerated carriers to the TiO_2 surface. This constraint was not met for rutile TiO_2 electrodes at $7 \leq pH \leq 14$, so recombination was significant under our model photocatalytic conditions. We have also demonstrated the importance of explicitly including rates for electron transfer, hole transfer, electron/hole pair generation, and recombination in a kinetic model for TiO_2-based photocatalysis. Our experimental measurements of O_2 reduction at rutile TiO_2 were in reasonable agreement with prior estimates for the rate of electron transfer from the TiO_2 conduction band at pH 7, but did not yield the expected pH dependence of this rate constant. Improved flux-matching conditions were thus not observed as the pH was varied with O_2 as the electron acceptor. At a fixed pH, improvements in the flux matching condition were observed upon addition of alternate electron acceptors to the electrolyte. Platinization of the TiO_2 also yielded an improved flux-matching condition in the presence of O_2. These data and theoretical analysis should therefore provide a useful framework to evaluate the behavior of systems using TiO_2 for photocatalytic degradation of organic donors.

Acknowledgments

We gratefully acknowledge ARPA (NAV 5 HFMN N0001 1492J1901) for support of this work, and JMK acknowledges the National Science Foundation for a pre-doctoral fellowship. We thank Dr. Corn for a preprint of ref. 52.

References

(1) Mao, Y.; Schöneich, C.; Asmus, K.-D. *J. Phys. Chem.* **1991**, *95*, 10080.

(2) Kormann, C.; Bahnemann, D. W.; Hoffmann, M. R. *Environ. Sci. Technol.* **1991**, *25*, 494.

(3) Minero, C.; Aliberti, C.; Pelizzetti, E.; Terzian, R.; Serpone, N. *Langmuir* **1991**, *7*, 928.

(4) Pruden, A. L.; Ollis, D. F. *Environ. Sci. Technol.* **1983**, *17*, 628.

(5) Pelizzetti, E.; Minero, C.; Carlin, V.; Vincenti, M.; Pramauro, E. *Chemosphere* **1992**, *24*, 891.

(6) Hidaka, H.; Nohara, K.; Zhao, J.; Serpone, N.; Pelizzetti, E. *J. Photochem. Photobiol. A: Chem.* **1992**, *64*, 247.

(7) Hidaka, H.; Zhao, J.; Kitamura, K.; Nohara, K.; Serpone, N.; Pelizzetti, E. *J. Photochem. Photobiol. A: Chem.* **1992**, *64*, 103.

(8) Hidaka, H.; Kubota, H.; Grätzel, M.; Serpone, N.; Pelizzetti, E. *Nouv. J. de Chimie* **1985**, *9*, 67.

(9) Finklea, H. O. In *Semiconductor Electrodes*; Finklea, H. O., Ed.; Elsevier: New York, 1988; Vol. 55.

(10) Fenton, H. J. H., M.A. *J. Chem. Soc. Trans.* **1894**, *65*, 899.

(11) Gerischer, H.; Heller, A. *J. Phys. Chem.* **1991**, *95*, 5261.

(12) Gerischer, H.; Heller, A. *J. Electrochem. Soc.* **1992**, *139*, 113.

(13) Wang, C.-M.; Heller, A.; Gerischer, H. *J. Am. Chem. Soc.* **1992**, *114*, 5230.

(14) Bideau, M.; Claudel, B.; Faure, L.; Kazouan, H. *J. Photochem. Photobiol. A.: Chem* **1991**, *61*, 269.

(15) Izumi, I.; Fan, F.-R. F.; Bard, A. J. *J. Phys. Chem.* **1981**, *85*, 218.

(16) Kraeutler, B.; Bard, A. J. *J. Am. Chem. Soc.* **1978**, *100*, 2239.

(17) Parkinson, B.; Decker, F.; Juliao, J. F.; Abramovich, M.; Chagas, H. C. *Electochimica Acta.* **1980**, *25*, 521.

(18) Tafalla, D.; Salvador, P. *Ber. Bunsenges. Phys. Chem.* **1987**, *91*, 475.

(19) Marcus, R. A.; Sutin, N. *Biochimica et Biophysica Acta.* **1985**, *811*, 265.

(20) Marcus, R. A. *J. Phys. Chem.* **1990**, *94*, 1050.

(21) Marcus, R. A. *J. Phys. Chem.* **1991**, *95*, 2010.

(22) Lewis, N. S. *Annu. Rev. Phys. Chem.* **1991**, *42*, 543.

(23) The reorganization energy for the electron in the solid is assumed to be neglibible relative to that for the acceptor ion in the electrolyte, yielding $\lambda \approx \lambda_{A/A^-}$.

(24) Morrison, S. R. *Electrochemistry at Semiconductor and Oxidized Metal Electrodes*; Plenum: New York, 1980.

(25) Memming, R. In *Electroanalytical Chemistry*; Bard, A. J., Ed.; Marcel Dekker, Inc.: New York, 1979; Vol. 11; pp 1.

(26) Koval, C. A.; Howard, J. N. *Chem. Rev.* **1992**, *92*, 411.

(27) Gerischer, H. *Adv. Electrochem. Electrochem. Engr.* **1961**, *1*, 139.

(28) Gerischer, H. In *Physical Chemistry: An advanced Treatise*; Eyring, H., Henderson, D., Yost, W., Eds.; Academic: New York, 1970; Vol. 9A; pp 463.

(29) Gerischer, H. *J. Phys. Chem.* **1991**, *95*, 1356-1359.

(30) Bard, A. J.; Faulkner, L. R. *Electrochemical Methods: Fundamentals and Appplications*; John Wiley & Sons: New York, 1980.

(31) Marcus, R. A. *J. Chem. Phys.* **1965**, *43*, 679.

(32) Marcus, R. A. *Electrochimica Acta.* **1968**, *13*, 995.

(33) Finklea, H. O. *J. Electrochem. Soc.* **1982**, *129*, 2003.

(34) Kogo, K.; Yoneyama, H.; Tamura, H. *J. Phys. Chem.* **1980**, *84*, 1705.

(35) Gronet, C. M.; Lewis, N. S. *J. Phys. Chem.* **1984**, *88*, 1310.

(36) Seaman, C. H.; Anspaugh, B. E.; Downing, R. G.; Estey, R. S. In *Proceedings of the Photovoltaic Specialists Conference*; 14th IEEE: San Diego, 1980; p 494.

(37) Kobayashi, T.; Yoneyama, H.; Tamura, H. *J. Electrochem. Soc.* **1983**, *130*, 1706.

(38) Clechet, P.; Martelet, C.; Martin, J. R.; Olier, R. *Electrochimica Acta* **1979**, *24*, 457.

(39) Nozik, A. J. *Ann. Rev. Phys. Chem.* **1978**, *29*, 189.

(40) *Photoinduced Electron Transfer*; Fox, M. A.; Chanon, M., Ed.; Elsevier: Amsterdam, 1988; Part D.

(41) Rajeshwar, K.; Singh, P.; DuBow, J. *Electrochimica Acta.* **1978**, *23*, 1117.

(42) Izumi, I.; Dunn, W. W.; Wilbourn, K. O.; Fan, F.-R. F.; Bard, A. J. *J. Phys. Chem.* **1980**, *84*, 3207.

(43) Al-Sayyed, G.; D'Oliveira, J.-C.; Pichat, P. *J. Photochem. Photobiol. A: Chem.* **1991**, *58*, 99.

(44) Bansal, A.; Tan, M. X.; Tufts, B. J.; Lewis, N. S. *J. Phys. Chem.* **1993**, *97*, 7309.

(45) Meier, A.; Uhlendorf, I.; Meissner, D. *Conf. Proceed., Electrochemical Soc.:* Honolulu, 1993; p 909.

(46) Nakato, Y.; Ueda, K.; Yano, H.; Tsubomura, H. *J. Phys. Chem.* **1988**, *92*, 2316.

(47) Yeager, E.; Scherson, D.; Simic-Glavaski, B. *Proceedings of the Symposium on The Chemistry and Physics of Electrocatalysis*, The Electrochemical Society: San Fransisco, 1983; p 247.

(48) A similar treatment was independently developed by Gerischer, who reached similar conclusions regarding "rate-determining" steps in photocatalysis: Gerischer, H. In *Photocatalytic Purification of Water and Air*; Ollis, D. F., Al-Ekabi, H., Eds.; Elsevier: Amsterdam, 1993; p 1.

(49) Sze, S. M. *The Physics of Semiconductor Devices*, 2nd ed.; Wiley: New York, 1981.

(50) Fonash, S. J. *Solar Cell Device Physics*; Academic: New York, 1981.

(51) Fox, M. A. In *Photocatalysis: Fundamentals and Applications*; Serpone, N., Pelizzetti, E., Eds.; John Wiley & Sons: New York, 1989.

(52) Lantz, J. M.; Baba, R.; Corn, R. M. *J. Phys. Chem.* **1994**, 98, 4899.

(53) Warman, J. M.; de Haas, M. P.; Pichat, P.; Serpone, N. *J. Phys. Chem.* **1991**, *95*, 8858.

Tables

Table I. Summary of RDE Data.

Potential (mV vs. SCE)	n_e	k_n' (cm s^{-1})
-1000	1.8 ± 0.5	0.003 ± 0.001
-1100	3.0 ± 0.9	0.009 ± 0.003
-1200	3.0 ± 0.9	0.010 ± 0.003
-1300	3.4 ± 0.7	0.009 ± 0.003

Figures

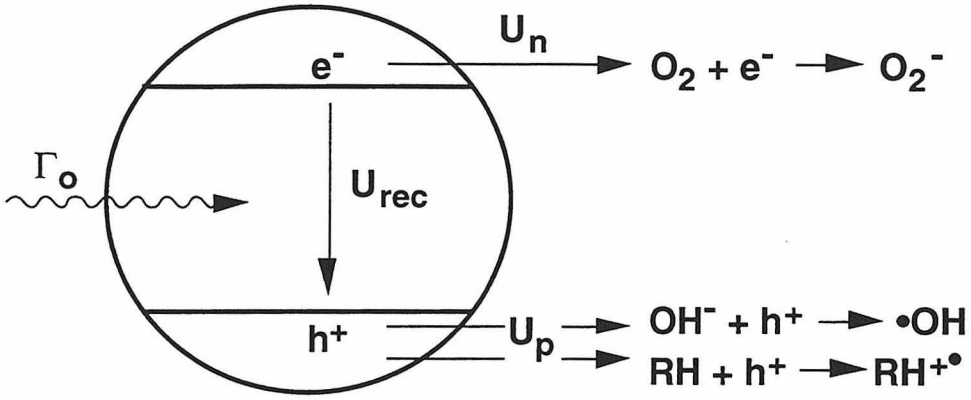

Figure 1. Schematic representation of the charge carrier fluxes in a TiO_2 particle operating as a photocatalyst. Γ_o is the flux of electrons and holes created by the light absorbed by the particle; U_{rec} is the flux of electrons and holes that recombine in the particle; U_n is the flux of electrons transferred to O_2 or other electron acceptor species; and U_p is the flux of holes being transferred to the organic, water, or other hole acceptor species in the solution.

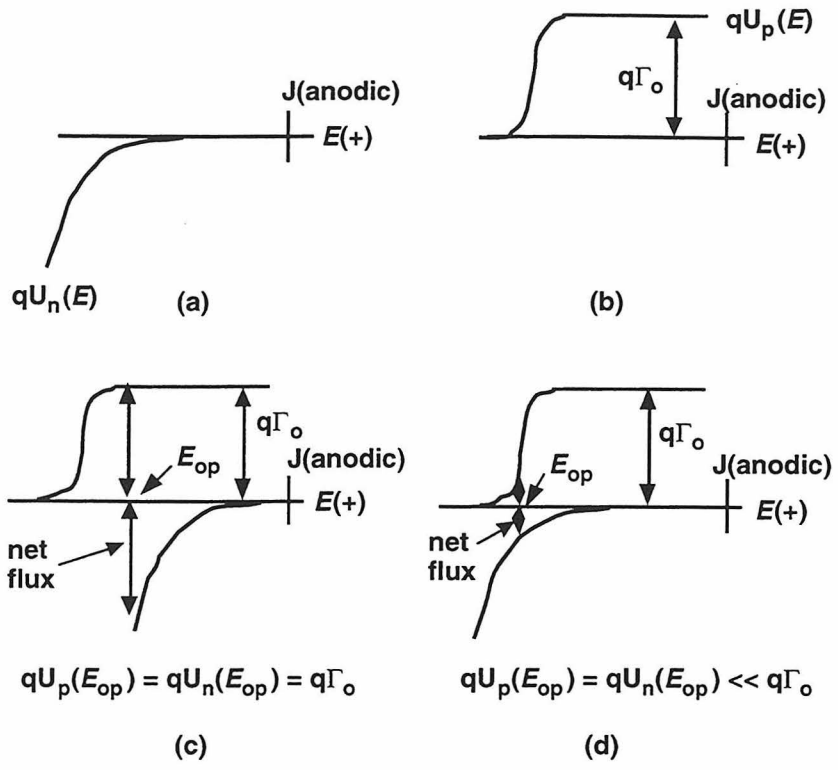

Figure 2. Schematic diagram of the photoelectrochemical behavior of TiO_2 in aqueous solutions. Flux-matching conditions for two possible cases are shown. (a) Dark oxygen reduction current density in an air-saturated solution as a function of potential, $qU_n(E)$. (b) Oxidation of H_2O/organic under solar illumination, $qU_p(E)$. The quantity $q\Gamma_o$ is the limiting photogenerated minority carrier current density, which equals the electron-hole pair generation flux multiplied by the charge on an electron, at the voltage indicated. (c) Flux-matching condition when the net flux of electrons *and* holes out of the particle equals the generation flux, and the photocatalytic process is predicted to be light limited. (d) Flux-matching condition when the net flux is less than the limiting generation flux. In this situation, photocatalytic reactions at TiO_2 are limited by the rate of charge transfer across the semiconductor/liquid interface. The behavior demonstrated in (d) would predict low efficiencies for photodegradation reactions due to recombination losses in the TiO_2.

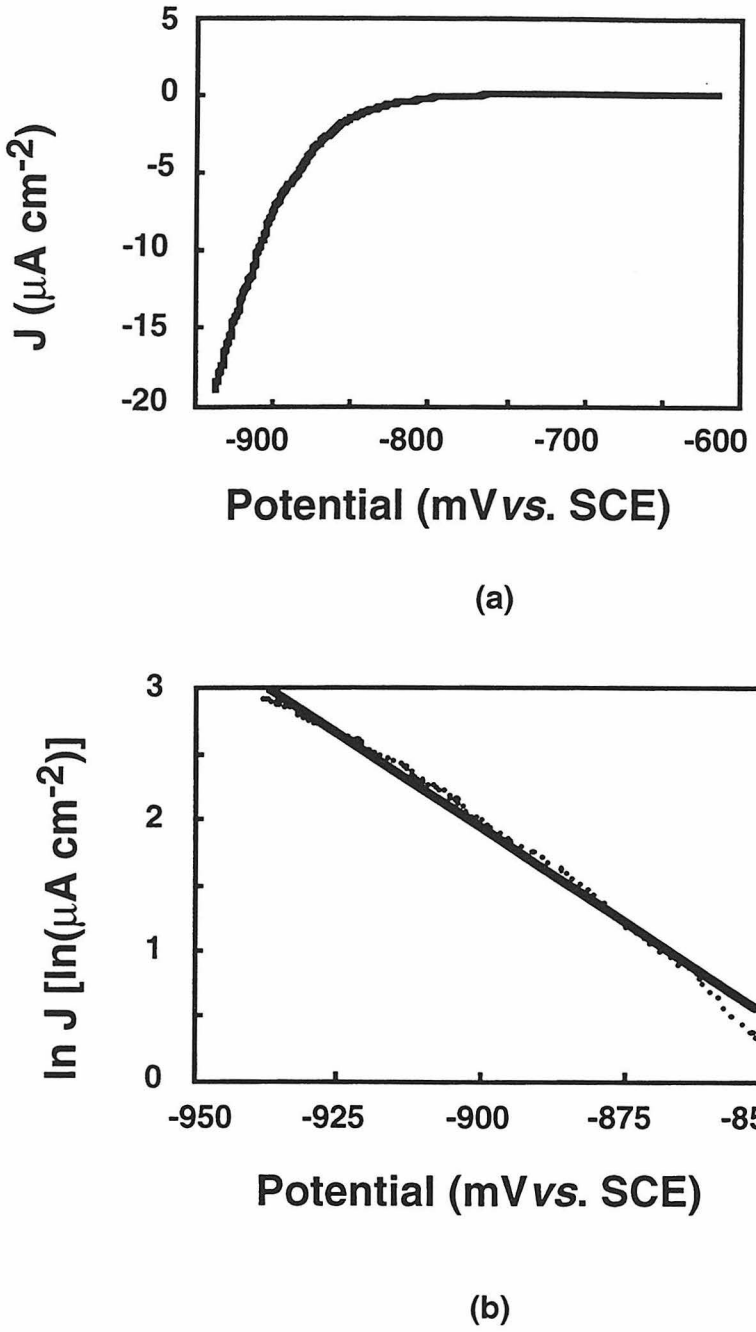

Figure 3. (a) Current density vs. voltage observed for the reduction of O_2 in the dark at TiO_2 in an air-saturated 1.0 *M* NaOH (aq) solution. (b) Plot of ln J vs. *E* for the data of (a). The diode quality factor determined from this plot was 1.4 and the exchange current density was 2×10^{-18} A cm^{-2}.

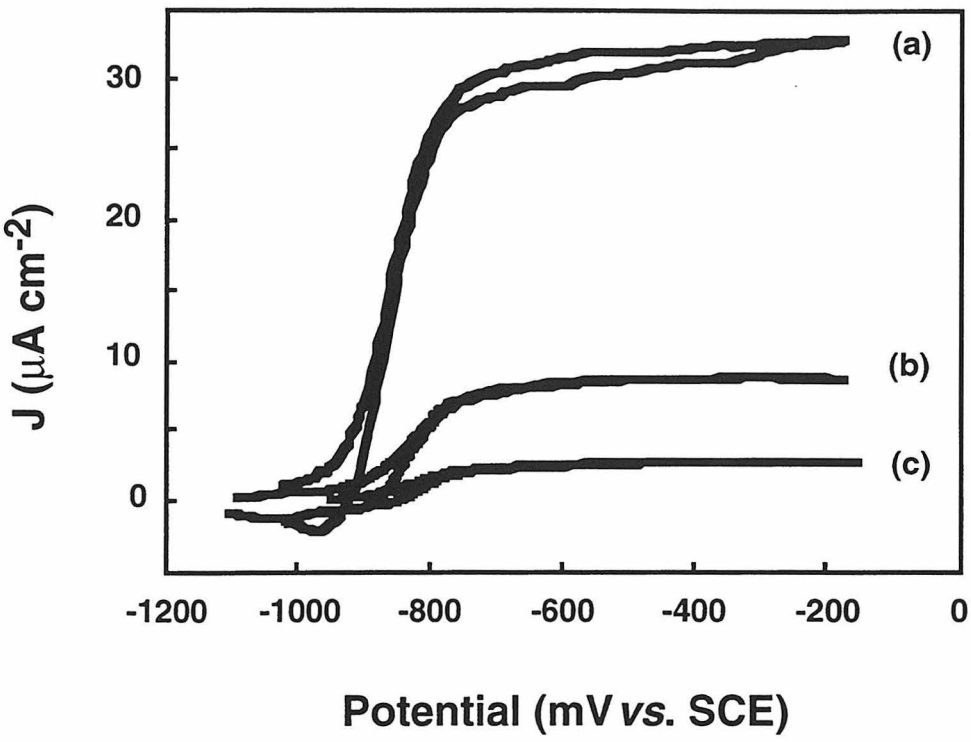

Figure 4. Photooxidation of water at TiO_2 under various light intensities. The solution was N_2-purged 1.0 *M* NaOH (aq). (a) Γ_o = 2.0 x 10^{14} electrons cm^{-2} s^{-1} (b) Γ_o = 5.2 x 10^{13} electrons cm^{-2} s^{-1} (c) Γ_o = 1.4 x 10^{13} electrons cm^{-2} s^{-1}.

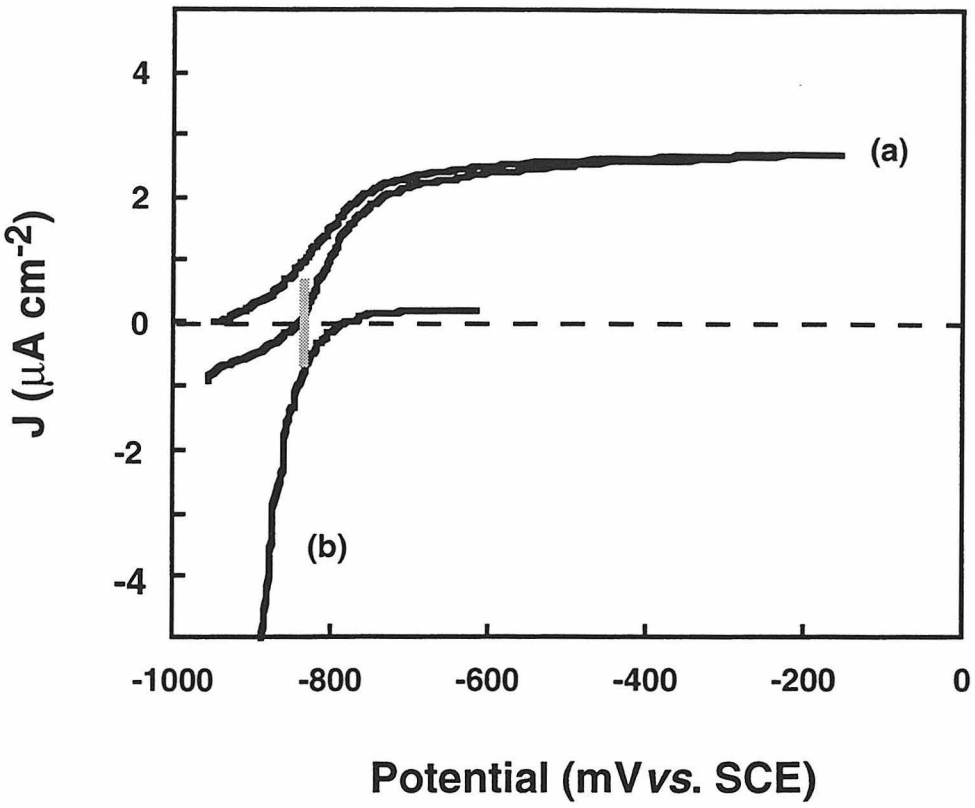

Figure 5. Flux-matching condition for single crystal rutile TiO_2 in 1.0 *M* NaOH(aq). (a) Photooxidation of H_2O; $\Gamma_o = 1.7 \times 10^{13}$ electrons $cm^{-2}s^{-1}$. (b) Dark reduction of O_2 in air-saturated solution. The bar indicates the potential at which the oxidative and reductive current densities were equal, and also indicates the magnitude of the electron and hole fluxes that would flow through a TiO_2 sample under photocatalytic conditions. Note that the net flux of both electrons and holes when $U_n(E) = U_p(E)$ was much less than the electron-hole pair generation flux.

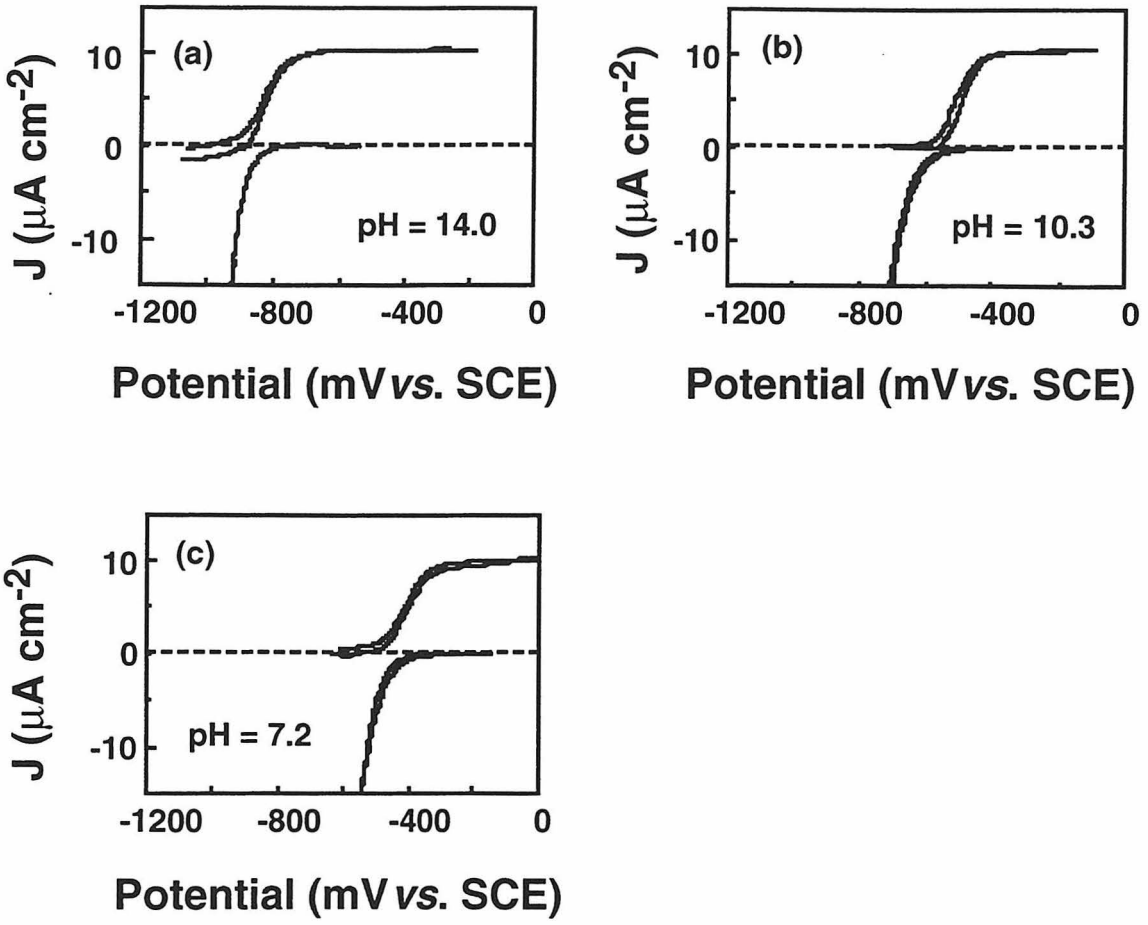

Figure 6. pH dependence of the flux-matching behavior of TiO_2. Each graph shows the dark reduction of O_2 in an air-saturated solution, and the photooxidation of water in a N_2 purged solution. The limiting photocurrent in each case corresponds to 6.2 x 10^{13} electrons cm^{-2} s^{-1}. (a) 1.0 *M* NaOH (aq), pH = 14.0 (b) 0.50 *M* $Na_2CO_3/NaHCO_3$ (aq), pH = 10.3 (c) 0.25 *M* TRIZMA HCl/TRIZMA Base, pH = 7.2. The potential at which the dark reduction current density equaled the photooxidation current density shifted negative by approximately 60 mV per pH unit. However, the magnitude of the predicted net flux was similar for all three cases and was much less than the photogeneration rate.

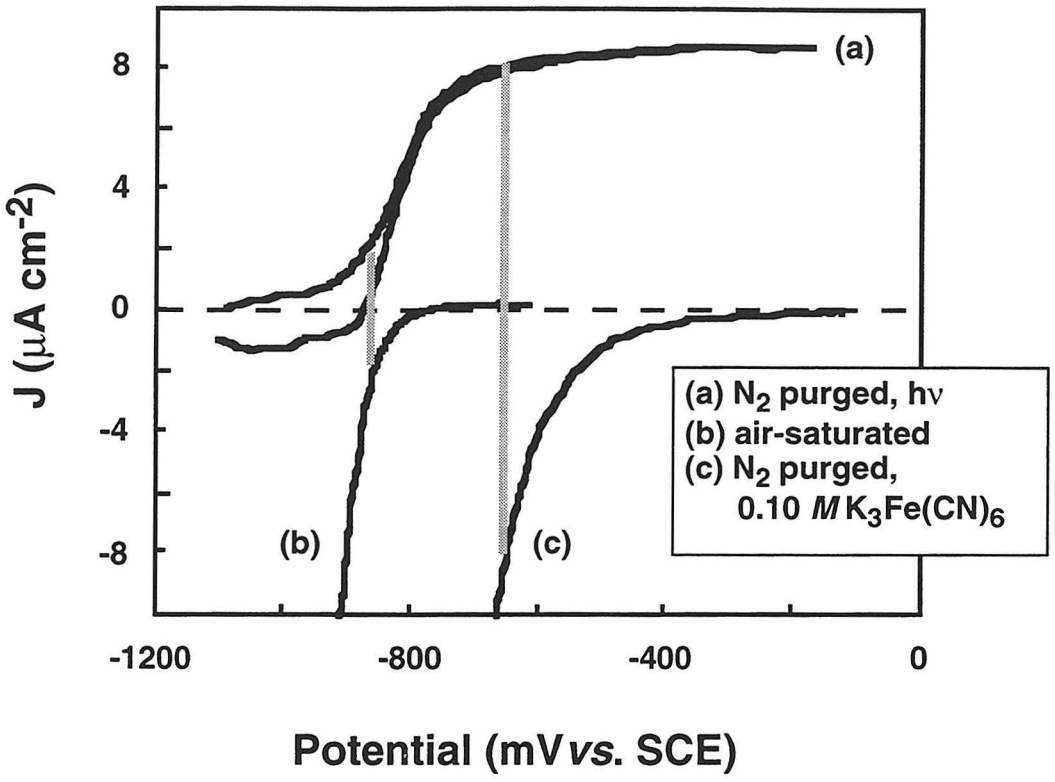

Figure 7. Effect of using an alternate electron acceptor on the flux-matching behavior at TiO_2 in 1.0 *M* NaOH (aq) in a N_2-purged solution. (a) Photooxidation of water (no added acceptor) (b) Dark reduction of dioxygen in an air-saturated solution (no added acceptor) (c) Dark reduction of 0.10 *M* $K_3Fe(CN)_6$ in a N_2-purged solution. The bars indicate the positions and magnitudes of the flux-matching conditions for the case when dioxygen was the electron acceptor and for the case when $K_3Fe(CN)_6$ was the electron acceptor.

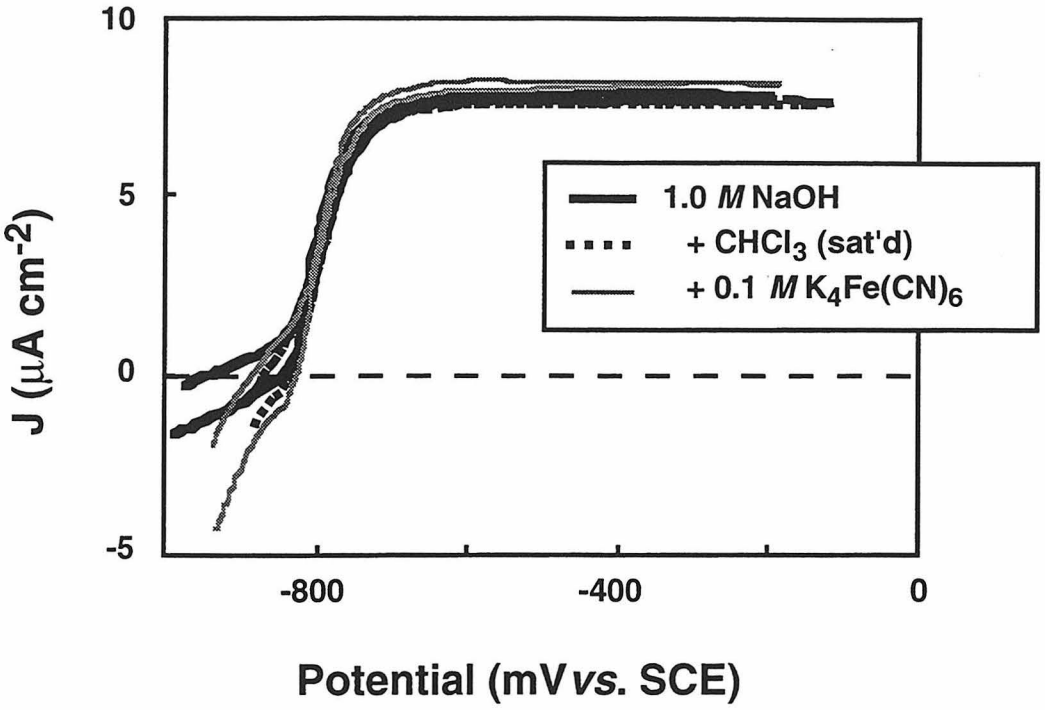

Figure 8. Effect of added donor on the photooxidation curves of TiO_2 in N_2-purged 1.0 *M* NaOH (aq) solution. The data shown are from experiments in electrolyte alone, electrolyte + $CHCl_3$ (saturated), and electrolyte + 0.10*M* $K_4Fe(CN)_6$.

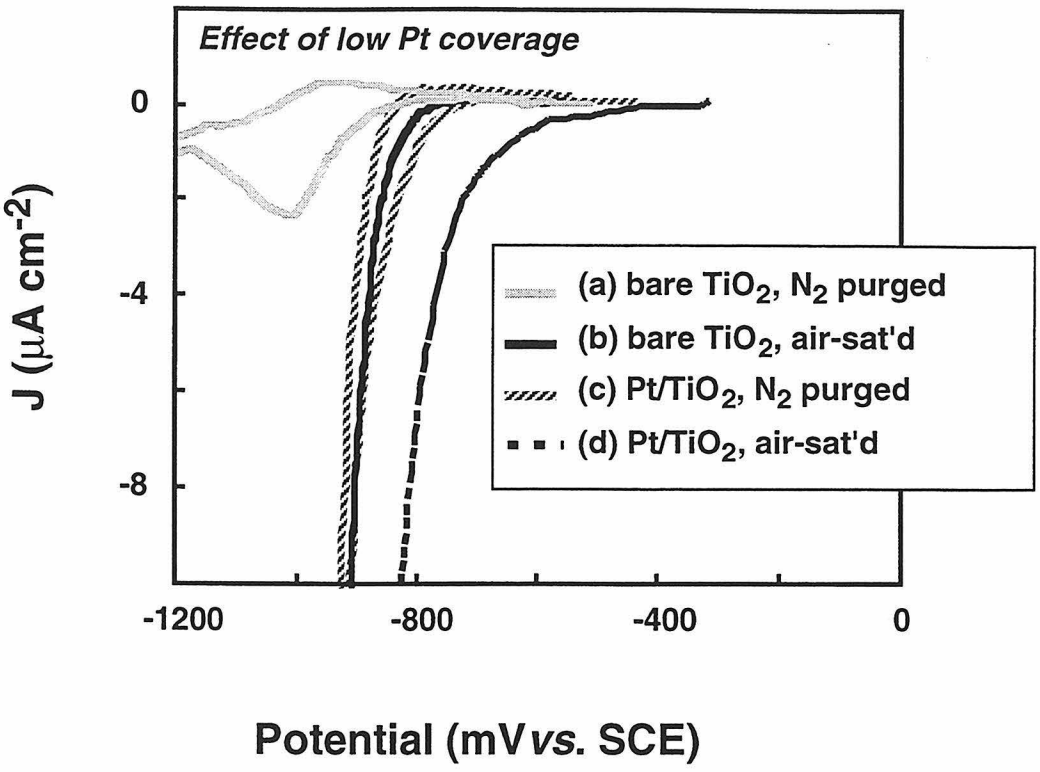

Figure 9. Comparison of the dark J-*E* behavior for bare and platinized (low coverage) TiO_2 electrodes in 1.0 *M* NaOH. (a) bare TiO_2, N_2 purged solution; (b) bare TiO_2, air-saturated solution; (c) platinized TiO_2 (150Å), N_2 purged solution; (d) platinized TiO_2 (150Å), air-saturated solution. The ratio of the Pt(4d3) peak to the Ti(2p) peak in XPS was 0.4 indicating approximately 6 Å of Pt on the surface. The electrode was tested for Schottky diode behavior as described in the text and was found not to behave as a Schottky diode.

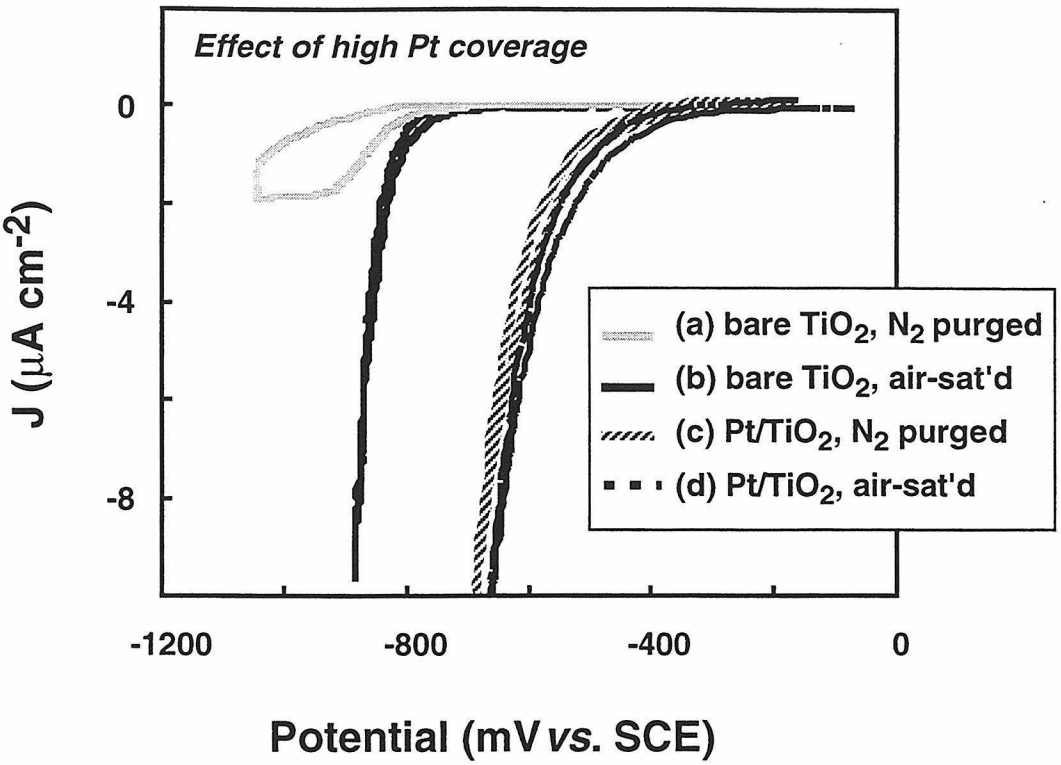

Figure 10. Comparison of the dark J-*E* behavior for bare and platinized (high coverage) TiO_2 electrodes in 1.0 *M* NaOH. (a) bare TiO_2, N_2 purged solution; (b) bare TiO_2, air-saturated solution; (c) platinized TiO_2 (4600Å), N_2 purged solution; (d) platinized TiO_2 (4600Å), air-saturated solution. The ratio of the Pt(4f5/2) peak to the Ti(2p) peak in XPS was 30 indicating approximately 70 Å of Pt on the surface. This electrode exhibited Schottky diode behavior as described in the text.

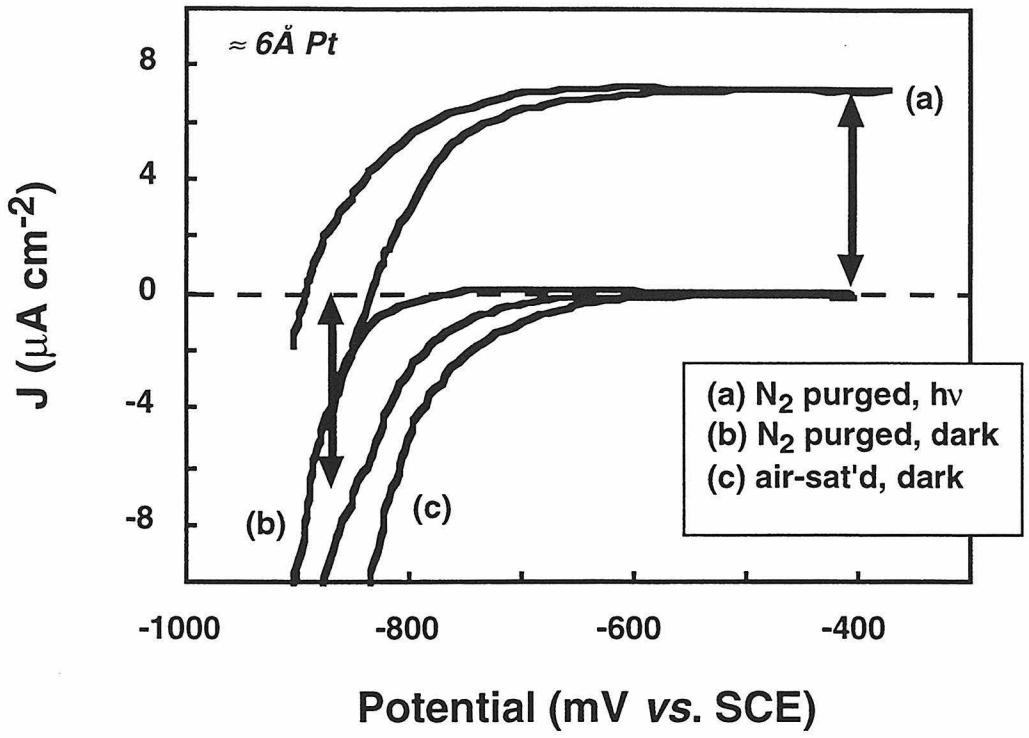

Figure 11. Flux-matching analysis in 1.0 *M* NaOH(aq) for the platinized TiO_2 electrode described in Figure 9 (≈ 6 Å Pt). (a) Photooxidation current density in a N_2-purged solution. (b) Reduction current density in a N_2-purged solution in the dark. (c) Reduction current density in an air-saturated solution in the dark. As described in the text, electron and hole fluxes could not be determined independently for this electrode. The relevant comparison is the limiting photooxidation current density and the reduction current density in the dark for the N_2-purged solution at E_{oc} of the light curve, as indicated by the arrows. These data predict that electron hole pair generation would be rate-limiting for this system.

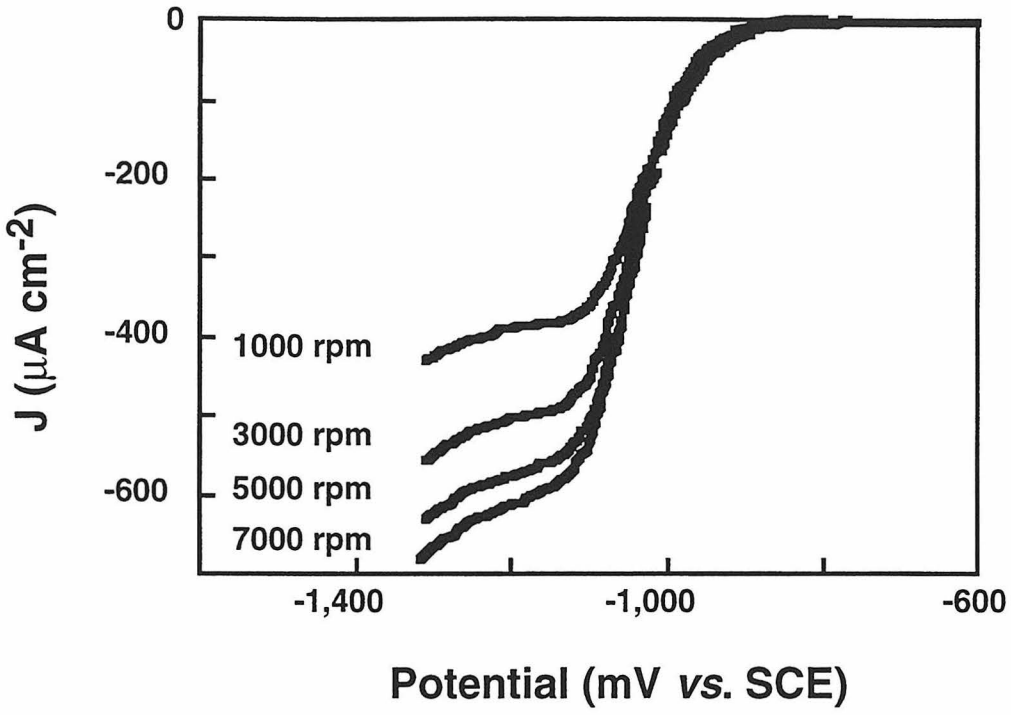

Figure 12. Representative plot of oxygen reduction current density vs. potential for TiO_2 RDE in air-saturated 1.0 *M* KOH(aq) solution. The current depended on the rotation rate of the electrode, with increasing rotation rates yielding increasing currents. The data illustrated were collected at 1000, 3000, 5000, and 7000 revolutions per minute, as indicated.

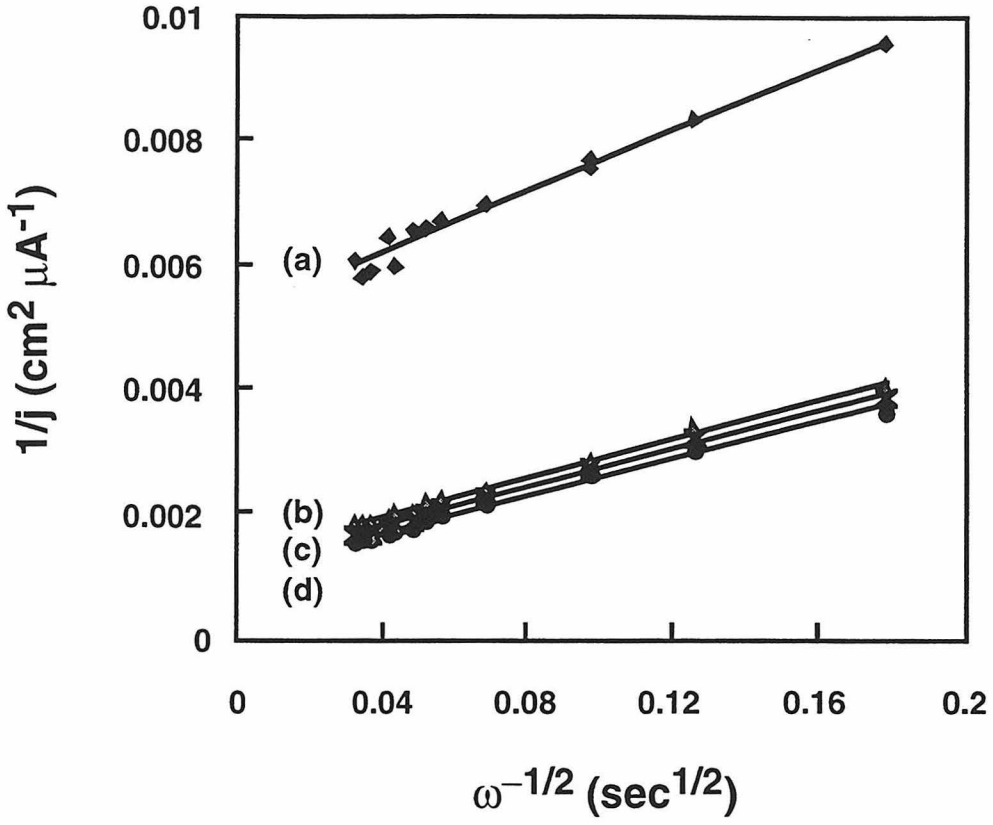

Figure 13. Koutecky-Levich plots at several potentials for the RDE data in Figure 12. (a) -1000 mV vs. SCE; (b) -1100 mV vs. SCE; (c) -1200 mV vs. SCE; (d) -1300 mV vs. SCE. The slope of these plots was proportional to the number of electrons transferred, n_e, and the y-intercept was inversely proportional to the rate constant for O_2 reduction, k_n'. The average values of n_e and k_n' for a series of data sets is summarized in Table I.

Chapter 3.

Electrochemical Production of •OH at Polycrystalline TiO_2 Electrodes and Quantification of •OH and Direct Oxidation Pathways

Abstract

The use of TiO_2 as a photocatalyst for the destruction of organic pollutants in aqueous waste streams has been extensively studied. One obstacle to the effective utilization of these systems is the relatively inefficient use of the solar spectrum by the photocatalyst. In addition, light delivery to the photocatalyst can be impeded by UV absorbing components in the waste stream. In this paper, we present a novel use of TiO_2 as a catalyst for the destruction of organic pollutants that uses a potential source instead of light to generate reactive oxidants. Application of an anodic bias of >+2 V vs. NHE to titanium electrodes coated with niobium-doped, polycrystalline TiO_2 particles electrochemically generates hydroxyl radicals at the TiO_2 surface. This process has been demonstrated to degrade efficiently a variety of environmentally important pollutants. In addition, these electrodes offer a unique opportunity to probe mechanistic questions in TiO_2 catalysis. By comparing substrate degradation rates with increases in current density upon substrate addition, the extent of degradation due to direct oxidation and •OH oxidation can be quantified. It is found that the branching ratio for these pathways depends on the organic substrate. Formate is shown to degrade primarily via a hydroxyl radical mechanism at these electrodes whereas the current increase data for compounds like 4-chlorocatechol indicate that a higher percentage of their degradation may occur through direct oxidation. In addition, the direct oxidation pathway is shown to be more important for 4-chlorocatechol, a strongly adsorbing substrate, than for 4-chlorophenol which does not adsorb to TiO_2.

Introduction

The use of TiO_2 as a photocatalyst for the destruction of organic pollutants in aqueous waste streams has been studied extensively.[1, 2] Light absorption in TiO_2 at $\lambda \leq$ 385 nm effects the promotion of an electron from the valence band to the conduction band of the semiconductor.[2] This excitation process creates an electronic charge carrier in the conduction band and an electron vacancy (a hole) in the valence band. Because the valence band edge of TiO_2 occurs at approximately +3.2 V vs. the normal hydrogen electrode, NHE, at pH 0 (the position of the band edge is pH dependent[3, 4]), the hole is a very powerful oxidizing agent and is capable of oxidizing a variety of organic molecules as well as generating hydroxyl radicals in water. Illuminated slurries of TiO_2 have been shown to oxidize a wide range of organic pollutants, leading to the formation of CO_2.[5-8] There is a great deal of interest in using TiO_2 for waste treatment due to the low cost of the TiO_2 catalyst as well as the potential for using sunlight as the energy source. However, the quantum yields for photodegradation of organics in aqueous solution are low.[9, 10] Commercial applications employ systems involving immobilization of the photocatalyst onto a solid support and the use of UV lamps instead of sunlight to enable continuous operation of the reactor.[11]

In a novel application of TiO_2 as a catalyst for the destruction of organic pollutants, Weres and Hoffmann have developed polycrystalline TiO_2 electrodes that are capable of generating hydroxyl radicals under an anodic bias (Figure 1).[12-14] Kamat and co-workers have used an applied bias to enhance the separation of photogenerated charge carriers in polycrystalline TiO_2 electrodes.[15, 16] However, the Weres and Hoffmann system is the first, to our knowledge, to generate hydroxyl radicals at the surface of TiO_2 using only an applied voltage. Significant levels of hydroxyl radical generation are not observed at typical metal electrodes, such as platinum, because the four electron oxidation of water to dioxygen occurs at a potential (+1.23 V at pH = 0) well below that required for the one electron oxidation of water to •OH (+2.74 V at pH = 0).[17] Thus,

most metal electrodes are sufficiently catalytic for the four electron process that the O_2 production pathway predominates at potentials high enough to generate •OH. In contrast, these degenerately doped TiO_2 electrodes have been demonstrated to effectively destroy a variety of environmentally important pollutants in aqueous solutions.[12-14]

The use of TiO_2 electrodes also allows the experimental determination of certain quantities that are not readily measureable on TiO_2 particles. A previous study in this laboratory used single crystal rutile TiO_2 electrodes to examine the possibility that oxygen reduction was rate-limiting in the TiO_2-photocatalyzed decomposition of organic compounds in water.[18] The goal of the present investigation is to demonstrate the production of hydroxyl radicals at the polycrystalline TiO_2 electrodes. The question in TiO_2 photocatalysis of whether oxidation occurs by direct hole transfer or by hydroxyl radical attack has been repeatedly asked, and evidence in support of both mechanisms has been obtained.[19-25] Ideally, a direct measure of the amount of hydroxyl radical production, for example through use of radical traps, would be desirable.[26, 27] However, common hydroxyl radical traps can be directly oxidized at very positive potentials, so an alternative approach was sought to distinguish between hydroxyl radical production and direct oxidation of the organic molecules.

Two sets of experiments were carried out in order to assess the production of hydroxyl radicals at degenerately-doped, polycrystalline TiO_2 electrodes. The first protocol involved comparison of the degradation rates of a series of chlorinated acetates on TiO_2 to the known rate constants for reaction of these same reagents with hydroxyl radicals. The rate constants for reaction of these acetates with hydroxyl radicals follow the trend.[25]

$$ClCH_2CO_2^- > Cl_2CHCO_2^- > CH_3CO_2^- >> Cl_3CO_2^- \qquad (1)$$

This trend occurs because the electronegative chlorine weakens the C-H bond, so the hydrogen atom in chloroacetate and dichloroacetate is more readily abstracted by the •OH relative to the hydrogen atom abstraction from acetate. Trichloroacetate, however, possesses no abstractable hydrogens and is degraded only slowly by hydroxyl radicals.

In contrast, the oxidation potentials of these acetates are expected to increase with an increasing degree of chlorination. Direct oxidation through hole transfer from the TiO_2 to the organic would thus be expected to follow the trend:

$$CH_3CO_2^- > ClCH_2CO_2^- > Cl_2CHCO_2^- > Cl_3CO_2^- \qquad (2)$$

Measurement of the degradation rates of these acetates at polycrystalline TiO_2 can then determine if the oxidation process occurs primarily through the direct electron transfer pathway or through hydroxyl radical attack.

The second set of experiments was designed to quantify the extent of degradation occurring through •OH attack relative to direct oxidation. Figure 2 shows the current-branching behavior expected during electrocatalysis at degeneratively doped TiO_2 electrodes. The rates of direct oxidation and •OH mediated oxidation should have different kinetic dependencies on the concentration of the organic substrate. For oxidation mediated by hydroxyl radicals, water is the species being oxidized at the electrode surface. Since the water concentration is constant, the observed current for this pathway should be independent of the concentration of organic substrate. In contrast, for oxidation occurring by direct electron transfer, the current should increase as the concentration of organic substrate increases. The magnitude of the increase in current observed upon addition of substrate can thus be used to place an upper limit on the percentage of substrate degradation that occurs through direct oxidation. Assuming that the observed current increase corresponds to direct oxidation, the magnitude of the

current increase, divided by the total degradation rate, yields the percentage of substrate degradation that proceeds through the direct oxidation pathway.

Experimental

Chemicals

Sodium acetate trihydrate (99+%), sodium chloroacetate (98%), potassium dichloroacetate (98%), and sodium trichloroacetate (97%) were purchased from Aldrich Chemicals (Milwaukee, MN). Sodium mono- and di-basic phosphate and sodium formate (99%) were purchased from EM (Gibbstown, NJ). 4-chlorophenol was purchased from Aldrich (Milwaukee, MN). 4-chlorocatechol was purchased from TCI America (Portland, OR) and was purified by recrystallization from hot heptane. Except for the 4-chlorocatechol, all chemicals were used as received. All solutions were prepared using Millipore Milli-Q^{UV} Plus 18 MΩ cm resistivity deionized water.

Fabrication and Lifetimes of Nb-doped Polycrystalline TiO_2 Electrodes

TiO_2 electrodes were provided by Sonoma Research, Inc., and the details of their manufacture are described in the U.S. patent literature.[12] In general, the electrodes are made by coating a titanium substrate with Nb-doped TiO_2 particles, followed by annealing the film under hydrogen. The electrodes used in this work were cylindrical rods with diameters of 6 mm and lengths of approximately 35 mm. After an initial "break in" period, the electrode behavior was stable through the course of many experiments when operated at the low current densities used in this work. However, when the electrodes were operated at higher current densities, their lifetimes were significantly

shortened. Extended use of the electrodes generally resulted in a gradual decrease in the observed current for a given electrode potential, sometimes followed by an increase in current. The failure mechanisms of these electrodes have not yet been determined. Nominally identical electrodes often displayed different absolute current densitites at a given potential (see Table 2), thus kinetic trends were evaluated for the same electrode operated in a controlled series of experiments.

Electrochemical Cells and Instrumentation

Chemical degradation and electrochemical experiments were carried out in a two compartment Pyrex cell (Figure 3). The TiO_2 working electrode described above, and the $Hg/Hg_2SO_4/K_2SO_4(aq)$ reference electrode (+ 0.64 vs. NHE) were separated from the counter electrode (made from carbon fibers) by a fine porosity glass frit. The volume of solution in the working compartment was 60 mL or 500 mL, as noted in the figure captions.

An EG&G PAR Model 362 Scanning Potentiostat/Galvanostat (Princeton, NJ) was used for experiments performed at constant current. Constant potential experiments were performed on a BAS model CV50 Potentiostat (Lafayette, IN) using the bulk electrolysis mode.

Analytical Methods

Ion Chromatography. Acetate, chloroacetate, dichloroacetate, trichloroacetate, and formate were analyzed by ion chromatography. Samples were withdrawn at given time intervals and the substrate concentration was then analyzed using a Dionex BioLC (Sunnyvale, CA) equipped with a pulsed electrochemical detector and an Omnipac PAX-500 analytical column. The eluants consisted of 1 mM NaOH(aq), 200 mM NaOH(aq), and 5% MeOH(aq), and were mixed in various ratios to achieve good separation between

substrate and background electrolyte peaks with a minimum of analysis time. Since experiments were run in the presence of high concentrations of background electrolyte (either K_2SO_4 or phosphate), samples were diluted prior to analysis in order to avoid overloading the column.

HPLC. 4-chlorophenol and 4-chlorocatechol were analyzed by high pressure liquid chromatography (HPLC). A Hewlett-Packard ODS Hypersil, 5μm, 100 x 2.1 mm column was used. The instrument was a Hewlett-Packard Series II 1090 Liquid Chromatograph. The eluants consisted of aqueous phosphoric acid (pH 3) and HPLC grade acetonitrile. To remove any particles that might clog the column, the samples were filtered with Gelman Acrodisc 4 CR PTFE 0.45 μm filters (Ann Arbor, MI) prior to analysis.

CO_2 Production. CO_2 production was monitored by gas chromatography using a Carle AGC Series 400 gas chromatograph equipped with a Porapak QS column and a thermal conductivity detector (Loveland, CO). The oven temperature was maintained at 70 °C and these conditions afforded good separation between air and CO_2 peaks. Standards were prepared from Na_2CO_3 dissolved in the same background electrolyte that was used in the degradation experiments. To initiate the analysis, 0.5 mL of the standard or sample were injected into a 2mL glass vial with a Teflon septa cap. Prior to injection on the GC, 50 μm of concentrated H_2SO_4 was added to acidify the samples. 15 μL of the headspace was then injected onto the column.

Results

Degradation of Chlorinated Acetates

Figure 4 depicts the time dependence of the concentrations of acetate, chloroacetate, dichloroacetate, and trichloroacetate during electrolysis at a TiO_2 electrode. These experiments were carried out in 0.5 M phosphate buffer (pH = 6.4), at a constant current of 15 mA. The trichloroacetate concentration was essentially constant over the course of the five hour experiment, whereas significant descreases were observed in the chloroacetate and dichloroacetate concentrations over this same time period. Similar experiments were carried out using a pH stat to control the pH to 9.0 with potassium sulfate as the electrolyte. The results of these experiments are summarized in Table 1. For each set of experiments, the trend in reaction rate parallels the trend observed for reaction of •OH with the various acetates.

Current Density vs. Solution Composition

As described in the introduction, it is also informative to examine the dependence of the current density on the concentration of the organic substrate in the solution. Assuming that any increase in current density observed after addition of the organic species to the solution is due to the direct oxidation of this electroactive reagent, the magnitude of the current increase can be converted into an equivalent degradation rate of the organic substrate and compared to the observed degradation rate. If the number of electrons involved in the electrochemical reaction were known, this procedure would yield a quantitative measure of the kinetic branching ratio between the rate of direct oxidation and the rate of •OH production.

This experiment, in which the current density was monitored as a function of the concentration of the organic compound, was performed using formate, acetate, chloroacetate, trichloroacetate, 4-chlorophenol, or 4-chlorocatechol. Figure 5 shows the time dependence of the formate concentration, as well as the concurrent time dependence

of the concentration of CO_2, which is formed stoichiometrically as a two-electron oxidation product of formate at the Nb-doped polycrystalline TiO_2 electrodes. The experiment was run in constant current mode with I = 15 mA, and the potential range observed during the experiment was 3.10 ± 0.01 V vs. NHE. Figure 6a shows the current vs. time data for an electrode held at 3.10 V vs. NHE as formate is added. Additionally, Figure 6b depicts a plot of the magnitude of the observed current increase of the TiO_2 electrode as a function of the concentration of formate in the solution. A linear dependence of the current density on the formate concentration is expected for the direct oxidation of substrates that are dissolved homogeneously in the solution. For each of the compounds investigated, however, the magnitude of the current increase per unit change in substrate concentration decreased at higher total substrate concentrations. This behavior suggests that the direct oxidation pathway involves surface sorbed species which saturate the available surface sites on the TiO_2 electrode at high substrate concentrations.

Table 2 shows the total degradation rates and maximum percent direct oxidation data for the different substrates. The initial degradation rates (determined from linear fits to the data obtained for the substrate concentration as a function of time) for the compounds studied are shown in the second column of this table. The following column shows the magnitude of the current increase upon addition of 1 mM substrate, while the fourth column shows the degradation rate of the organic reagent that would correspond to the observed current increase. This column was calculated assuming 1 electron was transferred per molecule of substrate oxidized, except for formate, for which a 2-electron oxidation was assumed (vide infra). The final column contains the ratio of column 4 to column 2. The numbers shown in bold type were obtained using an electrode (TiO_2-1) that was operated at a constant current of 15 mA for the degradation experiments. The current increase experiments were performed at the potential observed during the

degradation experiments (3.1 V vs. NHE). The data shown in plain type were taken with a different electrode (TiO_2-2) that was operated at a constant potential of 2.9 V vs. NHE for both the degradation and current increase experiments. The steady-state currents observed during the degradation experiments using this latter electrode ranged from 9 to 10 mA.

Prior work indicates that the one electron oxidation product of formate is unstable and immediately injects another electron into the electrode (a process called "current doubling").[28, 29] Since formate was shown to undergo a two electron oxidation in our experiments as well, the current increase data were analyzed assuming that two electrons were transferred for each molecule of formate that was consumed from the solution.

direct: $$HCO_2H \rightarrow CO_2 + 2H^+ + 2e^- \quad (3)$$

•OH: $$HCO_2H + \bullet OH \rightarrow \bullet CO_2H + H_2O$$
$$\bullet CO_2H + \bullet OH \rightarrow CO_2 + H_2O \quad (4)$$

A comprehensive study of the reaction intermediates present in the solution was not performed for the other substrates, and so it is not known how many electrons are transferred per molecule of those substrates. The values given in Table 2 therefore assume only one electron transferred per substrate molecule (except for formate as noted above). If the direct oxidation reactions involve transfer of more than one electron to a given molecule of substrate, then the values for the percentage of direct oxidation quoted in Table 2 will be larger than the actual values (by a factor equal to the number of electrons transferred). These values can therefore only serve as upper limits on the actual branching ratio for all substrates except for formate.

The data in Table 2 indicate that formate is consumed primarily through an •OH mechanism under the conditions of our experiments. 4-chlorophenol and 4-chlorocatechol showed similar degradation rates to each other, as determined by the time dependence of the decrease in substrate concentration. However, 4-chlorocatechol, which is known to adsorb strongly to the surface of TiO_2,[30] causes a larger current increase per unit substrate concentration than does 4-chlorophenol, which does not adsorb to TiO_2.[31-33] These results suggest that a higher percentage of degradation occurs through the direct oxidation process for 4-chlorocatechol degradation than for 4-chlorophenol. The dependence of the results on the specific electrode and/or operating conditions can be seen by comparing the two results shown for acetate (see also experimental section). The first electrode indicated that as much as 65% of the degradation may have occurred via direct oxidation, whereas the second electrode showed only 15%. Within the series of experiments for the chlorinated acetates operated under the same conditions, the trend of the current increases agrees with the expected trend in oxidation potentials shown in equation 2. Acetate causes the largest current increase (i.e., is the easiest to oxidize), followed by dichloroacetate and trichloroacetate.

Discussion

The large increase in current per unit concentration of acetate observed with electrode TiO_2-1 was surprising given that the trend in degradation rates for the chlorinated acetates (taken with the same electrode and under the same operating conditions) agreed well with the trend expected for an •OH abstraction mechanism. However, as in the case of formate, the direct oxidation of acetate may involve transfer of multiple electrons before intermediates are released from the surface. In the extreme case

of complete oxidation for the direct pathway involving transfer of 6 electrons, only 11% of the loss of acetate would result from direct transfer.

An analysis of the products formed from •OH and photo-Kolbe oxidations of acetate in homogeneous solution has been performed by Schuchmann et al.[34, 35] Proposed mechanisms are shown below.

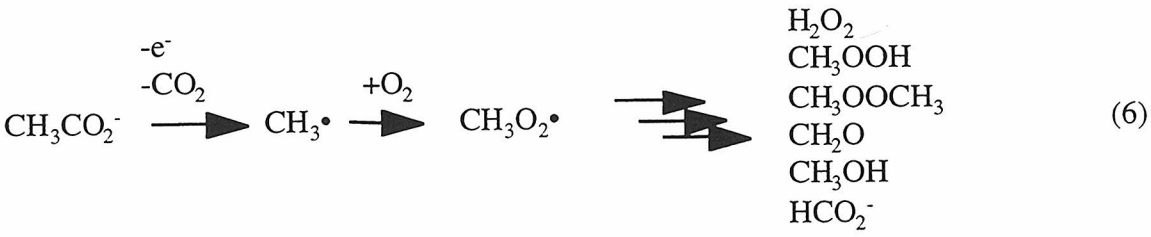

(6)

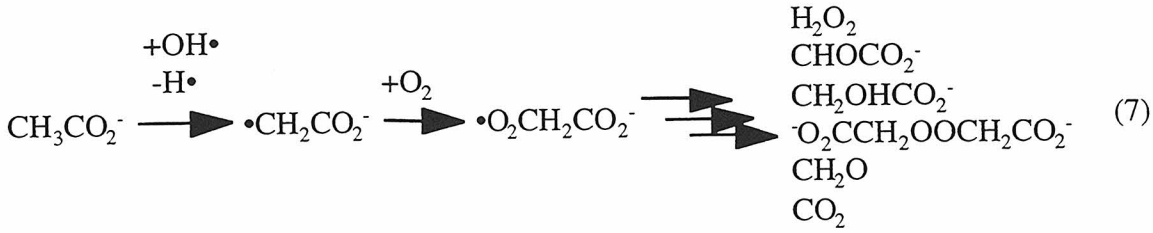

(7)

These mechanisms predict differences in the product distribution for the various kinetic pathways under consideration. For example, direct one-electron oxidation of acetate is expected to release one molecule of CO_2, and is also expected to produce a methyl radical that then reacts further with O_2 to produce a variety of intermediates. In contrast, the reaction of acetate with •OH also produces a carbon-centered radical which reacts with O_2, but which produces a different set of intermediates. Furthermore, CO_2 is not an initial product at all in the •OH pathway.

An analysis of the CO_2 production rate in our system during acetate degradation was therefore performed in order to assess the number of electrons transferred per acetate

molecule degraded in the direct oxidation mechanism. If a stoichiometric amount of CO_2 were observed, as in the case of formate degradation, then no intermediates are formed and the direct mechanism must have involved the complete 6 electron oxidation. However, only one molecule of CO_2 was produced per molecule of acetate degraded. This is consistent with a variety of kinetic pathways and does not allow assignment of the number of molecules transferred per acetate oxidized.

In related work, Carraway et al. have performed an extensive analysis of the products formed during acetate degradation at ZnO particles.[36] The concentrations of the observed products—formate, formaldehyde, organic peroxides, H_2O_2, and CO_2—were not in accord with expectations from either isolated kinetic pathway observed by von Sonntag. In order to explain their results, Carraway et al. postulated a surface-mediated/direct oxidation mechanism involving the two-electron oxidation of acetate.[36]

Our results indicate that both direct hole transfer and •OH abstraction are occurring simultaneously, with direct oxidation accounting for between 11 and 65% of the acetate degraded with electrode TiO_2-1 and only 2 to 15% of the acetate degraded with electrode TiO_2-2. Due to the similarity of the intermediates produced in the two homogeneous pathways, as well as the complicating factors involved in the potential participation of surface reaction processes such as those hypothesized by Carraway et al.,[36] further quantification of the kinetic pathways in our system would be difficult through analysis of the time dependence of concentrations of the intermediates. Thus, for molecules more complex than formate, only an upper limit on the percentage of oxidation that occurs through the direct oxidation pathway can be established.

Conclusions

The observed trend in acetate degradation rates as well as the increase in current per unit substrate concentration increase indicate the production of •OH at degenerately

doped polycrystalline TiO_2 electrodes under strong anodic bias. The electrochemical data allowed quantification of the extent of direct and •OH pathways for the degradation of a variety of compounds under our experimental conditions. Formate is shown to degrade primarily via a hydroxyl radical mechanism at these electrodes whereas the current increase data for compounds like 4-chlorocatechol indicate that a higher percentage of their degradation may occur through direct oxidation. In addition, current increase experiments suggest that surface adsorption plays an important role in determining the oxidation mechanisms in TiO_2 catalysis. Experiments with TiO_2 electrodes operated in the light at less positive potentials could also be used to determine these quantities for TiO_2 photocatalysis. The results may differ due to different surface interactions at the high potentials used in the electrocatalysis experiments. However, this approach should provide useful information in designing optimal waste treatment systems.

Acknowledgments

We are grateful to DARPA and ONR {NAV 5 HFMN N0001492J1901} for financial support. The authors would also like to thank Dr. Oleh Weres for supplying the TiO_2 electrodes and for helpful discussions. J. Kesselman acknowledges the NSF for a predoctoral fellowship.

References

(1) Ollis, D. F. In Homogeneous and Heterogeneous Photocatalysis; E. Pelizzetti and N. Serpone, Eds.; D. Reidel Publishing Company: 1986; p 651-656.

(2) Hoffmann, M. R.; Martin, S. T.; Choi, W.; Bahnemann, D. W. *Chem. Rev.* **1995**, *95*, 69-96.

(3) Finklea, H. O. In Semiconductor Electrodes; H. O. Finklea, Eds.; Elsevier: New York 1988; p 43-146.

(4) Nozik, A. J. *Ann. Rev. Phys. Chem.* **1978**, *29*, 189-222.

(5) Pruden, A. L.; Ollis, D. F. *Environ. Sci. Technol.* **1983**, *17*, 628-631.

(6) Hidaka, H.; Nohara, K.; Zhao, J.; Serpone, N.; Pelizzetti, E. *J. Photochem. Photobiol. A: Chem.* **1992**, *64*, 247-254.

(7) Hidaka, H.; Zhao, J.; Kitamura, K.; Nohara, K.; Serpone, N.; Pelizzetti, E. *J. Photochem. Photobiol. A: Chem.* **1991**, *64*, 103-113.

(8) Terzian, R.; Serpone, N.; Minero, C.; Pelizzetti, E.; Hidaka, H. *J. Photochem. Photobiol. A: Chem.* **1990**, *55*, 243-249.

(9) Choi, W.; Termin, A.; Hoffmann, M. R. *J. Phys. Chem.* **1994**, *98*, 13669-13679.

(10) Kormann, C.; Bahnemann, D. W.; Hoffmann, M. R. *Environ. Sci. Technol.* **1991**, *25*, 494-500.

(11) Al-Ekabi, H.; Safarzadeh-Amiri, A.; Sifton, W.; Story, J. *International Journal of Environment and Pollution* **1991**, *1*, 125-136.

(12) Weres, O.; Hoffmann, M. R. *Electrode, Electrode Manufacturing Process and Electrochemical Cell*; U.S. Patent# 5,419,824, May 30, 1995.

(13) Weres, O.; Hoffmann, M. R. *Electrochemical Method and Device for Generating Hydroxyl Free Radicals and Oxidizing Chemical Substances Dissolved in Water*; U.S. Patent# 5,364,508, Nov. 15, 1994.

(14) Weres, O.; Hoffmann, M. R. *Electrochemical Device for Generating Hydroxyl Free Radicals and Oxidizing Chemical Substances Dissolved in Water*; U.S. Patent# 5,439,577, Aug. 8, 1995.

(15) Vinodgopal, K.; Stafford, U.; Gray, K. A.; Kamat, P. V. *J. Phys. Chem.* **1994**, *98*, 6797-6803.

(16) Vinodgopal, K.; Hotchandani, S.; Kamat, P. V. *J. Phys. Chem.* **1993**, *97*, 9040-9044.

(17) Kläning, U. K.; Sehested, K.; Holcman, J. *J. Phys. Chem.* **1985**, *89*, 760-763.

(18) Kesselman, J. M.; Shreve, G. A.; Hoffmann, M. R.; Lewis, N. S. *J. Phys. Chem.* **1994**, *98*, 13385-13395.

(19) Nishimoto, S.-i.; Ohtani, B.; Kagiya, T. *J. Chem. Soc., Faraday Trans. 1* **1985**, *81*, 2467-2474.

(20) Prairie, M. R.; Evans, L. R.; Stange, B. M.; Martinez, S. L. *Environ. Sci. Technol.* **1993**, *27*, 1776-1782.

(21) Micic, O. I.; Zhang, Y.; Cromack, K. R.; Trifunac, A. D.; Thurnauer, M. C. *J. Phys. Chem.* **1993**, *97*, 7277-7283.

(22) Draper, R. B.; Fox, M. A. *Langmuir* **1990**, *6*, 1396-1402.

(23) Stafford, U.; Gray, K. A.; Kamat, P. V. *J. Phys. Chem.* **1994**, *98*, 6343-6351.

(24) Goldstein, S.; Czapski, G.; Rabani, J. *J. Phys. Chem.* **1994**, *98*, 6586-6591.

(25) Mao, Y.; Schöneich, C.; Asmus, K.-D. *J. Phys. Chem.* **1991**, *95*, 10080-10089.

(26) Brezova, V.; Stasko, A.; L. Lapcik, J. *J. Photochem. Photobiol. A: Chem.* **1991**, *59*, 115-121.

(27) Samuni, A.; Carmichael, A. J.; Russo, A.; Mitchell, J. B.; Riesz, P. *Proc. Natl. Acad. Sci. USA* **1986**, *83*, 7593-7597.

(28) Kerchove, F. V.; Vandermolen, J.; Gomes, W. P.; Cardon, F. *Ber. Bunsenges. Phys Chem.* **1979**, *83*, 230-236.

(29) Dutoit, E. C.; Cardon, F.; Gomes, W. P. *Ber. Bunsenges. Phys. Chem.* **1976**, *80*, 1285-1288.

(30) Martin, S. T.; Kesselman, J. M.; Park, D. S.; Lewis, N. S.; Hoffmann, M. R. *Env. Sci. Technol.* **1996**, *30*, 2535-2542.

(31) Tunesi, S.; Anderson, M. *J. Phys. Chem.* **1991**, *95*, 3399-3405.

(32) Mills, A.; Morris, S. *J. Photochem. Photobiol. A: Chem.* **1993**, *71*, 75-83.

(33) Cunningham, J.; Sedlák, P. *J. Photochem. Photobiol. A: Chem.* **1994**, *77*, 255-263.

(34) Schuchmann, H.-P.; Sonntag, C. v. *Z. Naturforsch.* **1984**, *39b*, 217-221.

(35) Schuchmann, M. N.; Zegota, H.; Sonntag, C. v. *Z. Naturforsch.* **1985**, *40b*, 215-221.

(36) Carraway, E. R.; Hoffman, A. J.; Hoffmann, M. R. *Environ. Sci. Technol.* **1994**, *28*, 786-793.

Tables

Table 1. Comparison Between Reaction Rates of Acetate With •OH and TiO_2 Electrodes.

I. Substrate	II. k_{OH} ($M^{-1}s^{-1}$)[a]	III. k_{meas} (min^{-1})[b]	IV. k_{meas} (min^{-1})[c]	V. k_{meas} (min^{-1})[d]
$CH_3CO_2^-$	(1-2) x 10^7	4.7 x 10^{-4} 4.4 x 10^{-4}	1.6 x 10^{-4} 2.6 x 10^{-4} 2.8 x 10^{-4}	3.3 x 10^{-3} 1.6 x 10^{-3}
$ClCH_2CO_2^-$	(4-8) x 10^7	1.2 x 10^{-3} 1.1 x 10^{-3} 1.3 x 10^{-3}	1.0 x 10^{-3} 5.6 x 10^{-4}	8.5 x 10^{-3} 3.4 x 10^{-3}
$Cl_2CHCO_2^-$	2.8 x 10^7	7.8 x 10^{-4} 9.9 x 10^{-4} 8.9 x 10^{-4}	3.5 x 10^{-4}	5.6 x 10^{-3} 3.8 x 10^{-3}
$Cl_3CO_2^-$	< 10^6	~ 10^{-5}	~ 10^{-5}	~ 10^{-4}

[a]taken from reference (25)
[b]3mM acetate, pH = 9.0, I = 15 mA, 0.1M K_2SO_4, 500 mL cell
[c]5mM acetate, pH = 9.0, I = 10 mA, 0.1M K_2SO_4, 500 mL cell
[d]3 mM acetate, pH = 6.4, I = 15 mA, 0.5 M phosphate buffer, 60 mL cell.

Table 2. Degradation of Organics by a Direct Oxidation Pathway at TiO_2 Electrodes.

I. Substrate	**II. Initial Degradation Rate (mM/min)**	**III. Current Increase (mA/mM)**	**IV. Direct Oxidation Rate *(Calculated)* (mM/min)**	**V. Maximum % Direct Oxidation**
formate	**0.0095**	**0.22**	**0.0011**[a]	**12**
4-chlorophenol	**0.0046**	**0.29**	**0.0030**	**65**
4-chlorocatechol	**0.0047**	**0.44**	**0.0046**	**97**
acetate	**0.0023**	**0.14**	**0.0015**	**65**
	0.0065	0.10	0.0010	15
dichloroacetate	0.0089	<0.01	<0.0001	<1
trichloroacetate	0.0002	<0.01	<0.0001	<50

[a]assuming 2 electrons transferred
Boldfaced type = electrode TiO_2-1, degradation at constant I = 15 mA
Plain type = electrode TiO_2-2, degradation at constant V= 2.9 V *vs.* NHE

Figures

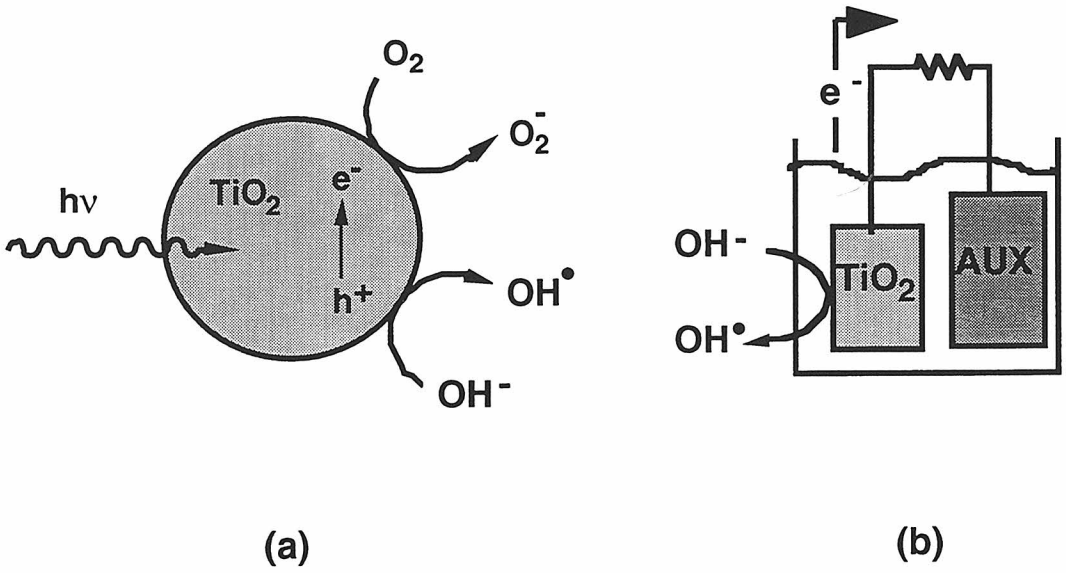

Figure 1. TiO_2 Photocatalysis vs. TiO_2 Electrocatalysis. (a) Schematic representation of the processes occurring in TiO_2 photocatalysis. (b) Schematic representation of TiO_2 electrocatalysis.

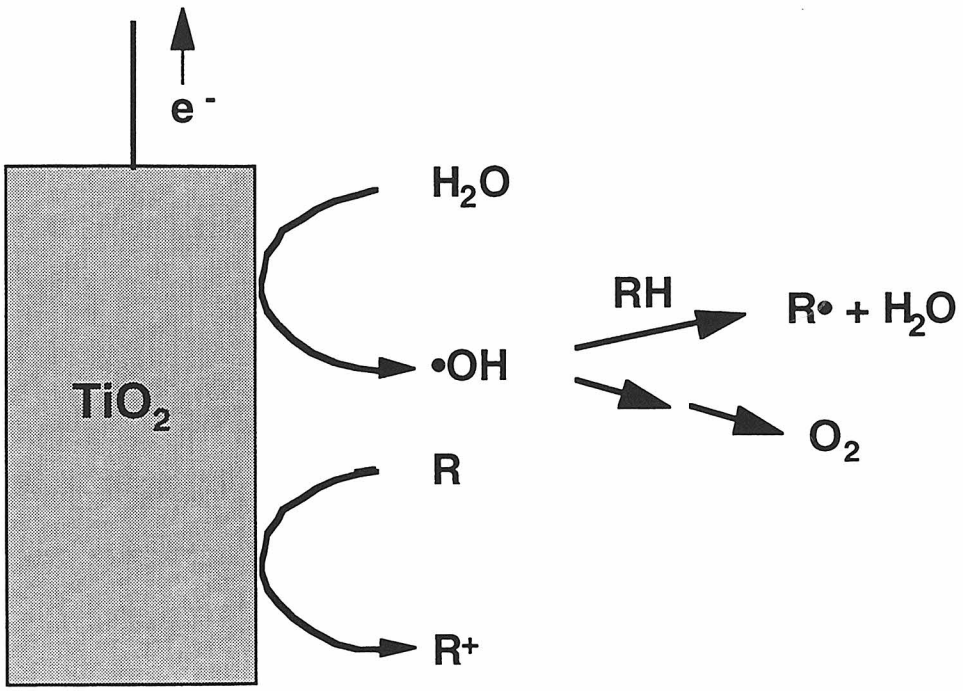

Figure 2. Schematic diagram illustrating differences in the expected current response between direct oxidation and hydroxyl radical mediated oxidation pathways.

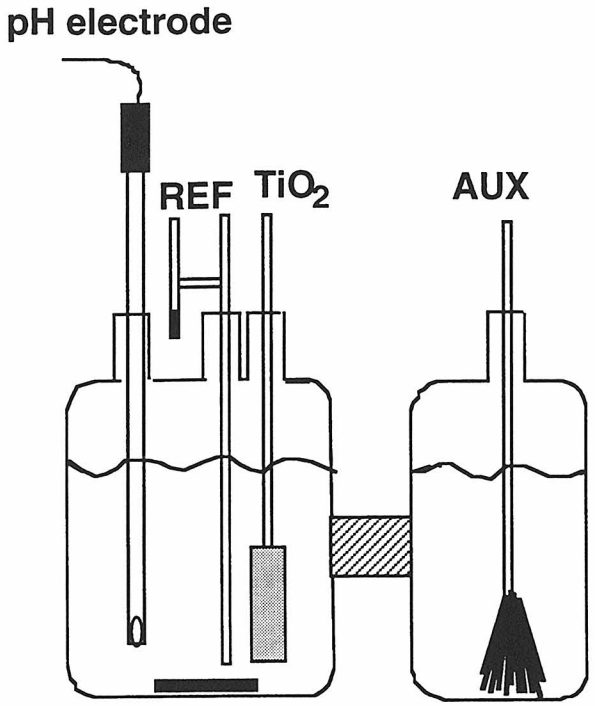

Figure 3. Schematic of the two compartment cell used in this work. The TiO_2 working electrode and the $Hg/Hg_2SO_4/K_2SO_4$(sat'd) or standard calomel reference electrodes (SCE) were separated from the carbon fiber auxilary electrode by a fine porosity glass frit.

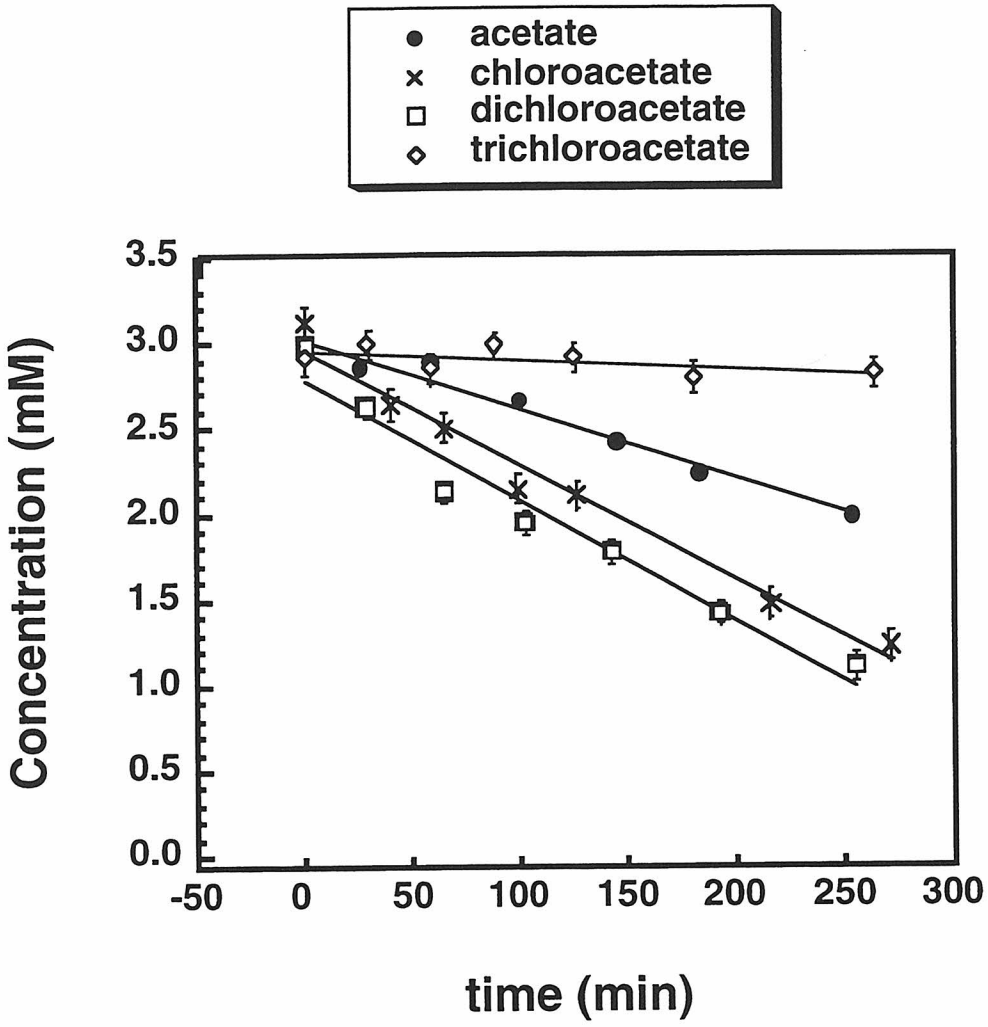

Figure 4. Concentration vs. time data during the bulk electrolysis of substituted acetates at polycrystalline TiO_2 electrodes. Experimental conditions: 0.5 M phosphate buffer, pH = 6.4; 3 mM initial acetate concentration; current = 15 mA; 60 mL of solution in the working electrode compartment. Trichloroacetate shows almost no change in concentration during the five hour experiment, consistent with its slow reaction rate with •OH. Chloroacetate and dichloroacetate react more quickly than acetate, as expected for an •OH abstraction process.

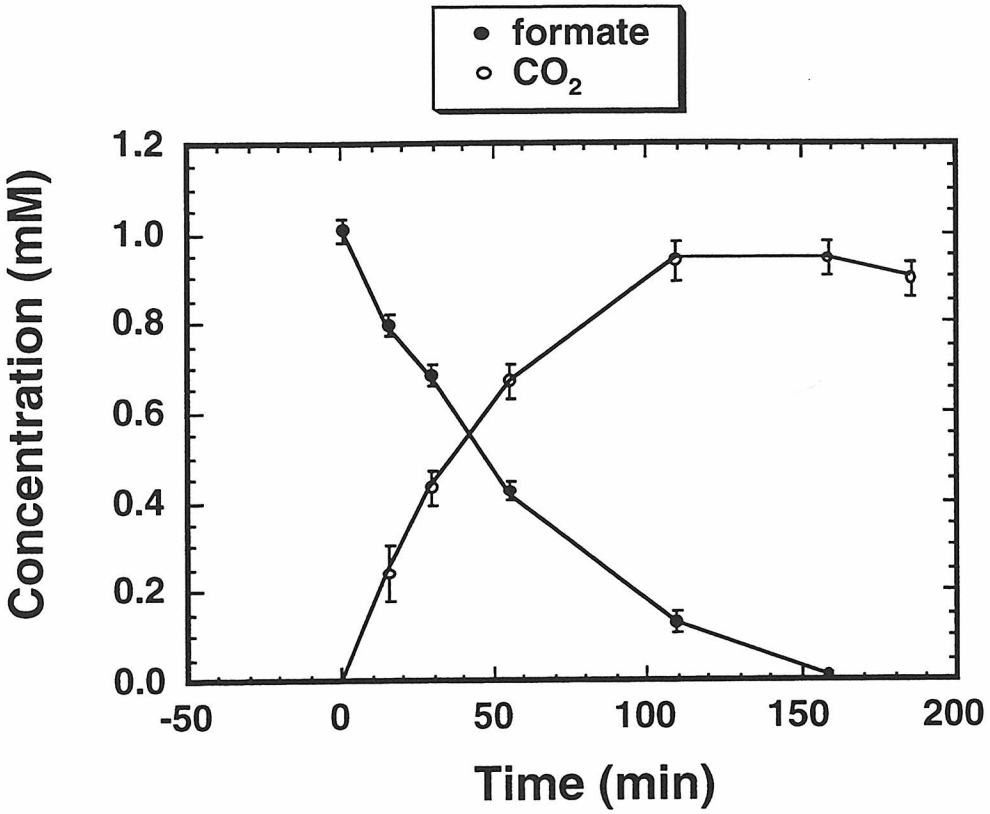

Figure 5. Concentration vs. time data for the bulk electrolysis of formate at a polycrystalline TiO_2 electrode. Also shown are concentration vs. time profiles for the appearance of CO_2 in the cell. The experimental conditions were as follows: I = 15 mA, 1 M phosphate buffer, pH = 6.4, 60 mL volume working compartment, closed cell.

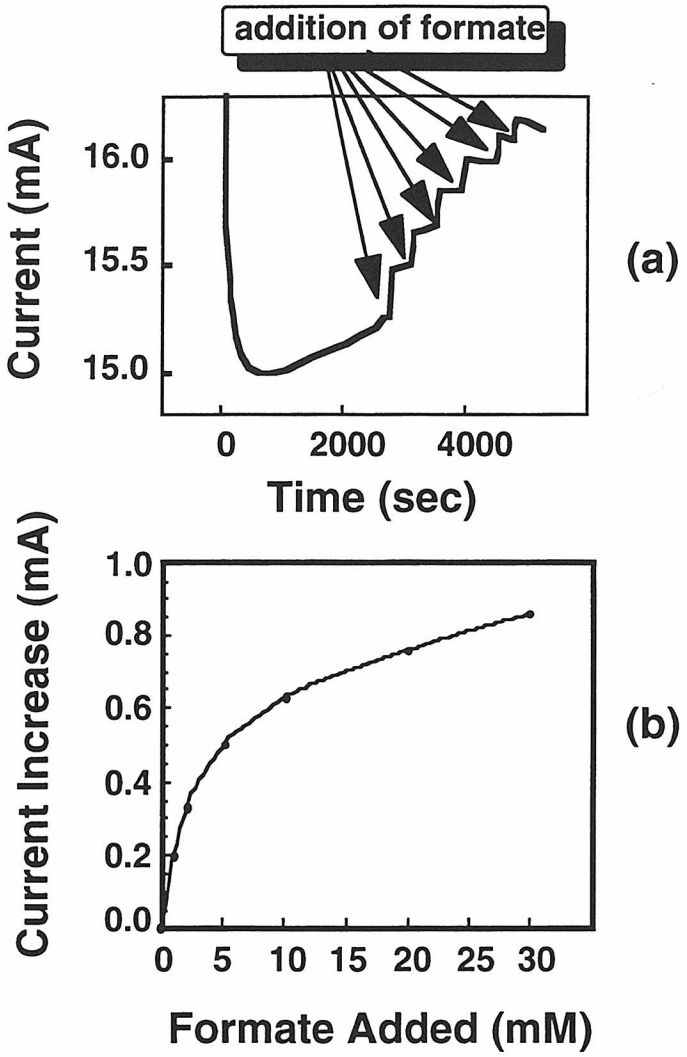

Figure 6. Current at a fixed potential of a polycrystalline Nb-doped TiO_2 electrode as a function of formate concentration. (a) Current vs. time data for an electrode held at +3.1 V vs. NHE in a 1 M phosphate solution at pH 6.4. As shown, the current increased abruptly when the formate was added to the solution. (b) Graph of the resulting current increase as a function of the total concentration of formate added to the solution. The graph displays a "saturation" behavior suggestive of electron transfer from adsorbed species.

Chapter 4.

Surface Structures of 4-Chlorocatechol Adsorbed on Titanium Dioxide

(The text of this chapter appeared in Martin, S. T.; Kesselman, J. M.; Park, D. S.; Lewis, N. S.; Hoffmann, M. R., *Env. Sci. Technol.*, **1996**, *30(8)*, 2535-2542.)

Abstract

TiO_2 has been extensively studied as a photocatalyst for the complete oxidation of a variety of organic pollutants commonly found in groundwater. In this paper, we investigate the surface structures formed between an organic substrate and TiO_2 in the context of understanding how these specific surface interactions affect photoreactivity. The surface complexes formed by 4-chlorocatechol (CT) sorbed on TiO_2 are investigated as a function of concentration and of pH. Singular-value decomposition of the IR spectra of CT adsorbed on TiO_2 indicate a single bidentate chemisorbed species is present over the pH range of 2 to 10. The surface-bound species appears to have 40% covalent and 60% ionic bond character. The pH dependence of the adsorption isotherms is modeled using a generalized electric double layer approach. The data are consistent with the formation of a bidentate binuclear surface group for solution CT concentrations below 50 μM followed by nonspecific multilayer partitioning at concentrations above 100 μM. (Figure 3)

Introduction

TiO_2 catalyzes the oxidation of chlorinated hydrocarbons in the presence of UV radiation at photon energies equal to or greater than the band gap energy of 3.2 eV (λ = 385 nm) (1). The quantum efficiency of the process is influenced by electronic processes (2-6), reactor design (7), solution composition (8), the organic substrate (9), light intensity (10, 11), and surface interactions (12-15). In addition, the interactions between organic ligands and metal oxide surfaces has been the focus of much attention (16-21). However, the relationship between surface complexation and its effects on TiO_2/UV quantum efficiency has not received as much attention. In this paper, we investigate the surface structures formed between an organic substrate and TiO_2 in the context of understanding how these specific surface interactions affect photoreactivity.

In a previous study, we demonstrated that the trichloroacetate anion is oxidized more quickly at low pH due to electrostatic attraction between the negatively charged anion and the positively charged surface (10). On the other hand, the chloroethylammonium cation is oxidized more rapidly as the pH is increased. The interactions between the substrate and surface can be interpreted in part in terms of Gouy-Chapman theory for the activity of the ion at the surface. However, Cunnningham et al. (12, 13) found that the rate of photocatalytic oxidation of substituted salicylic acids and monochlorophenols does not correlate with the extent of adsorption. Tunesi et al. (22) suggested that salicylate undergoes direct hole transfer at low pH, when it is directly adsorbed to TiO_2, and is attacked by hydroxyl radicals at high pH, when it is found predominantly in solution. Gray (23) reported that although the rate of 4-CP loss is independent of catalyst loading, the rate of TOC loss in the same system increases with catalyst loading due to surface-catalyzed thermal reactions. Vasudevan and Stone (18, 19) showed that extent of adsorption of substituted catechols on TiO_2 depends on ionic

strength, pH, molecular structure, and the crystalline phase of TiO_2 (i.e., rutile or anatase). Furthermore, the quantum efficiency for the photooxidation of selenite on TiO_2 appears to correlate with the concentration of deprotonated surficial titanol groups (24).

In this study using ATR-FTIR spectroscopy, we investigate the surface structures of 4-chlorocatechol (CT) on TiO_2. 4-Chlorocatechol, which adsorbs strongly to metal oxides, is formed as an intermediate in the TiO_2 catalyzed photooxidation of 4-chlorophenol (8, 25-27). In addition, it is photochemically stable above 340 nm. The C-O stretching frequencies of CT, which shift upon adsorption, occur in an experimentally accessible window of 1000-1500 cm^{-1}.

Experimental Section

Materials.

4-Chlorocatechol (TCI America) is purified by recrystallization from heptane. Titanium dioxide (Degussa P25) is dialyzed against 18 MΩ–cm resistivity water (Millipore) for four hours to remove 30 μmol/g HCl. This process is repeated three times until the conductivity remains constant. The TiO_2 (1 g/L) is stored up to six weeks at 4 °C before use. The B.E.T. surface area is 49 m^2/g without thermal activation. All other chemicals are reagent grade.

Acid-base titrations.

In a 1L wide-mouth Teflon beaker with screw-top lid, a calomel reference electrode (Beckman) is immersed in electrolyte. A salt bridge (3 wt.% agar) connects the reference beaker to the beaker containing the TiO_2 dispersion in order to minimize the

effect of the suspension (28). In the sample beaker, a pH electrode (Beckman), a bubbler for continuous Ar sparging, and a tube for acid delivery are immersed in 800 mL of 1.25 g/L TiO_2. Both beakers are sealed against the atmosphere and are immersed in a temperature regulated (25.0 °C) water bath. A typical titration is carried out by adjusting the ionic strength to 1 mM KNO_3 (80.9 mg) and sparging for 60 min with Ar to remove CO_2 and O_2. CT must be handled under anaerobic conditions for pH values above pK_{a1} (8.63) to avoid oxidative coupling (29). The pH is adjusted to 10 with NaOH, and 0.1000 N HNO_3 (Baker) is introduced at the rate of 1 mL/hr using a syringe pump (Orion Sage model 361). The syringe pump is calibrated by the mass of titrant added. The pH is continuously monitored using a glass electrode (Beckman) interfaced to Labview$^{@}$ for Macintosh (National Instruments). At pH 4, the ionic strength is increased, the pH is returned to 10, and the acid titration is repeated. Blank titrations are carried out in the absence of P25. The H^+ adsorbed on the P25 at any pH is determined by subtracting the moles of H^+ to reach that pH in the absence of P25 from the moles of H^+ necessary to reach that pH in the presence of P25 (30). The program FITEQL (31) is employed to fit the surface adsorption data to the electric double layer model to evaluate the total surface concentration of titanol groups and pK_{a1} and pK_{a2} (32).

Fluoride titration.

800 mL of 1.25 g/L P25 and 10 mM KNO_3 are prepared in a 1 L Teflon beaker (16). A combination pH electrode (Beckman), a combination fluoride electrode (Orion 9609B), and an Ar bubbler are immersed in the beaker. The pH is adjusted to 5.5 with HNO_3. The fluoride titration is carried out by adding 80.00 mM NaF at the rate of 233.4 μM/hr. The fluoride concentration is continuously monitored with Labview. The F^- adsorbed on TiO_2 is calculated by subtracting the measured solution concentration of fluoride from the total amount of fluoride added to the system.

Batch Adsorption.

In a 250 mL 3-neck round bottom flask, 100 mL of 1 g/L TiO_2 and 10 mM KCl are suspended. A combination pH electrode, a 10 mL burette, and 6" needles for sampling and Ar sparging enter the sealed flask through rubber septa and stoppers. To carry out a typical adsorption experiment at a fixed pH, 4-chlorocatechol is added as a 1 mL aliquot. After allowing 30 min for equilibration, 500 μL is filtered through 0.45 μm filters. The sample is transferred to a 250 μL reduced volume cuvette and diluted as 10:11 in 1 M HCl. The UV/Vis spectrum is recorded with a HP 8452A diode array spectrophotometer. Both residual TiO_2 and 4-chlorocatechol contribute to the observed spectrum. The components are resolved and quantified by spectral decomposition using Mathematica (Wolfram Research, Champaign, IL). The amount of CT adsorbed to the TiO_2 is calculated by subtracting the measured solution concentration of CT from the total amount of CT added to the solution. To construct the entire adsorption isotherm, further aliquots of CT are added. Samples are taken for analysis on HPLC to confirm the absence of oxidative coupling products according to previously described methods (25). Similar adsorption experiments at a fixed concentration of CT and a varying pH are carried out from pH 2 to pH 10. The pH is returned to 2 and a measurement is taken in order to demonstrate the reversibility of adsorption.

FTIR-ATR measurements.

The approach is based upon the methods of Hug and Sulzberger (21). (For a general review of reflectance spectroscopy, see ref. 33.) The ZnSe crystals (trapezoid, 45°, 52.5 mm × 20 mm × 2mm) are freshly coated for each experiment with 2.65 mg TiO_2 on each side by application of 50 μL of 53 g/L TiO_2. The spectra are recorded using 1024 scans (ca. 40 min.) at 8 cm^{-1} resolution on a PE 1600 FTIR spectrophotometer equipped with a Janos F90 ATR optical bench and liquid sample

holder. In a typical experiment at a constant pH, the sparged CT solution (10 mM KCl) is flowed through the cell continuously. After at least a 30 min equilibration period, spectra are recorded. The reported spectra are calculated from the subtraction of the spectrum obtained with 10 mM KCl and no CT from the spectrum recorded in the presence of CT. In a typical experiment at a constant [CT] and varying pH, the experiment is carried out by recirculating a 4 L reservoir through the sample cell.

FTIR spectra calculations.

Full details of the computational approach are reported by Hug and Sulzberger (21). The elements of the data matrix, A_{ij}, are absorbance values where i corresponds to the wavenumber and j corresponds to the experimental conditions (e.g., [CT]). Thus, each row contains the absorbance at a fixed wavenumber as a function of changing experimental conditions and each column contains a spectrum. The A matrix may be decomposed by singular-value decomposition as $\mathbf{A} = \mathbf{U}\,\mathbf{S}\,\mathbf{V}^{\mathbf{T}}$ where **U** contains the (unrotated) spectral components, **S** the singular values, and $\mathbf{V}^{\mathbf{T}}$ the loadings. **U**, **S**, and $\mathbf{V}^{\mathbf{T}}$ are reduced according to the number of components implied by S_{ii} (34, 35). Furthermore, $\mathbf{A} = \mathbf{B}\,\mathbf{P}$ where **B** contains the physical spectral components (e.g., a surface-adsorbed CT and solution phase CT) and **P** contains the concentrations of those components as a function of experimental conditions. Before the experiment, **B** is unknown, but the form of P_{ij} is known. For example, when the first component has the form of a Langmuir isotherm, $P_{1j} = K\,[CT]_j/(1 + K\,[CT]_j)$ where $[CT]_j$ is known and K is unknown. There exists some matrix **C** such that $\mathbf{A} = \mathbf{U}\,\mathbf{S}\,\mathbf{C}\,\mathbf{C}^{-1}\,\mathbf{V}^{\mathbf{T}}$ so that $\mathbf{B} = \mathbf{U}\,\mathbf{S}\,\mathbf{C}$ and $\mathbf{P} = \mathbf{C}^{-1}\,\mathbf{V}^{\mathbf{T}}$. The matrix $\mathbf{C}^{-1}$ rotates $\mathbf{V}^{\mathbf{T}}$ into **P**. We wish to minimize the following objective function:

$$\left\|\mathbf{S}\left(\mathbf{V}^{\mathrm{T}} - \mathbf{CP}\right)\right\| \qquad (1)$$

The number of unknowns in the function equals the total number of elements in the C matrix plus the n unknowns in the **P** matrix (e.g., K). To carry out the minimization, we use Mathematica and the simplex method (36). If the model chosen for the **P** matrix is correct, then **P** and $\mathbf{V}^{\mathbf{T}}$ both span the same subspace and the **C** matrix obtained should yield real components in the **B** matrix. On the other hand, if the model incorporated in the **B** matrix is not correct, a poor minimum is expected and quite possibly negative components in the **B** matrix. Using this technique, we are thus able to decompose the FTIR spectra observed as a function of an experimental condition (e.g., [CT]) into the contributing component spectra and the parameters (e.g., K) of the model in the **P** matrix.

Results

Figure 1 (top) shows the IR spectrum of CT adsorbed to TiO_2 as a function of pH. Principal component analysis indicates one component accounts for 96% of the total variance. The remaining 4% arises from instabilities in the baseline. The sensitivity of detection (ca. 1 μM) has increased significantly because the CT adsorbed to the TiO_2 film is within the penetration depth of the evanescent wave eminating from the ATR crystal. By contrast, the sensitivity towards CT in solution is ca. 10 mM. Figure 1 (bottom) shows the relative extent of adsorption of CT on TiO_2 as a function of pH. The maximum adsorption is observed at pH = 8.

Figure 2 shows the IR spectra of H_2CT, HCT^-, and CT^{2-} in solution as determined from the singular-value decompostion of spectra of CT recorded from pH 2 to 14. The total concentration of CT was 40 mM. The minimization of eq 1 yields pK_{a1} = 8.2 and pK_{a2} = 12.7; the values obtained by Vasudevan and Stone from titration are 8.8 and 12.7, respectively (19).

Figure 3 (top) shows IR spectra of CT as a function of concentration (2 μM to 100 mM) in contact with a TiO_2 film on the ATR element at pH = 5.0 and is qualitatively representative of data recorded from pH = 3 to 8. The IR spectra are due to contributions from CT adsorbed to TiO_2 and to CT in solution. The spectra are decomposed using a single Langmuir-type binding site on TiO_2 and a linear component in solution. The binding constant obtained from this fitting procedure is 97,000 M^{-1}. Other adsorption models (i.e., Freundlich adsorption or two-site Langmuir models) yield negative peaks in the component spectra. The component spectra determined from the single Langmuir-type binding site are shown in Figure 3 (middle). Residuals (Figure 1, top) are calculated by **A** - **B** **P**. Figure 3 (bottom) shows the measured contribution of component #1 to the IR spectra and the calculated contribution based on the Langmuir sorption assumption. The Langmuir model underpredicts the observed spectra for 2 and 5 μM while it over-predicts the spectra for 50-500 μM. This error is not accounted for by baseline instabilities and indicates the Langmuir model does not provide a perfect fit. The model fit obtained from the data in Figure 4 and the model in Tables 1 and 2 shows an improved fit with the FTIR data.

The adsorption isotherms of CT at pH = 3, 5, and 8 are shown in Figure 4. At low concentrations (< 50 μM), a saturation effect is observed. At high concentrations (> 50 μM), linear sorption behavior is observed. The linear region continues to at least 4 mM (data not shown). In the linear region, CT adsorbs to a lesser extent at pH = 8 than at pH = 3 and 5. The interaction of protons and CT with the surface of TiO_2 is modeled according to the general double layer theory (32). The mass law equations, mole balance equations, and charge-potential relationship used in the model are shown in Table 1. A bidentate binuclear bond between CT and TiO_2 is denoted by $\equiv Ti_2CT$, and a bidentate mononuclear group is shown by ≡TiCT[-] and carries an overall -1 charge. Different sites of surface groups are denoted by the subscripts A and B. The binding constants of

CT at sites A and B are allowed to vary, but the acidity constants for each site are assumed to be the same. The results of considering several surface models constrained by the adsorption isotherms (Figure 4) are shown in Table 2. The best goodness of fit, as indicated by the minimum overall variance (32), is obtained for the model including one type of specifically binding bidentate binuclear site on the surface of TiO_2 as well as nonspecific partitioning from the solution to a surface monolayer of CT on the TiO_2. The fit obtained with this model is shown in Figures 3 and 4. The linear region observed in the batch adsorption data of Figure 4 is absent in the FTIR data (Figure 3, bottom).

The adsorption isotherms of 49.8 and 498 μM CT on TiO_2 as a function of pH are shown in Figure 5. At both high and low concentrations (i.e., 498 and 49.8 μM), CT is adsorbed most strongly over the range of pH from 7 to 9. At high concentrations, the amount adsorbed varies from 30 to 110 μM from pH = 2 to 8, whereas at low concentrations it varies from 10 to 45 μM. The sensitivity of adsorption to pH is thus greater at higher [CT]. The fits shown in Figure 5 are an empirical guide and do not arise from an underlying model. In fact, none of the models proposed in Table 2 can adequately reproduce the data shown in Figure 5 under the constraints that the acidity constants $pK_{a1} = 5.8$ and $pK_{a2} = 7.1$, as derived from the data in Figure 6.

The charge due to protons adsorbed on TiO_2 as a function of pH and ionic strength is shown in Figure 6 (top). The data are fit to the generalized electrical double layer model. The reactions are shown in Table 1. Model fits are shown (Figure 6, top) for optimized values of $[\equiv TiOH] = 75 \pm 5$ μM, $pK_{a1}^{int} = 5.8 \pm 0.4$, and $pK_{a2}^{int} = 7.1 \pm 0.4$. The charge due to adsorbed protons diverges from the model at basic pH for high electrolyte concentrations. The pH_{zpc} obtained from the best fit model is 6.4; other authors have reported for P25 that $pH_{zpc} = 6.6$ (37), 6.5 (18), and 6.4 (38). In Figure 6 (bottom), the fluoride adsorption isotherm is shown. The model calculations use the

values of pK_{a1}^{int} and pK_{a2}^{int} and optimize for [≡TiOH] and log K_{F-}, which are found to be 35 μM and 10.3 (M^{-2}), respectively.

Discussion

The IR spectra of H_2CT, HCT^-, and CT^{2-} in aqueous solution as deduced from SVD analysis of the pH dependent spectra are shown in Figure 2. The bands for H_2CT from 1472 through 1338 cm^{-1} have been assigned to the tangential C-C normal modes of the aromatic rings, the bands at 1276 and 1246 arise from radial stretching vibrations including the C-O groups, at 1198 from in-plane O-H vibrations, and at 1116 and 1084 from in-plane C-H bending (39). Monodeprotonation (Figure 2, middle) broadens all bands due to the formation of two resonance structures of the hydrogen-bonded bridged species. In addition, all bands are observed to shift to lower energies relative to the neutral form of CT due to the presence of a negative charge that electrostatically destabilizes the molecule and reduces the force constants (40). The spectrum of the doubly deprotonated species (Figure 2, bottom) shows a further shift to lower energies due to electrostatic repulsion. For example, the C-C normal mode shifts from 1490, to 1486, and finally to 1474 while the C-O bond moves from 1276, to 1270, to 1254 for the neutral, singly deprotonated, and doubly deprotonated species. The 1198 out-of-plane O-H wag is absent for the doubly deprotonated species.

The IR spectrum of CT adsorbed onto TiO_2 is shown in Figure 3 (middle, component #1). We conclude by the similarities between this spectrum and that of the doubly deprotonated CT^{2-} (Figure 2, bottom) that CT forms a bidentate structure on TiO_2. In this case, the band at 1484 arises from C-C normal modes and 1268 from C-O vibrations. The relative oscillator strengths between these bands and those at 1380 and 1292 in Figure 2 have increased five-fold. The peaks at 1484 and 1268 in the adsorbed

CT spectrum lie between the corresponding peaks for the singly and doubly deprotonated solution phase CT. A linear interpolation based on the peak positions of the solution phase species as a function of charge suggests the CT adsorbate carries a charge of -1.2. In a purely covalent bond, we would expect the charge to be 0. This analysis suggests that the bond may be described as having 60% ionic and 40% covalent character. Within experimental error, the peak positions in the IR spectrum of the CT adsorbate do not depend on pH.

The surface adsorbed component is shown in Figure 1 (top) to be qualitatively identical from pH = 2 to 10, though the extent of adsorption differs (Figure 1, bottom). Furthermore, the linewidths are of comparable broadness to those of CT in solution (Figure 2). The heterogeneity of surface energies is thus less than or equal to the distribution of energies found in a solvation shell of water (40).

As indicated by the IR spectrum of component #1 in Figure 3, CT forms a bidentate group at the surface of TiO_2. Bidentate mononuclear and binuclear structures are both possible, as follows:

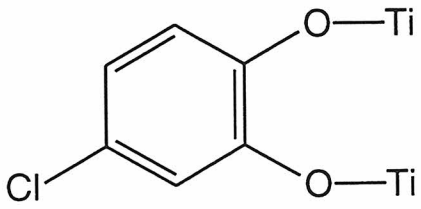

Bidentate Binuclear
$\equiv Ti_2CT$

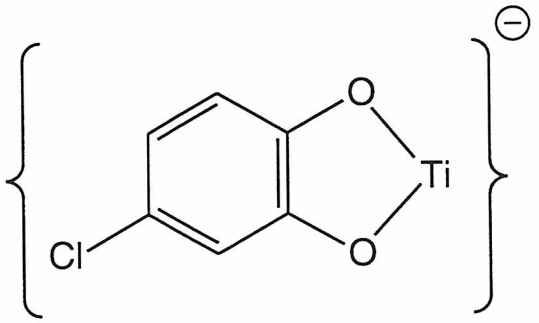

Bidentate Mononuclear
$\equiv TiCT^-$

The reaction stoichiometries for the formation of $\equiv Ti_2CT$ and $\equiv TiCT^-$ are as follows:

$$2 \equiv TiOH + H_2CT \rightarrow \equiv Ti_2CT + 2\ H_2O \quad (2)$$

$$\equiv TiOH + H_2CT \rightarrow \equiv TiCT^- + H^+ \quad (3)$$

The corresponding mass law equations are shown in Table 1 as K_A' and K_A, respectively. The concentration of the bidentate mononuclear surface group thus has an explicit dependence upon pH; however, both the binuclear and mononuclear surface groups depend implicity upon pH due to the speciation of ≡TiOH, H_2CT, and the surface charge with pH. The pH-dependent adsorption isotherm (Figure 4) should distinguish between the binuclear and mononuclear surface structures.

As shown in Table 2, the adsorption data fit neither a single-site bidentate mononuclear surface structure nor a single-site bidentate binuclear structure. The fit is improved by considering two surface sites, A and B, with different binding affinities for a bidentate mononuclear structure. However, the total concentration of TiO_2 surface sites (785 μM = 8 sites/nm^2) is much larger than measured for proton affinities (75 μM) or fluoride affinities (35 μM) in Figure 6. The best fit, as indicated by the minimum in V_y and a consistent concentration of surface sites (86 μM), is obtained for a model including a single-site bidentate binuclear surface complex and nonspecific multilayer partitioning from the solution phase according to the following mass law equation:

$$\equiv Ti_2CT + H_2CT \rightarrow CT'_{Ads} \qquad (4)$$

The mole balance equation is as follows:

$$H_2CT \rightarrow CT'_{Ads} \qquad (5)$$

Incorporated into FITEQL, the mass law equation provides increasing affinity for the TiO_2 surface as $[\equiv Ti_2CT]$ increases (i.e., as a monolayer forms) while the mole balance equation indicates the conversion of a solution phase H_2CT to a surface adsorbed species without changing $[\equiv Ti_2CT]_T$ (i.e., nonspecific adsorption).

In order to assess each of the proposed models in Table 2, the appropriate suite of reactions is selected from Table 1. These reactions are constrained by the results of the surface-charge titration (Figure 6, top) for which $pK_{a1} = 5.8 \pm 0.4$ and $pK_{a2} = 7.1 \pm 0.4$. The electric double layer model succeeds in adequately describing the titrations at low ionic strengths, but it underpredicts the surface charge at high ionic strengths and strongly negative surfaces. The TiO_2 employed in the experiments consists of 30 nm primary crystallites agglomerated into 1 μm porous structures (41, 42). The surface charge-potential relationship (i.e., capacitance) in the interstitial pores depends upon the local geometry and should be highly heterogeneous. The double layer model thus, at best, provides an averaged description of the structure of the TiO_2 since it incorporates Gouy-Chapman theory, which is based upon a flat plane. At low ionic strengths, the Debye-length is several times the size of the primary crystallites and, thus, the pore sizes so that the flat plane description may be adequate. At high ionic strengths, however, the Debye-length compresses and the heterogeneity of the TiO_2 is revealed. Deviation at high ionic strengths from the double layer theory are thus expected.

As shown in Figure 3 (bottom), the specifically adsorbed component observed in the IR spectra approaches saturation above 100 μM. Based upon the bidentate binuclear model description deduced from the data in Figure 4, we have calculated the expected concentration of $[\equiv Ti_2CT]$. However, because the path length of the ATR cell and the extinction coefficient of the adsorbed species are unknown, a direct comparison between the calculated concentration and the concentration observed in the IR measurements is not possible. Instead, the IR data are calibrated by using the adsorption measurements to provide a best fit of the observed shape. In this case, 1 unit of relative contribution in Figure 3 (bottom) corresponds to 62 μmol specifically adsorbed CT per gram of TiO_2. Although the $\equiv Ti_2CT$ surficial complex is identified by the singular-value decomposition of the IR spectra, the nonspecifically adsorbed $CT^{'}_{Ads}$ is not observed in the FTIR

measurements. A nonspecifically associated CT layer should have an IR spectrum similar to the solution phase molecule. In this case, the basis spectra of the two of the three components (i.e., specifically adsorbed, nonspecifically adsorbed, and solution phase CT) are nearly degenerate so that the SVD procedure reveals only two components. The linear component (Figure 3, middle, #2) exhibits broadening of the 1438, 1366, 1246, and 1198 cm^{-1} bands relative to the pure solution CT (Figure 2, top). The line broadening is consistent both with the heterogeneities in a multilayer environment and two similar components contributing to a single spectrum obtained by SVD.

The IR spectra (Figure 1, top) show CT at 10 μM adsorbs to the greatest extent near pH = 8 and adsorbs to a lesser extent under more acidic or more alkaline conditions. The IR measurements are supported by the batch adsorption experiments made as a function of pH (Figure 5) at [CT] = 49.8 μM. However, a cross-section of data at [CT] = 50 μM from Figure 4 (top) indicates that the highest concentration of adsorbed CT occurs at pH = 5. The reproducibility of the experiments is indicated by the error bars. The apparent inconsistencies between the data sets may be understood by considering the reaction conditions. In the adsorption data of Figure 4, the TiO_2 is held at a constant pH for the time course of the experiment (ca. 5 hours). In the case of Figures 1 and 5, the TiO_2 is exposed to the highly acidic conditions of pH = 2 for 30 min and the pH is then adjusted upwards. The highly acidic conditions may promote irreversible surface reconstruction. The adsorption behavior of CT on TiO_2 thus depends upon the sample history.

Kummert and Stumm studied the adsorption of catechol on γ-alumina (17). Based on the difference in surface charge during titration in the presence and absence of catechols, they conclude that catechol forms a mononuclear monodentate complex on γ-alumina that binds through a single phenolate bridge. However, they also seem to allow for a mononuclear bidentate structure analogous to solution complexes. A bidentate

binuclear structure is excluded based on titration data as well as the distance between adjacent hydroxo groups on γ-alumina. McBride and Wesselink studied the adsorption of catechol on a variety of alumina surfaces using FTIR (43). The IR spectrum of catechol adsorbed on amorphous alumina is similar to the spectrum we observed for CT on TiO_2. McBride and Wesselink postulate a bidentate structure based on the IR data as well as the much stronger adsorption seen for compounds with ortho functional groups. In contrast to the OH groups on γ-alumina, those of amorphous alumina are close enough to accommodate bidentate binuclear complexes.

Vasudevan and Stone (19) studied the adsorption of a variety of catechols including CT on TiO_2, and their data agree with those shown in Figure 5. Using the contraints of $pK_{a1} = 3.9$, $pK_{a2} = 8.7$, and 3-4 sites/nm^2, these authors conclude that CT binds to TiO_2 as negatively charged surface complex as follows:

$$>S + CT \longrightarrow [>S\text{-}CT]^- + H^+ \qquad (6)$$

where >S denotes a neutral TiO_2 surface group. Note the difference in pH dependence between this model and our proposed model of adsorption as given by Equation 2. As previously discussed, the pH dependence observed in Figures 4 and 5 differ due to exposure of the TiO_2 particles to extreme pH conditions in the case of Figure 5. The data in Figure 4 were used to model the pH dependence of CT adsorption in our experiments. The added information provided by FTIR data support our hypothesis of a bidentate, binuclear complex.

Unlike Hug and Sulzberger (21) who were able to distinguish multiple binding modes for sulfate and oxalate on TiO_2, we observe only one specific binding mode for adsorbed catechol in our experiments. The additional information provided by the

titration and batch adsorption experiments and the resulting modeling studies lends confidence to our hypothesis of one specifically adsorbed surface species.

In conclusion, 4-chlorocatechol adsorbs as a bidentate binuclear surface complex on TiO_2 at solution concentrations below 50 μM. Above that concentration, CT adsorbs nonspecifically in a multilayer environment. The specifically adsorbed CT appears to have 40% covalent and 60% ionic bond character. In ongoing work, we will study the photoreactivity of CT in the TiO_2/UV process. Based upon this work, when [CT] = 50 μM, maximum quantum efficiencies are expected to occur at pH = 5. When [CT] = 500 μM, catalyst poisoning may occur due to charge-carrier recombination if an electron acceptor is unable to penetrate the CT multilayer.

Acknowledgments

We are grateful to ARPA and ONR {NAV 5 HFMN N0001492J1901} for financial support. Drs. Ira Skurnick and Harold Guard provided generous support and encouragement. S. Martin is supported by a National Defense Science and Engineering Graduate Fellowship. J. Kesselman is the recepient of a National Science Foundation Predoctoral Fellowship. D. Park is a Summer Undergraduate Research Fellow. Wonyong Choi, Peter Green, and Nicole Peill provided critical analyses and stimulating discussion.

References

(1) Hoffmann, M. R.; Martin, S. T.; Choi, W.; Bahnemann, D. W. *Chem. Rev.* **1995**, *95*, 69.

(2) Martin, S. T.; Herrmann, H.; Choi, W.; Hoffmann, M. R. *J. Chem. Soc. Faraday Trans.* **1994**, *90*, 3315.

(3) Martin, S. T.; Herrmann, H.; Hoffmann, M. R. *J. Chem. Soc. Faraday Trans.* **1994**, *90*, 3323.

(4) Kesselman, J. M.; Shreve, G. A.; Hoffmann, M. R.; Lewis, N. S. *J. Phys. Chem.* **1994**, *98*, 13385.

(5) Herrmann, H.; Martin, S. T.; Hoffmann, M. R. *J. Phys. Chem.* **1995**, *99*, 16641.

(6) Choi, W.; Termin, A.; Hoffmann, M. R. *J. Phys. Chem.* **1994**, *98*, 13669.

(7) Peill, N. J.; Hoffmann, M. R. *Environ. Sci. Tech.* **1995**, *29*, 2974.

(8) Martin, S. T.; Lee, A. T.; Hoffmann, M. R. *Environ. Sci. Technol.* **1995**, *29*, 2567.

(9) Carraway, E. R.; Hoffman, A. J.; Hoffmann, M. R. *Environ. Sci. Technol.* **1994**, *28*, 786.

(10) Kormann, C.; Bahnemann, D. W.; Hoffmann, M. R. *Environ. Sci. Technol.* **1991**, *25*, 494.

(11) Hoffman, A. J.; Carraway, E. R.; Hoffmann, M. R. *Environ. Sci. Technol.* **1994**, *28*, 776.

(12) Cunningham, J.; Sedlák, P. *J. Photochem. Photobiol. A: Chem.* **1994**, *77*, 255.

(13) Cunningham, J.; Al-Sayyed, G. *J. Chem. Soc. Faraday Trans.* **1990**, *86*, 3935.

(14) Stafford, U.; Gray, K.; Kamat, P.; Varma, A. *Chem. Phys. Lett.* **1993**, *205*, 55.

(15) Moser, J.; Punchihewa, S.; Infelta, P. P.; Grätzel, M. *Langmuir* **1991**, *7*, 3012.

(16) Sigg, L.; Stumm, W. *Coll. Surf.* **1981**, *2*, 101.

(17) Kummert, R.; Stumm, W. *J. Coll. Int. Sci.* **1980**, *75*, 373.

(18) Stone, A. T.; Torrents, A.; Smolen, J.; Vasudevan, D.; Hadley, J. *Environ. Sci. Technol.* **1993**, *27*, 895.

(19) Vasudevan, D.; Stone, A. T. *Environ. Sci. Technol.* **1996**, *30*, 1604.

(20) Biber, M. V.; Stumm, W. *Environ. Sci. Technol.* **1994**, *28*, 763.

(21) Hug, S. J.; Sulzberger, B. *Langmuir* **1994**, *10*, 3587.

(22) Tunesi, S.; Anderson, M. *J. Phys. Chem.* **1991**, *95*, 3399.

(23) Gray, K., 1995, *personal communication.*

(24) Gruebel, K.; Davis, J.; Leckie, J. *Environ. Sci. Technol.* **1995**, *29*, 586.

(25) Martin, S. T.; Morrison, C. L.; Hoffmann, M. R. *J. Phys. Chem.* **1994**, *98*, 13695.

(26) Mills, A.; Morris, S. *J. Photochem. Photobiol. A: Chem* **1993**, *71*, 285.

(27) Mills, A.; Davies, R. H.; Worsley, D. *Chem. Soc. Rev.* **1993**, *22*, 417.

(28) Bates, R. G. *Determination of pH: Theory and Practice*; 2nd; John Wiley & Sons: New York, 1973.

(29) Taylor, W.; Battersby, A. *Oxidative Coupling of Phenols*; Marcel Dekker: New York, 1967.

(30) Yates, D. E., "The Structure of the Oxide/Aqueous Electrolyte Interface," Thesis, University of Melbourne, 1975.

(31) Herbelin, A.; Westall, J. C., FITEQL 3.1, Report No. 94-01, Department of Chemistry, Oregon State Univeristy, 1994.

(32) Dzombak, D.; Morel, F. *Surface Complexation Modeling: Hydrous Ferric Oxide*; John Wiley & Sons: New York, 1990.

(33) Wendlandt, W.; Hecht, H. *Reflectance Spectroscopy*; John Wiley & Sons: New York, 1966.

(34) Pullin, M.; Cabaniss, S. *Environ. Sci. Technol.* **1995**, *29*, 1460.

(35) Shrager, R. I.; Hendler, R. W. *Anal. Chem.* **1982**, *54*, 1147.

(36) Carley, A. F.; Morgan, P. H. *Computational Methods in the Chemical Sciences*; John Wiley & Sons: New York, 1989.

(37) Herrmann, V. M.; Boehm, H. P. *Z. Anorg. Allg. Chem.* **1969**, *368*, 73.

(38) Schindler, P. W.; Gamsjäger, H. *Kolloid - Z. u. Z. Polymere* **1972**, *250*, 759.

(39) Varsanyi, G. *Assignments for Vibrational Spectra of Seven Hundred Benzene Derivatives*; John Wiley & Sons: New York, 1974.

(40) Urban, M. W. *Vibrational Spectroscopy of Molecules and Macromolecules on Surfaces*, John Wiley & Sons: New York, 1993.

(41) Degussa Technical Bulletin No. 56, 1990.

(42) Bickley, R. I.; Gonzalez-Carreno, T.; Lees, J. S.; Palmisano, L.; Tilley, R. J. D. *J. Solid State Chem.* **1991**, *92*, 178.

(43) McBride, M.B.; Wesselink, L.G. *Environ. Sci. Technol.* **1988**, *22*, 703.

Table 1: Mass law and mole balance equations
for model fits shown in Table 2, Figure 4, and Figure 6.

Components: H^+, $\equiv TiOH_A$, $\equiv TiOH_B$, K^+, NO_3^-, F^-, H_2CT

Species: H^+, OH^-, $\equiv TiOH_A$, $\equiv TiOH_2^+{}_A$, $\equiv TiO_A^-$, $\equiv TiCT^-{}_A$, $\equiv Ti_2CT_A$, $\equiv TiOH_B$, $\equiv TiOH_2^+{}_B$, $\equiv TiO_B^-$, $\equiv TiCT^-{}_B$, $\equiv Ti_2CT_B$, K^+, NO_3^-, F^-, $\equiv TiF_A$, H_2CT, HCT^-, CT^{2-}, CT_{Ads}, CT'_{Ads}

Mass Law Equations

$[H^+]$	=	$[H^+]^1$							
$[OH^-]$	=	$[H^+]^{-1}$	a^{-2}					K_w	
$[K^+]$	=					$[K^+]^1$			
$[NO_3^-]$	=		a^{-2}				$[NO_3^-]^1$		
$[H_2CT]$	=				$[H_2CT]^1$				
$[HCT^-]$	=	$[H^+]^{-1}$	a^{-2}		$[H_2CT]^1$				$10^{-8.63}$
$[CT^{2-}]$	=	$[H^+]^{-2}$	a^{-6}		$[H_2CT]^1$			$10^{-21.33}$	
$[\equiv TiOH_A]$	=			$[\equiv TiOH_A]^1$					
$[\equiv TiOH_2^+{}_A]$	=	$[H^+]^1$	a^1	$[\equiv TiOH_A]^1$	γ^1			$(1/K_{a1}{}^{int})$	
$[\equiv TiO_A^-]$	=	$[H^+]^{-1}$	a^{-1}	$[\equiv TiOH_A]^1$	γ^1			$K_{a2}{}^{int}$	
$[\equiv TiCT^-{}_A]$	=	$[H^+]^{-1}$	a^{-1}	$[\equiv TiOH_A]^1$	γ^1	$[H_2CT]^1$		K_A	
$[CT_{Ads}]$	=	$[H^+]^{-1}$	a^{-1}	$[\equiv TiOH_A]^1$	γ^1	$[H_2CT]^2$			K_{Ads}
$[\equiv Ti_2CT_A]$	=			$[\equiv TiOH_A]^m$		$[H_2CT]^1$		K_A'	
$[CT'_{Ads}]$	=			$[\equiv TiOH_A]^m$		$[H_2CT]^2$			K_{Ads}'
$[\equiv TiOH_B]$	=			$[\equiv TiOH_B]^1$					
$[\equiv TiOH_2^+{}_B]$	=	$[H^+]^1$	a^1	$[\equiv TiOH_B]^1$	γ^1			$(1/K_{a1}{}^{int})$	
$[\equiv TiO_B^-]$	=	$[H^+]^{-1}$	a^{-1}	$[\equiv TiOH_B]^1$	γ^1			$K_{a2}{}^{int}$	
$[\equiv TiCT^-{}_B]$	=	$[H^+]^{-1}$	a^{-1}	$[\equiv TiOH_B]^1$	γ^1	$[H_2CT]^1$		K_B	
$[\equiv Ti_2CT_B]$	=			$[\equiv TiOH_B]^m$		$[H_2CT]^1$		K_B'	
$[F^-]$	=							$[F^-]^1$	
$[\equiv TiF_A]$	=	$[H^+]^1$		$[\equiv TiOH_A]^1$				$[F^-]^1$	K_{F-}

Mole Balance Equations

TOT[H]	=	$[H^+] - [OH^-] - [HCT^-] - 2[CT^{2-}] + [\equiv TiOH_2^+{}_A] - [\equiv TiO_A^-] - [\equiv TiCT^-{}_A] + [\equiv TiOH_2^+{}_B] - [\equiv TiO_B^-] - [\equiv TiCT^-{}_B] + [\equiv TiF_A]$
TOT[a]	=	$0.5\,[H^+] + 0.5\,[OH^-] + 0.5\,[K^+] + 0.5\,[NO_3^-] + 0.5\,[F^-] + 0.5\,[HCT^-] + 2[CT^{2-}]$
$TOT[\equiv TiOH_A]$	=	$[\equiv TiOH_A] + [\equiv TiOH_2^+{}_A] + [\equiv TiO_A^-] + [\equiv TiCT^-{}_A] + 2[\equiv Ti_2CT_A]$
$TOT[\equiv TiOH_B]$	=	$[\equiv TiOH_B] + [\equiv TiOH_2^+{}_B] + [\equiv TiO_B^-] + [\equiv TiCT^-{}_B] + 2[\equiv Ti_2CT_B]$
$TOT[K^+]$	=	$[K^+]$
$TOT[NO_3^-]$	=	$[NO_3^-]$
$TOT[F^-]$	=	$[F^-] + [\equiv TiF_A]$
$TOT[H_2CT]$	=	$[H_2CT] + [HCT^-] + [CT^{2-}] + [\equiv TiCT^-{}_A] + [\equiv Ti_2CT_A] + [\equiv TiCT^-{}_B] + [\equiv Ti_2CT_B] + [CT_{Ads}] + [CT'_{Ads}]$
$TOT[\gamma]$	=	$\equiv TiOH_2^+{}_A] - [\equiv TiO_A^-] - [\equiv TiCT^-{}_A] + [\equiv TiOH_2^+{}_B] - [\equiv TiO_B^-] - [\equiv TiCT^-{}_B] = \sigma(AS/F)$

Charge-Potential Relationship

$\sigma = 0.1174\, c^{1/2} \sinh(19.46\,\Psi)$

where σ is the surface charge (C/m^2), c is the ionic strength (M) and equals TOT[a], Ψ is the surface potential (volts), m is assumed to be 1 (16), a is the ionic strength correction term [Fiteql manual], γ is the electrostatic correction term given by $\exp(-F\Psi/RT)$, A is the surface area (m^2/g), S is the oxide loading (g/L), and $\equiv X$ denotes a surface species. Omitted equilibrium constants are unity. See further discussion in text.

Table 2: Summary of agreement between proposed adsorption models and experimental data (Figure 4). See Table 1 for definitions of symbols. V_y is the overall variance.

Description	Variance, Vy	[≡TiOH] (μM)	$[\equiv TiOH]_B$ (μM)	log K_A (-)	log K_B (-)	log K_A' (M^{-1})	log K_B' (M^{-1})	log K_{ads} (M^{-1})	log K_{ads}' (M^{-1})
1 bidentate mononuclear	1.55	264		-1.96					
2 bidentate mononuclear	0.54	751	34.1	-3.46	-0.66				
1 bidentate mononuclear 1 nonspecific binding	1.57	259		-1.93				-0.20	
1 bidentate binuclear	1.25	179				4.38			
1 bidentate binuclear 1 nonspecific binding	0.24	88.5				5.27			8.93
2 bidentate binuclear	1.13	86.0	108			4.65	3.97		
1 bidentate mononuclear 1 bidentate binuclear	1.27	179		-5.17		4.38			

Figures

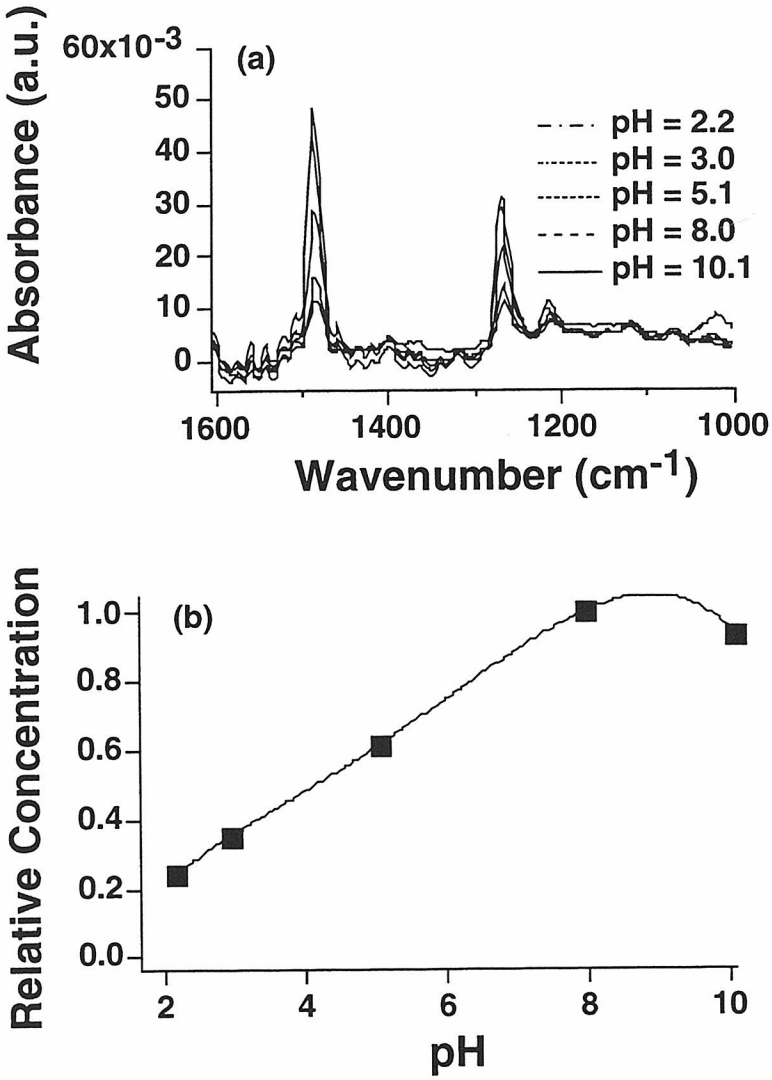

Figure 1. (a) IR spectra of 10 μM 4-chlorocatechol adsorbed to TiO_2 at several pH's in 10 mM KCl. Principal component analysis yields one component that explains 96% of the total variance. (b) Relative concentration of adsorbed 4-chlorocatechol as a function of pH (determined by the linear contribution of the first principal component).

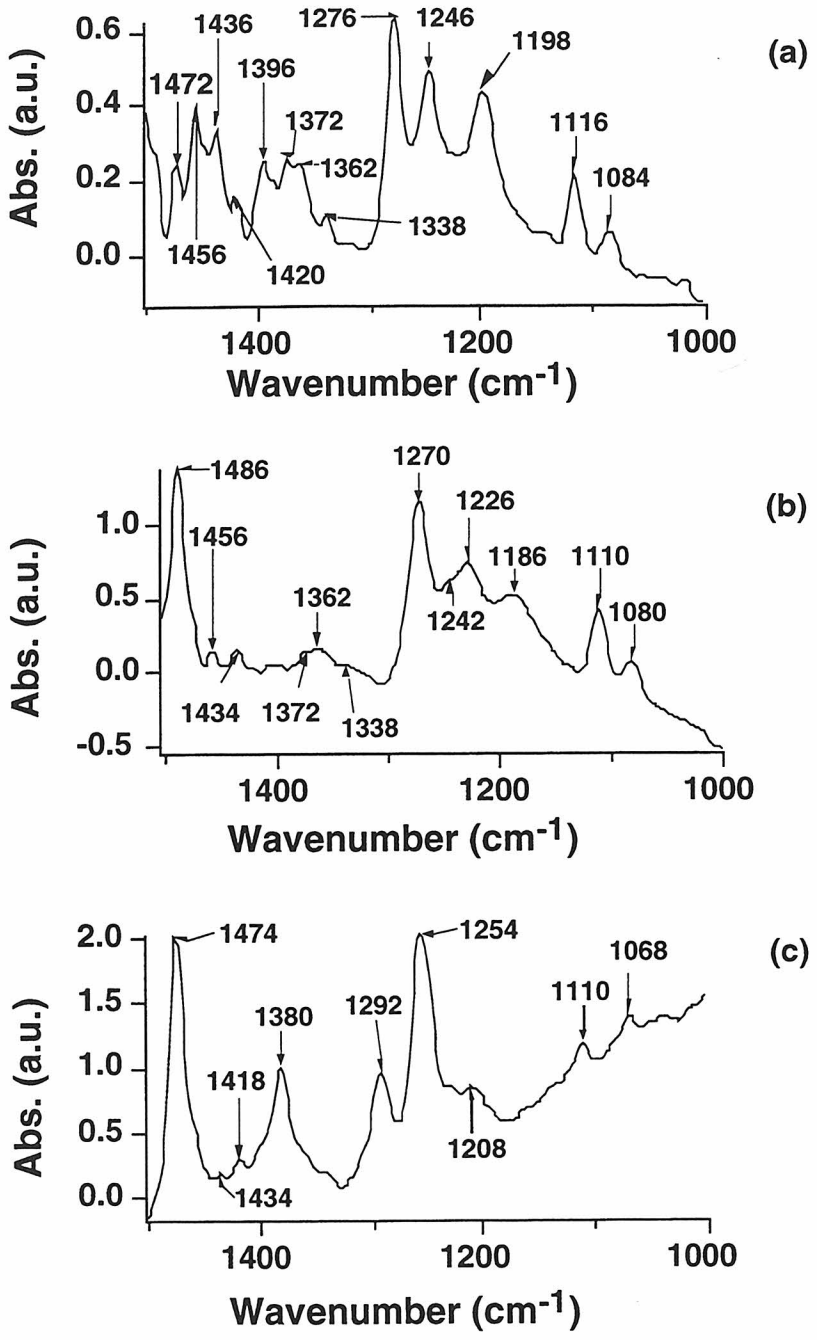

Figure 2. IR spectra of 4-chlorocatechol: (a) H_2CT, (b) HCT^-, (c) CT^{2-}. These basis spectra were determined from the singular-value decomposition of 12 spectra recorded at pH = 2.72, 5.94, 7.12, 8.02, 8.51, 9.12, 9.6, 11.5, 12.0, 12.6, 13.4, and 13.8.

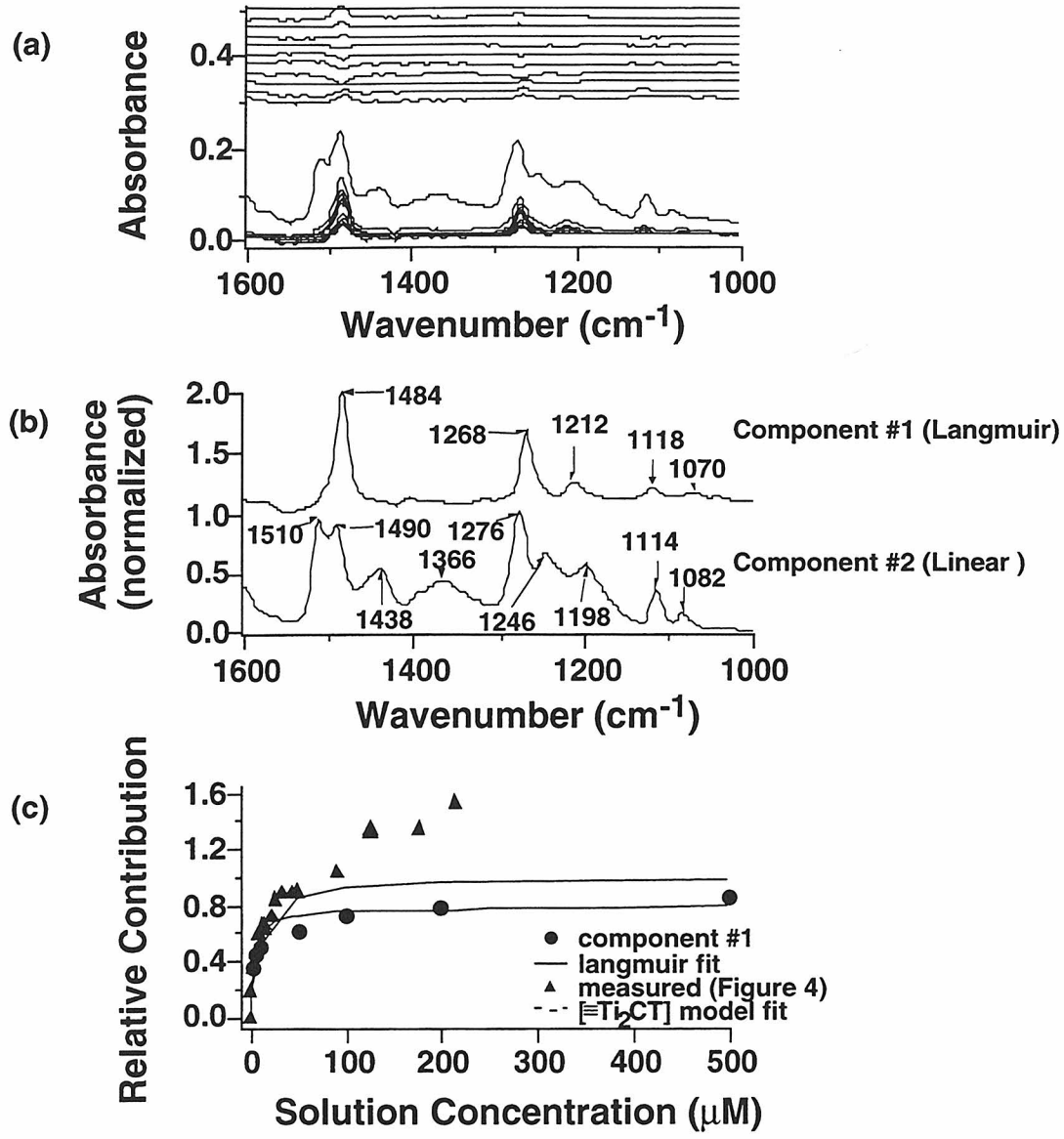

Figure 3. (a) IR spectra of 4-chlorocatechol adsorbed on TiO_2 at pH = 5.0 in 10 mM KCl at concentrations of 0.002, 0.005, 0.01, 0.05, 0.1, 0.2, 0.5, 1, 2, 10, and 100 mM and the residuals of a fit with a single Langmuirian site (K = 96,577 M^{-1}). (b) Component spectra determined from IR data set. (c) Relative concentration of component #1 as compared to measured adsorbed CT (Figure 4).

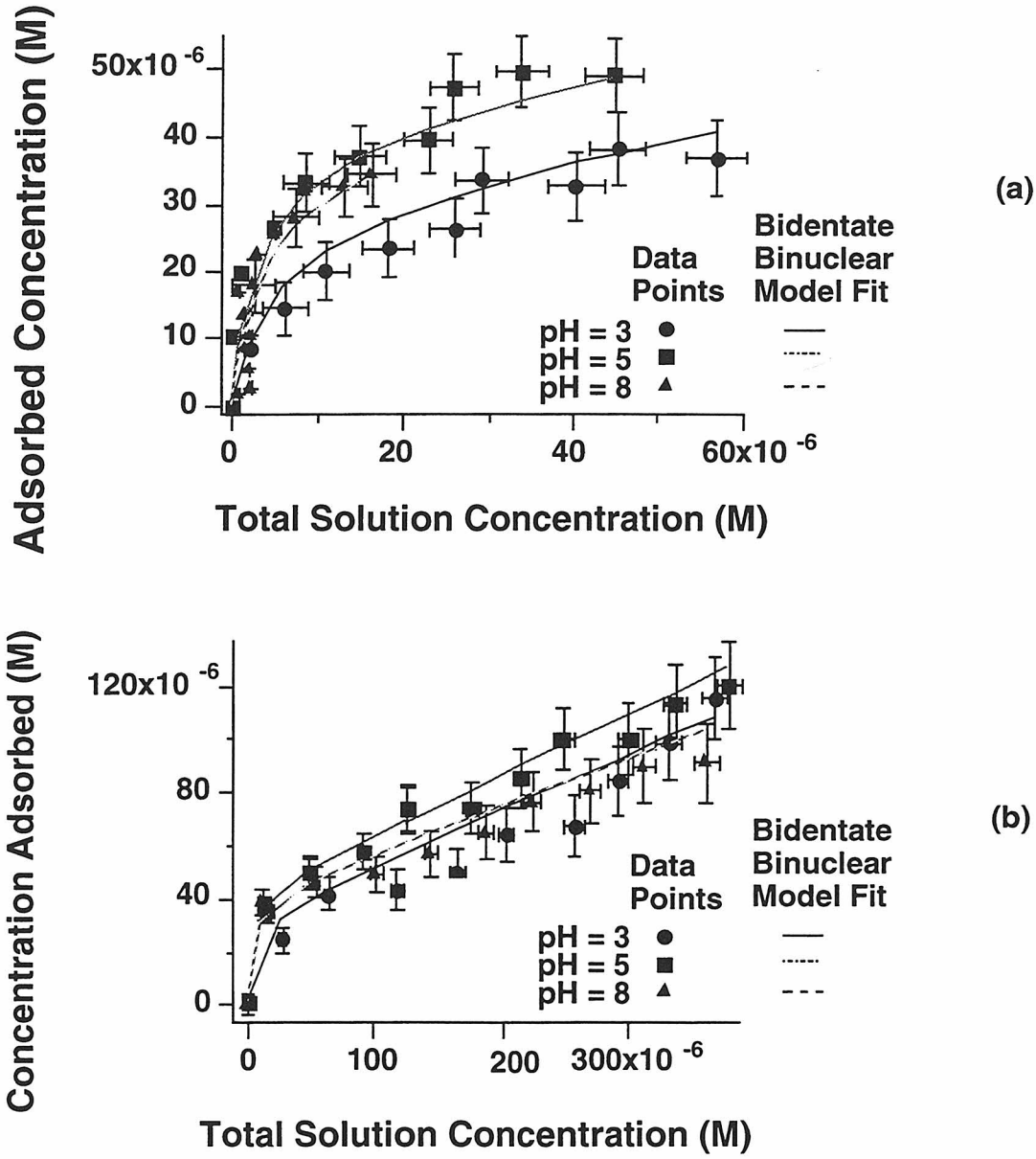

Figure 4:. Adsorption of 4-chlorocatechol on TiO_2 at pH = 3.0, 5.0, and 8.0 as a function of total solution concentration. (a) 60 μM maximum concentration. (b) 400 μM maximum concentration. $\sigma_{rel} = 0.02$, $\sigma_{abs} = 2.5$ μM, and $V_y = 0.24$ for model fit (see main text). Some error bars are omitted from the figure for clarity. Conditions: 1 g/L TiO_2, 10 mM KCl, and 25 °C.

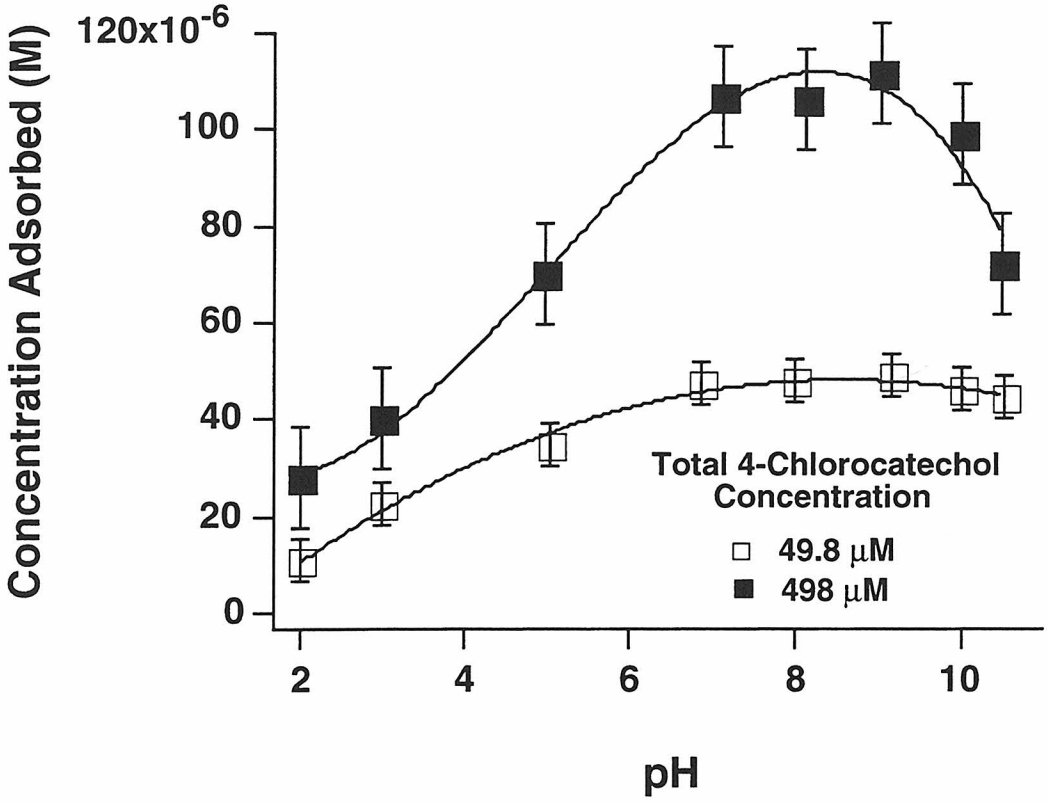

Figure 5. Adsorption of 4-chlorocatechol on TiO_2 from pH = 2 to pH = 11. The total concentration of 4-CC is shown in the legend. Conditions: 1 g/L TiO_2, 10 mM KCl, and 25 °C.

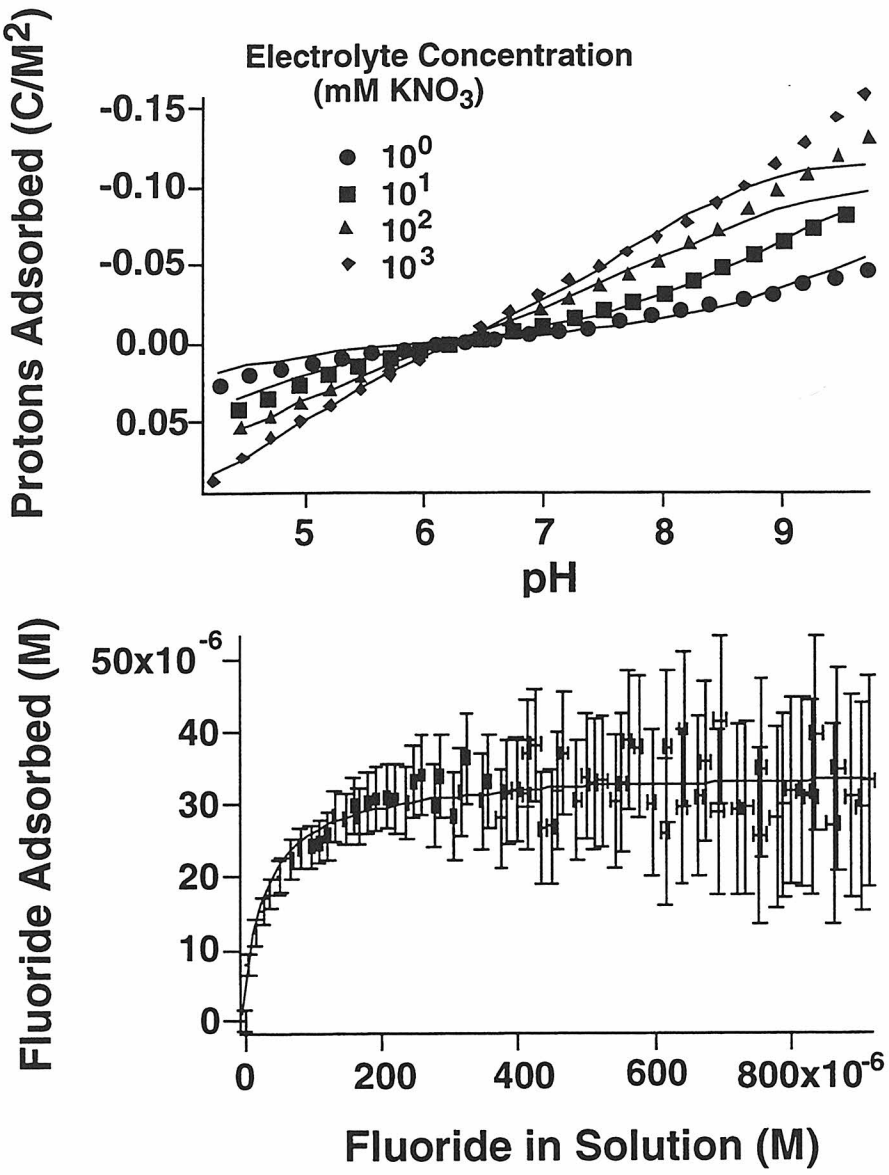

Figure 6. (a) Surface charge density due to adsorbed protons as a function of pH and electrolyte concentration as determined by acid titration. Model fits are shown for [≡TiOH] = 75 ± 5 μM, pK_{a1}^{int} = 5.8 ± 0.4, and pK_{a2}^{int} = 7.1 ± 0.4. (b) Adsorbed fluoride concentration as a function of solution concentration of fluoride (pH = 5.5 ± 0.2, 10 mM KNO_3). Model fit is shown for [≡TiOH] = 35 μM and log K_{F-} = 10.3 M^{-2}. Conditions: 1.25 g/L TiO_2, Ar sparging, and 25.0 ± 0.1 °C.

Chapter 5.

Photoelectrochemical Degradation of 4-Chlorocatechol at TiO_2 Electrodes: Comparison Between Sorption and Photoreactivity

Abstract

The TiO_2-catalyzed photodegradation of a strongly adsorbing substrate, 4-chlorocatechol, has been investigated as a function of solution concentration and pH at illuminated polycrystalline TiO_2 electrodes operated at a constant current density. The results are compared to the previously determined sorption behavior of 4-chlorocatechol. The initial rates of 4-chlorocatechol photodegradation measured at pH 3, 5, and 8 and solution concentrations of 20, 50, and 200 μM show a linear correlation with the concentration of the sorbed substrate.

Introduction

When irradiated with light of energy greater than 3.2 eV (band gap of TiO_2) (1-4), aqueous suspensions of TiO_2 particles catalyze the degradation of a variety of organic pollutants In general, however, the quantum yields for this process are low — typically less than 0.1 (5, 6) — and recent work has focused on understanding the basic processes occurring in TiO_2 photocatalysis and how various system parameters affect quantum efficiencies. Sorption of the organic substrate is generally considered to be an important parameter in determining photocatalytic degradation rates (as evidenced by the frequent use of the Langmuir-Hinshelwood kinetic model (3, 7, 8)), and the sorption of organic molecules to the TiO_2 surface has been investigated by many authors (9-18). Studies correlating experimental sorption and degradation data obtained under the same conditions, however, are limited.

Previous work in this laboratory has determined the sorption properties of 4-chlorocatechol on TiO_2 over the pH range of 2 to 10 and for 4-chlorocatechol solution concentrations up to 4 mM (12). Quantitative measurements of 4-chlorocatechol sorption were obtained by measuring the loss of 4-chlorocatechol from solution upon equilibration with TiO_2 particles. Attenuated total reflectance Fourier transform infrared spectroscopy (ATR-FTIR) was used to study the modes of 4-chlorocatechol sorption to the surface. The data were modeled using one specifically adsorbed component bound as a bidentate, binuclear complex (Fig. 1), and one non-specifically sorbed component that adheres to the initially formed 4-chlorocatechol monolayer.

The present contribution reports TiO_2-catalyzed photodegradation rates for 4-chlorocatechol at pH 3, 5, and 8 and for 4-chlorocatechol solution concentrations of 20, 50, and 200 μM. Quantitative correlations between these photodegradation rates and previously obtained sorption data (12) are made.

As reported previously (12), 4-chlorocatechol is subject to homogeneous oxidative coupling in basic, aerated solutions (12). In order to avoid complications due to this competing reaction, sorption and photodegradation studies were performed in nitrogen-purged solutions. It has been shown, however, that sustained photodegradation in TiO_2 slurry reactors requires the presence of oxygen or an alternative electron acceptor (2, 3). Photogenerated electrons can be removed from TiO_2 electrodes, in the absence of solution phase electron scavengers, by application of a potential bias (19). Illuminated TiO_2 electrodes have been shown to degrade 4-chlorophenol in nitrogen purged solutions (20, 21). TiO_2 electrodes are thus used in the present study to investigate the effect of sorption on photoreactivity for the TiO_2/4-chlorocatechol system.

Experimental Section

Chemicals

4-Chlorocatechol (TCI America, Portland, OR) was purified by recrystallization from heptane. Titanium dioxide (Degussa P25, Ridgefield Park, NJ) was used as received. Potassium chloride and potassium hydroxide (Mallinckrodt, Paris, KY), and hydrochloric acid (J. T. Baker, Phillipsburg, NJ) were also used as received. All solutions were prepared with MilliQ^{UV} Plus 18.2 MΩ•cm resistivity water (Millipore, Van Nuys, CA).

Fabrication of TiO_2 Electrodes

The polycrystalline TiO_2 electrodes used in this study were made by applying 0.5 mL of a 0.024 g/mL suspension of Degussa P25 TiO_2 to a glass slide that had been

coated with a conductive film of indium tin oxide (ITO) on one side ($\leq 20\ \Omega$/square) and an anti-reflection coating on the other side (Delta Technology, Lmtd., Stillwater, MN). The TiO_2 coated slides were annealed at 400 °C for 1 hour (20, 21). The resulting TiO_2 film covered an area of approximately 4.4 cm^2. Electrical contact was made by attaching a copper wire with silver print to an uncoated section at the top of the slide. The contacting wire and the edges of the electrode were then sealed with epoxy (Dexter Corp., Seabrook, NH). Because the TiO_2 did not adhere well at the edges of the film, the amount of TiO_2 on the electrode is less than that applied. However, after the edges had been sealed with epoxy, the electrodes were reasonably stable over a series of experiments, as shown by the reproducibility of the degradation rate data. Due to the variation between electrodes, however, comparisons are made only for data that were taken with the same electrode.

Electrochemical Cell and Instrumentation

Degradation experiments were carried out in a two compartment Pyrex cell. The polycrystalline TiO_2 working electrode described above and the Standard Calomel reference Electrode, SCE, (+ 0.24 vs. NHE) were separated from the Pt foil counter electrode by a fine porosity glass frit. The TiO_2 electrodes were illuminated from the back (through the ITO) to achieve more stable photocurrents. The volume of solution in the working compartment was 50 mL. Reactions were carried out in nitrogen-purged solutions with background electrolyte concentrations of 10 mM potassium chloride. The TiO_2 electrode was pre-equilibrated for one hour in 150 mL of solution of the same concentration and pH as the reaction medium. The pH of the solution in the working compartment was monitored and controlled by a Beckman combination pH electrode

connected to a Radiometer model PHM84 pH meter, TTT80 titrator, and ABU80 autoburette (Westlake, OH) charged with potassium hydroxide (approx. 40 mM).

A Pine Instruments Co. RDE Potentiostat/Galvanostat (Grove City, PA) was used for experiments performed at constant current. Controlled potential experiments were performed on a BAS model CV50 Potentiostat (Lafayette, IN).

UV Illumination was provided by a 1000 Watt xenon arc lamp fitted with a 10 cm water IR filter (Model 6269, Oriel, Stratford, CT). Two additional glass IR filters reduced heat buildup in the reaction vessel, and a 340 nm cut-off filter was used to prevent direct photochemical degradation of the 4-chlorocatechol.

Analytical Methods

Degradation rates for 4-chlorocatechol were determined by measurement of the loss of 4-chlorocatechol from the reaction solution. The concentration of 4-chlorocatechol as a function of time was determined by HPLC. Samples (0.5 mL) were withdrawn from the reaction vessel at specified time intervals, filtered with Nalgene 0.2 μM nylon filters (Rochester, NY) to remove any particles that might clog the column, and immediately acidified with 5 μM concentrated hydrochloric acid to prevent oxidative coupling. The HPLC instrument was a Hewlett-Packard Series II 1090 Liquid Chromatograph equipped with a Hewlett-Packard ODS Hypersil, 5 μm, 100 x 2.1 mm column. The eluants consisted of aqueous phosphoric acid (pH 3) and HPLC grade acetonitrile.

Results

Photoelectrochemical Characterization of TiO_2 Electrodes

The photoelectrochemical behavior of our polycrystalline TiO_2 electrodes was determined from current-potential curves obtained both in the dark and under UV illumination. Figure 2 shows the results for an electrode in a N_2-purged solution of background electrolyte (10 mM KCl). The cathodic current in the absence of illumination (Figure 2a) is due to the reduction of water. The band edge positions of TiO_2 shift (relative to a pH independent reference such as SCE) by -59 mV for each unit increase in pH (22) . The dark reduction curves in Figure 2a show qualitatively the same trend. Figure 2b shows the photocurrent obtained for this electrode as a function of pH. The limiting photocurrent depended on the pH of the solution, with the maximum limiting photocurrent occurring at pH 5. These results indicate that, for these polycrystalline electrodes, the efficiency at which the photogenerated electrons are collected at the back contact depends on the protonation of the TiO_2 surface. For this reason, 4-chlorocatechol degradation rates (vide infra) were compared for electrodes operated at the same current instead of at the same potential. At sufficiently positive biases, 4-chlorocatechol can be directly oxidized at these TiO_2 electrodes even in the absence of illumination (Figure 3), presumably by electron tunneling into the conduction band. The pH dependence of the onset potential for oxidation also qualitatively follows the pH dependence of the band edge positions of TiO_2. To preclude the possibility of direct oxidation of 4-chlorocatechol during the photodegradation experiments, the potential of the working electrode was monitored to ensure that it remained more negative than the onset potential for direct oxidation.

Photoelectrochemical Degradation of 4-chlorocatechol at TiO_2 Electrodes

Figure 4 is a representative graph of the time dependence of the 4-chlorocatechol concentration in the presence of an illuminated TiO_2 electrode operated at a constant current of 50 μA. The initial concentration of 4-chlorocatechol in solution was 50 μM,

and the solution was maintained at pH 5. Similar experiments were carried out at initial 4-chlorocatechol solution concentrations of 20, 50, and 200 μM and solution pH values of 3, 5, and 8. Degradation rates were determined from the slope of linear least squares fits to the data representing loss of the first 10 to 25% of 4-chlorocatechol from the solution. The degradation rate of 4-chlorocatechol depends both on the initial solution concentration of 4-chlorocatechol ($[4-CC]^{o}_{soln}$) and on the pH, as shown in Figure 5. For a given pH value, the degradation rate increases as the concentration of 4-chlorocatechol in solution increases. The pH dependence of the reaction rate, -d[4-CC]/dt, follows the trend: pH 8 > pH 5 > pH 3.

Figures 6a-c show plots of the initial degradation rates vs. the total concentration of 4-chlorocatechol sorbed to the TiO_2 (specifically + non-specifically bound) as determined from the sorption data in Martin et al. (12) and assuming 0.24 g TiO_2/L* in the present experiments. The error bars shown are estimated from the percent standard deviation determined from four trials employing experimental conditions of 20 μM initial solution concentration and pH 5. A linear fit of the degradation rates vs. sorbed 4-chlorocatechol concentration, $[4\text{-}CC]_{ads}$, at each pH according to

$$-\frac{d[4-CC]}{dt} = k'_{ads}[4-CC]_{ads} \qquad (1)$$

where k'_{ads} is the experimentally observed pseudo first-order degradation rate constant, yields k'_{ads} = 0.004 ± 0.001, 0.006 ± 0.001, and 0.007 ± 0.002 min^{-1} at pH 3, 5, and 8 respectively.

The experimentally-observed degradation rates at each pH are better correlated to the sorbed 4-chlorocatechol concentration than to the corresponding aqueous-phase

* Based on the amount of TiO_2 applied to each electrode and the volume of the reaction solution. While the actual concentration of TiO_2 will be somewhat less than 0.24 g/L (see experimental), the scaling factor is the same for all experiments and thus the comparisons are valid.

concentration. However, given the quality of the fits in Figure 6, the possibility of both sorbed and solution components contributing to the observed degradation rate could not be ruled out. The experimentally-determined degradation rates at each pH were analyzed in terms of the sum of the contributions of degradation due to sorbed and solution phase components according to the following two-term rate law:

$$v_i = -\frac{d[4-CC]}{dt} = k'_{ads}[4-CC]_{ads} + k_{soln}[4-CC]_{soln} \qquad (2)$$

subject to the following minimization:

$$\sum_{i=1}^{n}\left[v_i - \left(k'_{ads}[4-CC]_{ads,i} + k_{soln}[4-CC]_{soln,i}\right)\right]^2 \qquad (3)$$

using the Microsoft Excel solver application and constraining k'_{ads} and k_{soln} to be ≥ 0. In eq 2, v_i is the observed degradation rate of 4-chlorocatechol for experiment i and k_{soln} is the experimental rate constant for the pseudo first-order reaction of the solution phase 4-chlorocatechol. This analysis showed that $k_{soln} = 0$ at each pH and that $k'_{ads} = 0.0043$, 0.0053, and 0.0076 at pH 3, 5, and 8, respectively. Thus, the 4-chlorocatechol degradation rates can be described simply as linear functions of the sorbed concentrations with negligible contributions from solution phase degradation pathways.

Discussion

Initial degradation rates for photocatalysis on TiO_2 often follow Langmuir-Hinshelwood kinetics (6, 8, 23, 24). This dependence indicates that the reaction between surface sorbed substrates and photogenerated oxidants is dominant (2, 3). The Langmuir-Hinshelwood kinetic analysis has the following form:

$$\frac{-d[4-CC]}{dt} = k\theta_{4-CC} = k\left(\frac{K[4-CC]_{eq}}{1+K[4-CC]_{eq}}\right) \quad (4)$$

where k (moles/L•min) is the rate constant for reaction and is dependent on the catalyst used and the light intensity, $\theta_{4\text{-}CC}$ is the fraction of total surface sites occupied by the sorbate, K is the Langmuir-Hinshelwood sorption equilibrium constant, and $[4\text{-}CC]_{eq}$ is the equilibrium bulk solution concentration of 4-chlorocatechol (3). The constants, k and K, are readily determined from a double-reciprocal analysis of eq 4.

$$\frac{1}{\left(\frac{-d[4-CC]}{dt}\right)} = \frac{1}{k} + \frac{1}{kK[4-CC]_{eq}} \quad (5)$$

The concentration of sorbed 4-chlorocatechol (M) is given by

$$[4-CC]_{ads} = \theta C_{sites} \quad (6)$$

where C_{sites} is the total molar concentration of TiO_2 surface sites in the reaction medium. Thus, the reaction rate can also be written as

$$\frac{-d[4-CC]}{dt} = k'_{ads}[4-CC]_{ads} \quad (7)$$

where $k'_{ads} = k/C_{sites}$ and k'_{ads} has units of min^{-1}.

On the other hand, several authors have cautioned against interpreting conformity to the Langmuir-Hinshelwood equation as proof of a surface-mediated reaction mechanism (3, 25). Turchi et al. (25) have derived rate expressions for four different

reaction mechanisms—including the reaction of free •OH with solution phase substrate—that follow the general saturation form of the Langmuir-Hinshelwood equation.

There are several reports of the simultaneous investigation of sorption and photoreactivity on TiO_2, and the results seem to indicate that reaction mechanisms are more complicated than a simple Langmuir-Hinshelwood analysis indicates. Tunesi and Anderson (13) studied the sorption and photoreactivity of a variety of substituted benzenes including phenol and salicylate. The sorption of salicylate was studied at pH 3.7 and 5.7 and the data were fit to Freundlich isotherms (which are a reduced form of the Langmuir equation when $1 >> KC_{eq}$). Salicylate sorbed to a greater extent at low pH, and for an initial solution concentration of 40 μM (unsaturated surface), the first order degradation rate was also faster at low pH suggesting a positive correlation between sorbed concentration and the observed degradation rate. However, at low pH, as the solution concentration of salicylate was increased, the first order degradation rate decreased. The authors suggested that at higher concentrations, salicylate sorption blocked sites for •OH production and thus inhibited degradation. At high pH, where salicylate was not strongly sorbed, an increase in salicylate concentration resulted in an increase in the first-order degradation rate. The authors postulate that at low pH, salicylate degradation occurs through a direct oxidation mechanism of sorbed salicylate. At higher pH, when salicylate is not strongly sorbed, degradation occurs via a solution phase •OH mechanism. Phenol was found not to sorb appreciably to TiO_2. Its degradation rate was independent of the solution pH, and was similar to the degradation rate of salicylate at higher pH (13).

Cunningham and co-workers (14-16) have also investigated the sorption and photoreactivity properties of substituted benzenes on TiO_2. At low light intensities, the initial degradation rate of 4-chlorophenol as a function of solution concentration fit the Langmuir-Hinshelwood kinetic model despite the fact that the sorption of 4-chlorophenol

on TiO_2 was not well fit by a Langmuir isotherm (14). On the other hand, the sorption behavior of salicylate could be fit by a Langmuir isotherm, while the degradation rate as a function of solution concentration did not fit the Langmuir-Hinshelwood equation (15). In addition, the quantum yields for photodegradation of salicylate and other strongly sorbing substituted benzenes were less than those measured for non-sorbing chlorophenols. The authors proposed that hole trapping by sorbed substrates increased the charge carrier recombination rate and thus lowered the quantum yields for degradation (15). Investigation of the sorption and photoreactivity of benzyl alcohol, in both aqueous and acetonitrile solutions, indicated additional reactivity (over that predicted by a Langmuir-Hinshelwood equation) in aqueous solutions due to •OH release (16).

As reported in our earlier study (12), 4-chlorocatechol strongly sorbs to TiO_2 over the pH range of 3 to 8. The experimentally observed sorption was modeled using two components— one that specifically adsorbed to the TiO_2 surface according to a Langmuir isotherm and one that displayed a linear increase with solution concentration which was ascribed to non-specific binding to the monolayer of 4-chlorocatechol formed on the surface. Under the conditions of our experiments, the rate of 4-chlorocatechol photodegradation correlates with the concentration of 4-chlorocatechol sorbed to TiO_2 [where the sorbed concentration is the sum of both sorbed components]. In contrast to the results of Tunesi et al.,(13) no evidence was obtained for a decrease in oxidation rate caused by the blocking of photoactive sites due to 4-chlorocatechol sorption. An additional difference between our experiments and the studies summarized above is that our photodegradation studies were performed at a TiO_2 electrode operated at a constant current density. The observed dependence of the photocurrent on pH (vide supra) suggests that, in the absence of sorbed substrate, the rate of recombination of electrons and holes is pH-dependent. By operating our cell at a constant current density, however,

we have normalized out this effect (and the possible effect of increased recombination due to hole trapping by sorbed substrates proposed by Cunningham et al.). Our experiments indicate that for a given flux of holes (h_{vb}^+)/•OH to the surface, the rate of 4-chlorocatechol degradation is linearly dependent on the sorbed concentration of 4-chlorocatechol.

The fitted values for k'_{ads} show a slight increase with pH suggesting that k'_{ads} may be pH dependent. Additional experiments would be needed, however, to verify the statistical significance of this trend. The pH dependence of the homogeneous, hydroxyl-radical mediated oxidation of 4-chlorophenol has been previously studied by pulse radiolysis (26). Equal degradation rates were observed for 4-chlorophenol at pH 3 and pH 6, however, a slower degradation rate was observed at pH 9. Analysis of the transient intermediates indicated that at pH values below the pK_a of 4-chlorophenol, the reaction proceeded through a 4-chlorodihyroxycyclohexadienyl radical intermediate, while at higher pH values, the dominant intermediate was the 4-chlorophenoxyl radical. Thus the change in degradation rate could be explained by a change in the reaction mechanism. Since the first pK_a of 4-chlorocatechol is 8.8,(11) however, all of our degradation experiments were performed at pH values below the first pK_a. Interpretation of a possible pH dependence of k'_{ads} would be merely speculative at this point without a better understanding of the oxidation mechanisms at the surface of TiO_2 and additional experiments performed under controlled potential conditions to preclude changes in the driving force of the direct oxidation reaction due to the pH dependence of the band edge positions of TiO_2.

In conclusion, TiO_2-catalyzed photodegradation rates for 4-chlorocatechol have been determined at polycrystalline TiO_2 electrodes operated at 50 μA for initial solution concentrations of 20, 50, and 200 μM and for pH values of 3, 5, and 8. These results were compared to the extent of 4-chlorocatechol sorption previously determined under

similar conditions(12). Our results indicate that the rate of 4-chlorocatechol degradation can be described as a first-order reaction with respect to the concentration of sorbed 4-chlorocatechol. The experimentally determined rate constants are 0.004 ± 0.001, 0.006 ± 0.001, and 0.007 ± 0.002 min^{-1} at pH 3, 5, and 8, respectively.

Acknowledgments

We are grateful to ARPA and ONR {NAV 5 HFMN N0001492J1901} for financial support. J. Kesselman acknowledges NSF for a predoctoral fellowship. We would also like to acknowledge our earlier collaboration with Dr. Scot T. Martin.

References

(1) Matthews, R. W. *Wat. Res.* **1986**, *20*, 569-578.

(2) Hoffmann, M. R.; Martin, S. T.; Choi, W.; Bahnemann, D. W. *Chem. Rev.* **1995**, *95*, 69-96.

(3) Ollis, D. F.; Pelizzetti, E.; Serpone, N. In *Photocatalysis: Fundamentals and Applications*; N. Serpone and E. Pelizzetti, Eds.; John Wiley & Sons: New York 1989; p 603-637.

(4) Ollis, D. F. In *Homogeneous and Heterogeneous Photocatalysis*; E. Pelizzetti and N. Serpone, Eds.; D. Reidel Publishing Company: 1986; p 651-656.

(5) Choi, W.; Termin, A.; Hoffmann, M. R. *J. Phys. Chem.* **1994**, *98*, 13669-13679.

(6) Kormann, C.; Bahnemann, D. W.; Hoffmann, M. R. *Environ. Sci. Technol.* **1991**, *25*, 494-500.

(7) Al-Ekabi, H.; Serpone, N.; Pelizzetti, E.; Minero, C.; Fox, M. A.; Draper, R. B. *Langmuir* **1989**, *5*, 250-255.

(8) Al-Sayyed, G.; D'Oliveira, J.-C.; Pichat, P. *J. Photochem. Photobiol. A: Chem.* **1991**, *58*, 99-114.

(9) Tunesi, S.; Anderson, M. A. *Langmuir* **1992**, *8*, 487-495.

(10) Hug, S. J.; Sulzberger, B. *Langmuir* **1994**, *10*, 3587-3597.

(11) Vasudevan, D.; Stone, A. T. *Environ. Sci. Technol.* **1996**, *30*, 1604.

(12) Martin, S. T.; Kesselman, J. M.; Park, D. S.; Lewis, N. S.; Hoffmann, M. R. *Env. Sci. Technol.* **1996**, *30*, 2535-2542.

(13) Tunesi, S.; Anderson, M. *J. Phys. Chem.* **1991**, *95*, 3399-3405.

(14) Cunningham, J.; Sedlák, P. *J. Photochem. Photobiol. A: Chem.* **1994**, *77*, 255-263.

(15) Cunningham, J.; Al-Sayyed, G. *J. Chem. Soc. Faraday Trans.* **1990**, *86*, 3935-3941.

(16) Cunningham, J.; Srijaranai, S. *J. Photochem. Photobiol. A: Chem.* **1991**, *58*, 361-371.

(17) Stafford, U.; Gray, K. A.; Kamat, P. V.; Varma, A. *Chem. Phys. Lett.* **1993**, *205*, 55-61.

(18) Moser, J.; Punchihewa, S.; Infelta, P. P.; Grätzel, M. *Langmuir* **1991**, *7*, 3012-3018.

(19) Kesselman, J. M.; Shreve, G. A.; Hoffmann, M. R.; Lewis, N. S. *J. Phys. Chem.* **1994**, *98*, 13385-13395.

(20) Vinodgopal, K.; Stafford, U.; Gray, K. A.; Kamat, P. V. *J. Phys. Chem.* **1994**, *98*, 6797-6803.

(21) Vinodgopal, K.; Hotchandani, S.; Kamat, P. V. *J. Phys. Chem.* **1993**, *97*, 9040-9044.

(22) Finklea, H. O. In *Semiconductor Electrodes*; H. O. Finklea, Eds.; Elsevier: New York 1988; p 43-146.

(23) Mills, A.; Morris, S. *J. Photochem. Photobiol. A: Chem.* **1993**, *71*, 75-83.

(24) Matthews, R. W. *J. Catalysis* **1988**, *111*, 264-272.

(25) Turchi, C. S.; Ollis, D. F. *J. Catalysis* **1990**, *122*, 178-192.

(26) Stafford, U.; Gray, K. A.; Kamat, P. V. *J. Phys. Chem.* **1994**, *98*, 6343-6351.

(27) Stumm, W. In *Aquatic Chemistry: Interfacial and Interspecies Processes*; C. P. Huang, J. J. Morgan and C. R. O'melia, Eds.; American Chemical Society: Washington, D.C. 1995; p 1-32.

Figures

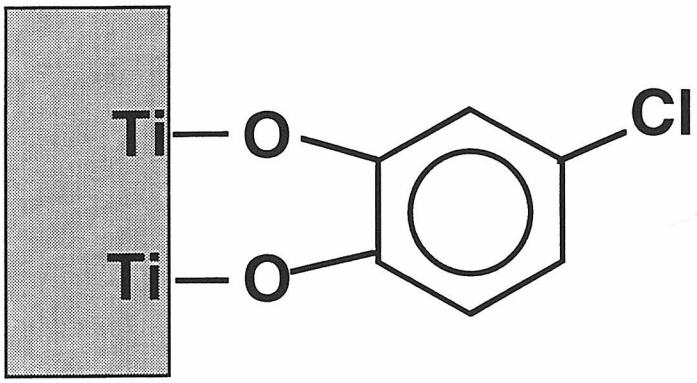

Figure 1. Bidentate binuclear structure of 4-chlorocatechol adsorbed on the surface of TiO_2 as determined by Martin et al. (12).

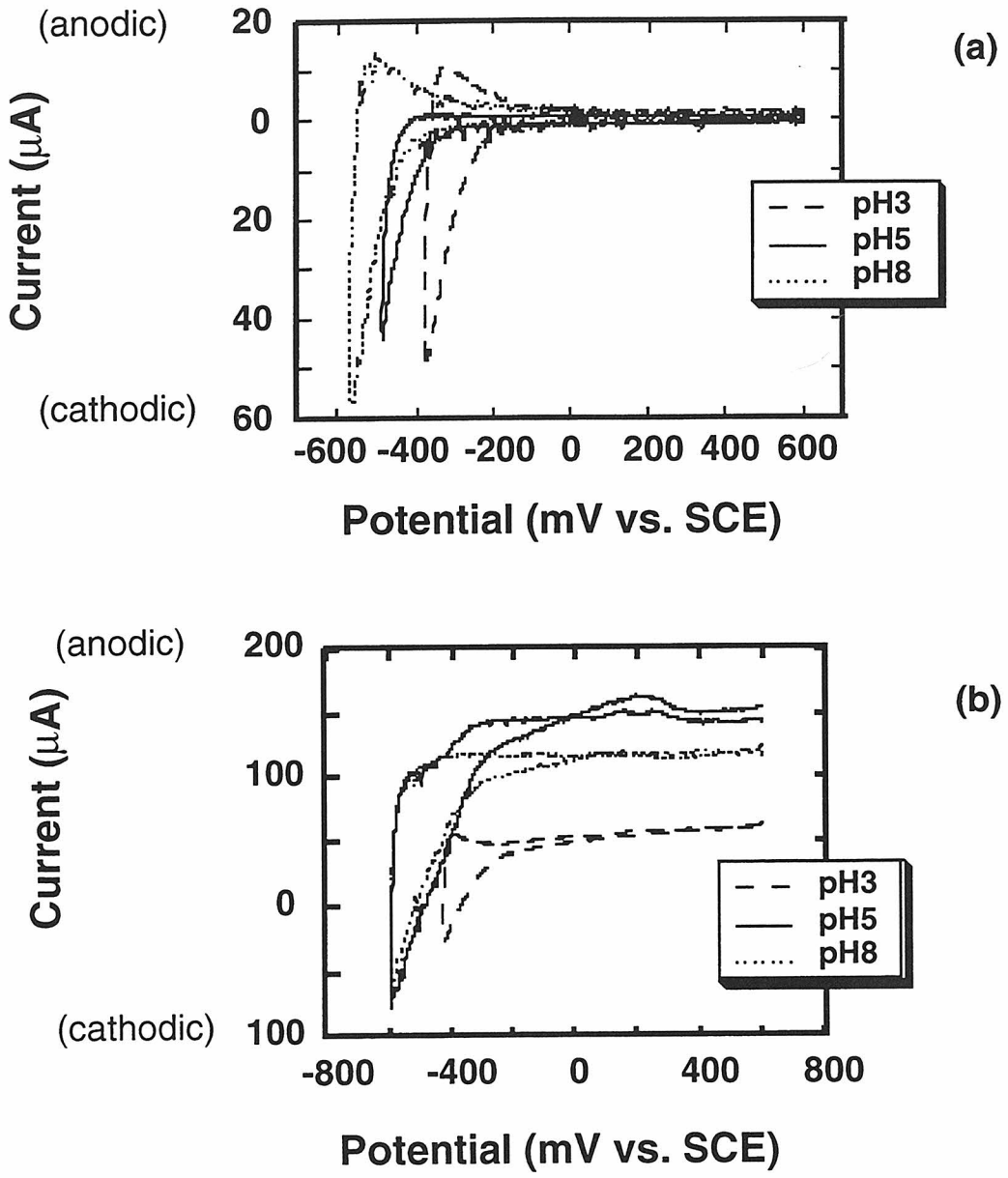

Figure 2. Current-potential curves for TiO_2 electrodes as a function of pH. Solutions are N_2-purged, 10 mM KCl (aq). (a) Current-potential behavior of TiO_2 electrodes in the absence of illumination. (b) Current-potential behavior of TiO_2 electrodes under UV-irradiation.

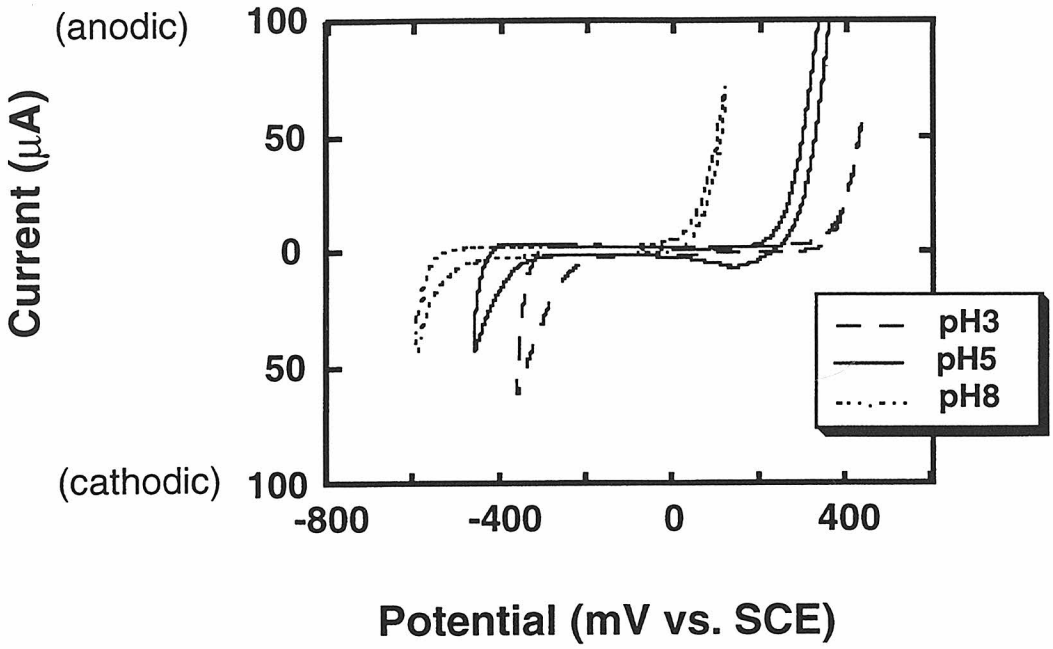

Figure 3. Current-potential behavior for TiO_2 electrodes in the presence of 500 μM 4-chlorocatechol with no illumination. Solutions are N_2-purged and contain a background electrolyte of 10 mM KCl (aq).

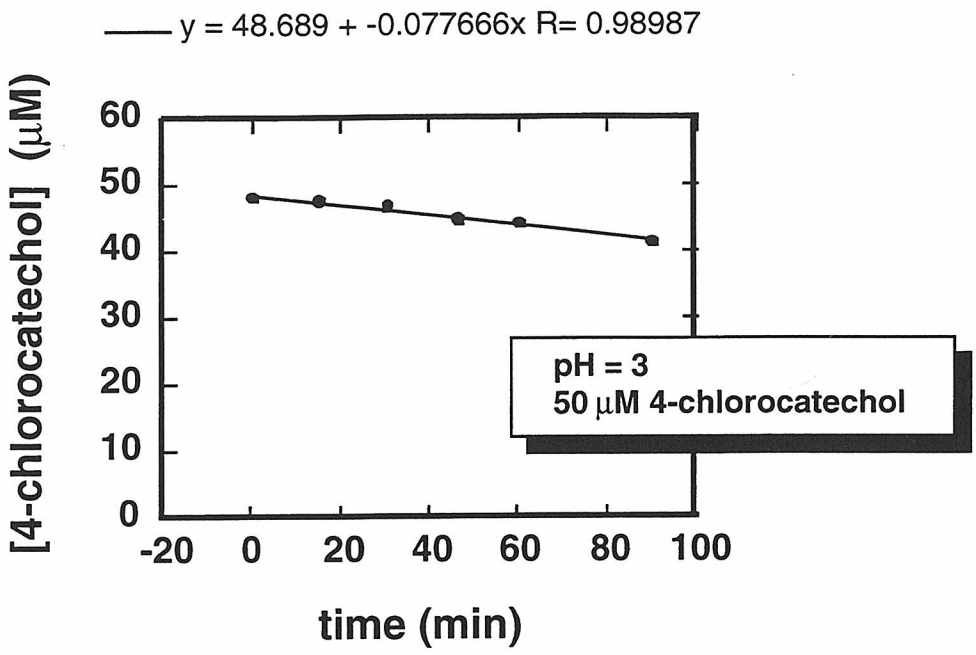

Figure 4. Time dependent concentration of 4-chlorocatechol in illuminated cell operated at 50 μA current. Solution pH equals 5. Equation shows linear least squares fit for the loss of 4-chlorocatechol as a function of time.

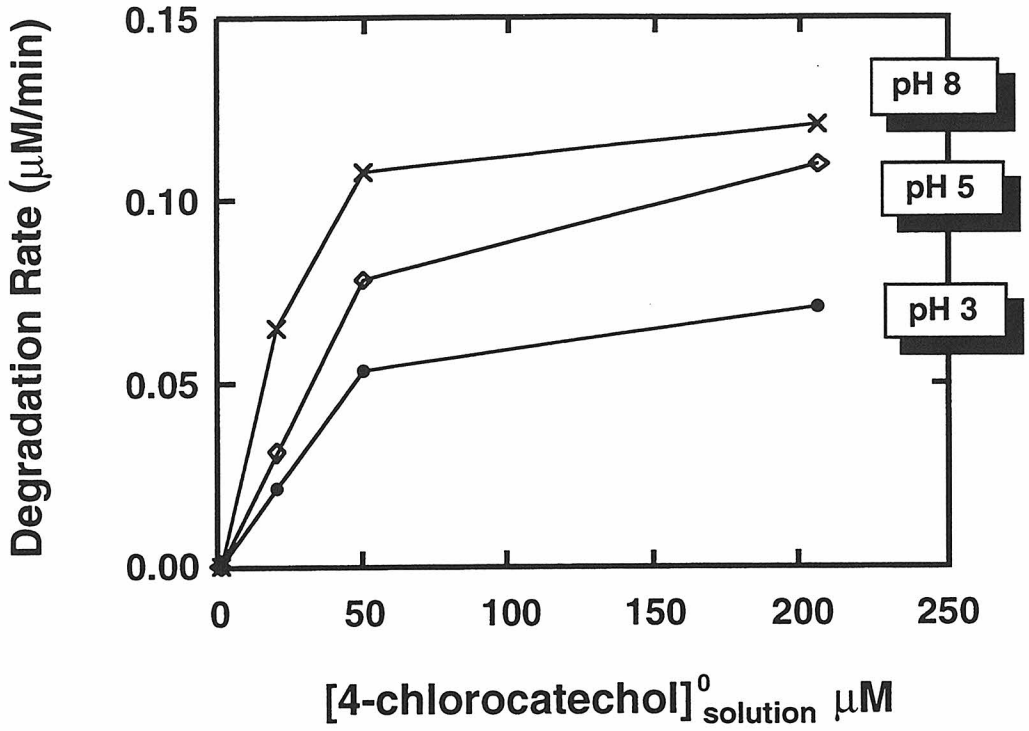

Figure 5. Initial degradation rate vs. initial bulk solution concentration of 4-chlorocatechol.

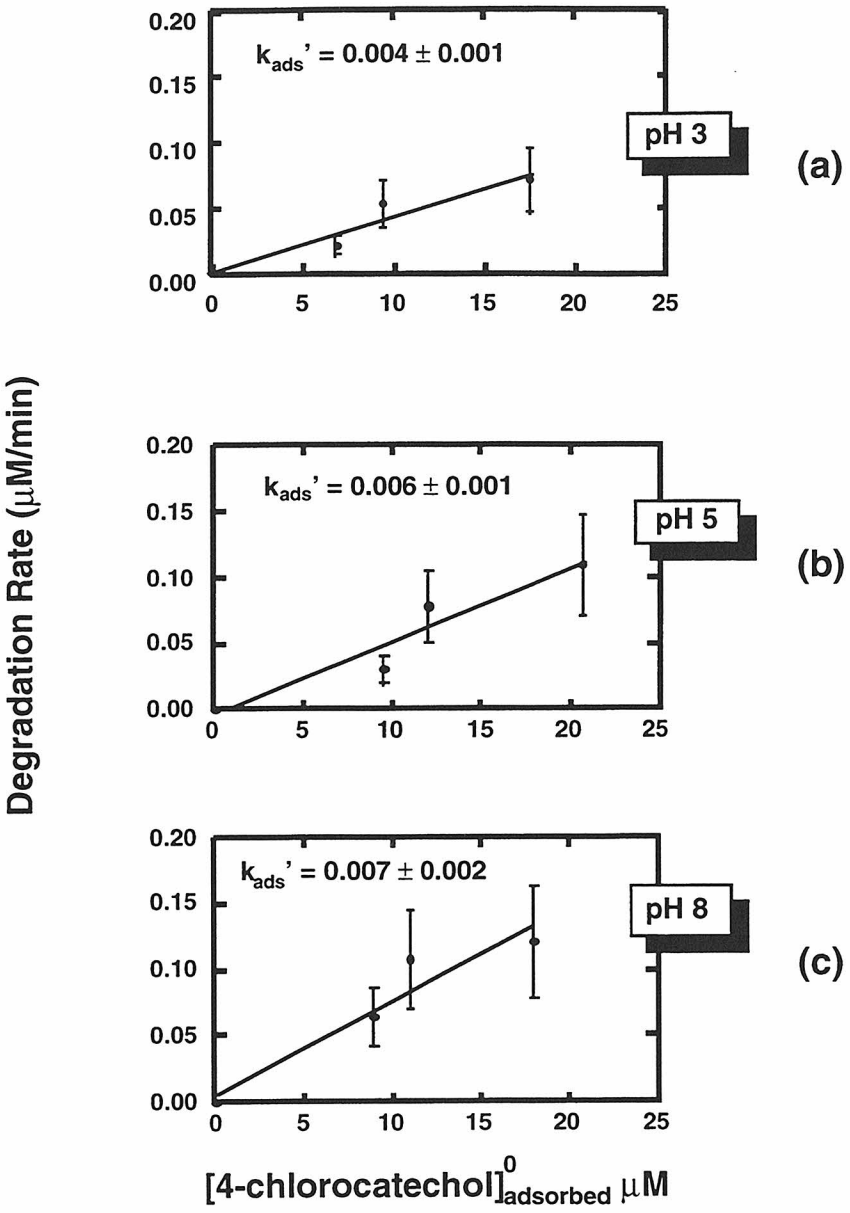

Figure 6. Initial degradation rate vs. concentration of sorbed 4-chlorocatechol on TiO_2. (a) pH = 3.0 ± 0.2; (b) pH = 5 ± 0.2; (c) pH = 8 ± 0.2. Concentrations of sorbed substrate were determined from data presented by Martin et al. (12) obtained under similar conditions.

Chapter 6.

Conclusions and Future Research Directions

This thesis describes research into the fundamental processes occurring in TiO_2 photocatalysis and correlates the results obtained with observed efficiencies for water treatment reactions. Oxidation mechanisms, charge transfer kinetics, and questions of molecular structure have been investigated along with more practically oriented studies of the effect of platinum deposits and organic sorption on photocatalytic efficiencies.

This research has contributed to our understanding of TiO_2 photocatalysis by determining the efficacy of oxygen as an electron scavenger in the TiO_2 photocatalytic process and by demonstrating that an increased flux of electrons across the TiO_2/H_2O interface at a given potential is achievable by using a more efficient electron acceptor. The interactions of a particular organic compound, 4-chlorocatechol, with the surface of TiO_2 have been investigated and have been shown to affect positively the resulting photodegradation rates.

In this thesis, an alternative technology using non-illuminated TiO_2 electrodes for waste water treatment has also been explored. At these electrodes, both direct and hydroxyl radical mediated oxidation mechanisms occur, with the precise distribution of kinetic events depending on the particular substrate being degraded.

As with all research, these results suggest new directions for future investigations. While it has been shown that the use of platinum or potassium ferricyanide would increase the flux of electrons across the TiO_2/H_2O interface at a given potential and should thus improve the quatnum yields for photodegradation, neither of these additives is feasible in a practical application. Research into alternative electron scavengers thus appears to be a promising avenue for future work. The preliminary study of the effect of sorption on the photoelectrocatalytic degradation rate of 4-chlorocatechol for a constant flux of oxidizing species should also be expanded to include other classes of specifically adsorbing compounds as well as compounds that are electrostatically associated with the surface. Current increase experiments, similar to those performed with Nb-doped

polycrystalline electrodes, using illuminated TiO_2 electrodes would allow comparison of the contribution of direct and hydroxyl radical mediated oxidation pathways for the two systems.

An interesting result reported by other researchers has noted the dramatic improvement in quantum yields for reactors operated under pulsed rather than steady-state illumination.[1] The mechanism of this improvement, however, has not been determined and merits further investigation. Given the results reported here for steady-state photocatalysis, it would be useful to determine the effect of substrate sorption and solution pH on systems operated under pulsed illumination. This is also an area in which the use of TiO_2 electrodes should provide additional insight.

While much has been learned over the past 20 years, it is still an open question whether TiO_2 photocatalysis will become a commercially viable treatment alternative for contaminated ground water and/or industrial effluents.[2] The Nb-doped, polycrystalline TiO_2 electrodes described in Chapter 3 have shown promising current efficiencies for the degradation of organic molecules and are currently being tested in pilot scale treatment systems for the reduction of the biological oxygen demand of industrial effluents.

References

(1) Sczechowski, J. G.; Koval, C. A.; Noble, R. D. *J. Photochem. Photobiol. A: Chem.* **1993**, *74*, 273-278.

(2) Wilson, E. In *Chem. Eng. News*, July 1, 1996; pp 29.